Univerzita Karlova v Praze

1. lékařská fakulta

Studijní program: Biochemie a patobiochemie

Studijní obor: YBICH

Ing. Alena Karnošová

Lipidované analogy peptidu uvolňujícího prolaktin jako potenciální antiobezitika: zkoumání mechanizmu účinku

Lipidized analogs of prolactin-releasing peptide as potential agents for obesity therapy: search for mechanism of action

Disertační práce

Vedoucí závěrečné práce/Školitel: RNDr. Lenka Maletínská, DSc.

Konzultant (byl-li): RNDr. Veronika Strnadová, Ph.D.

Praha, 2023

PROHLÁŠENÍ

Prohlašuji, že jsem závěrečnou práci zpracovala samostatně a že jsem řádně uvedla a citovala všechny použité prameny a literaturu. Současně prohlašuji, že práce nebyla využita k získání jiného nebo stejného titulu.

Souhlasím s trvalým uložením elektronické verze mé práce v databázi systému meziuniverzitního projektu Theses.cz za účelem soustavné kontroly podobnosti kvalifikačních prací.

V Praze, 27.3. 2023

Alena Karnošová

IDENTIFIKAČNÍ ZÁZNAM

KARNOŠOVÁ, Alena. Lipidované analogy peptidu uvolňujícího prolaktin jako potenciální antiobezitika: zkoumání mechanizmu účinku. [Lipidized analogs of prolactin-releasing peptide as potential agents for obesity therapy: search for mechanism of action. Praha, 2023. 97 stran, 2 přílohy. Disertační práce. Univerzita Karlova, 1. lékařská fakulta, Klinika / Ústav 1. LF UK 2008. Ústav organické chemie a biochemie Akademie věd České republiky, v.v.i. Vedoucí disertační práce Maletínská, Lenka.

ABSTRAKT

Obezita je jedním z nejvíce rozšířených onemocnění na světě, ale její současná léčba má mnoho omezení. Peptid uvolňující prolaktin (PrRP) je neuropeptid snižující příjem potravy po podání do třetí mozkové komory, tuto schopnost však ztrácí po periferním podání. Lipidizace peptidů zvyšuje jejich stabilitu v krevním řečišti a usnadňuje jejich centrální účinek po periferním podání. V naší laboratoři byly vyvinuty lipidizované analogy PrRP, které mohou být perspektivním řešením pro léčbu obezity. Dříve jsme prokázali, že lipidizované analogy PrRP při periferním podání významně snižují příjem potravy a tělesnou hmotnost u obézních myší. Palm-PrRP31 a palm^{11}-PrRP31 byly identifikovány jako klíčové analogy s těmito účinky a v této studii jsme se zaměřili na zkoumání mechanismu účinků těchto analogů in vitro.

Přirozený PrRP31 se váže ke svému receptoru GPR10 a s vysokou afinitou i na receptor pro neuropeptid FF 2. typu (NPFFR2), které jsou oba exprimovány v oblastech zapojených do regulace příjmu potravy. Palmitoylace PrRP31 zvýšila jejich vazebné a agonistické vlastnosti pro receptory GPR10 i NPFFR2. Lipidizované analogy také vykazovaly vyšší afinitu než přirozený PrRP31 k dalšímu receptoru neuropeptidu FF, NPFFR1, což naznačuje, že NPFFR1 by mohl být novým potenciálním cílem lipidizovaných PrRP31 analogů. V buňkách exprimujících receptory GPR10, NPFFR2 a NPFFR1 byly studovány buněčné signální dráhy, které by mohly být základem účinků palmitoylovaných analogů PrRP31. Palmitoylované analogy PrRP31 stimulovaly aktivaci několika signalizačních kaskád, jako jsou MAPK, Akt a CREB, a transkripčních faktorů c-Foc a c-Jun, které se účastní regulace různých buněčných procesů, jako je progrese buněčného cyklu, migrace a diferenciace.

Druhá část práce byla zaměřena na *in vivo* experimenty zahrnující metabolickou fenotypizaci myší s vyřazenými geny *Npffr2* a *Gpr10/Npffr2*, krmených buď standardní nebo vysokotukovou dietou, a jejich srovnáním s kontrolními myšmi. Delece receptoru NPFFR2 vedla ke glukózové intoleranci, která byla zhoršena vysokotukovou dietou. Navíc myši s vyřazeným genem *Npffr2* vykazovaly narušenou centrální signální dráhu PI3K/Akt. Delece receptorů GPR10 a NPPFR2 vedla ke změnám, které byly závislé na pohlaví a dietě, vedoucím k prediabetickým symptomům. Při podávání stravy s vysokým obsahem tuků vykazovala obě pohlaví hyperinzulinémii. Samice myší s deficitem GPR10/NPFFR2 také vykazovaly zhoršenou glukózovou toleranci a hyperglykémii, když byly krmeny vysokotukovou dietou.

KLÍČOVÁ SLOVA

Peptid uvolňující prolaktin; analogy; GPCR; obezita; buněčná signalizace; myši s vyřazenými geny pro GPR10 a NPFFR2

ABSTRACT

Obesity is a common metabolic condition that is becoming more prevalent globally, but current treatments have limitations. Prolactin-releasing peptide (PrRP), a neuropeptide that reduces food intake after administration to the third ventricle, loses this ability when administered peripherally. However, lipidization of peptides enhances their stability in the bloodstream and facilitates their central effect after peripheral administration. We developed lipidized analogs of PrRP, which have high potential as a treatment option for obesity. We previously demonstrated that peripheral administration of lipidized PrRP analogs led to a substantial reduction in food intake and body weight in mice, with palm-PrRP31 and palm^{11}-PrRP31 emerging as key analogs. In this study, we aimed to further investigate the mechanisms underlying the effects of these two PrRP31 analogs *in vitro*.

Natural PrRP31 binds to its receptor GPR10 and with high affinity to neuropeptide FF receptor type 2 (NPFFR2), which are both expressed in regions involved in food intake regulation. The palmitoylation of PrRP31 increased their binding and agonist properties for both GPR10 and NPFFR2 receptors. Lipidized analogs exhibited a stronger affinity also for another neuropeptide FF receptor, NPFFR1, suggesting that NPFFR1 could be a new potential target for PrRP31 analogs. The molecular mechanisms underlying the effects of palmitoylated PrRP31 analogs on cellular signaling pathways were studied in cells expressing GPR10, NPFFR2, and NPFFR1. Palmitoylated PrRP31 analogs stimulated the activation of multiple signaling kinases such as MAPK, Akt, and CREB, and transcription factors c-Foc and c-Jun, which are involved in regulation of various cellular processes such as cell cycle progression, migration, and differentiation.

The second part of the thesis was focused on *in vivo* experiments involving metabolic phenotyping of NPFFR2-deficient and GPR10/NPFFR2-deficient mice, fed either standard or high-fat diets, and comparing them to age-matched control mice. We observed that deficiency of NPFFR2 resulted in glucose intolerance impaired on a high-fat diet. Moreover, NPFFR2 knock-out mice showed a disrupted central PI3K/Akt signaling pathway. Deletion of both GPR10 and NPFFR2 receptors resulted in sex-specific and diet-dependent changes leading to prediabetic symptoms. When fed a high-fat diet, both sexes exhibited hyperinsulinemia. Moreover, female GPR10/NPFFR2-deficient mice also showed impaired glucose tolerance and hyperglycemia when fed high-fat diet.

KEY WORDS

prolactin-releasing peptide; analogs; GPCR; obesity; cell signaling; GPR10 and NPFFR2 knock-out mice

ACKNOWLEDGEMENT

I would like to express my deepest gratitude to my thesis supervisor Dr. Lenka Maletínská and my advisor Dr. Veronika Strnadová for their unwavering support, guidance, and patience throughout my doctoral studies. I also want to thank Dr. Jaroslav Kuneš, and Dr. Blanka Železná, for their feedback and valuable insights that greatly improved the quality of my work.

I am also grateful to my colleagues for creating a friendly atmosphere and for discussions that have helped my understanding of the subject of my thesis. Special thanks to my colleague Lucie Holá, MSc. for her constant support and encouragement. In addition, I would like to express my appreciation towards Martina Kojecká, MSc. for conducting metabolic parameter measurements and Hedvika Vysušilová for the technical assistance provided at the animal facility. Additionally, I want to express my gratitude towards Miroslava Blechová, MSc. for her peptide synthesis, and team of Dr. Aleš Marek for peptide iodination.

Furthermore, I would like to acknowledge the support and encouragement I received from my family and boyfriend. Their unwavering support and love kept me motivated and inspired throughout this challenging journey.

This Ph.D. theses was supported by the Grant Agency of the Czech Republic No. 21-03691S, the Academy of Sciences of the Czech Republic RVO:61388963, and research grant from Novo Nordisk.

CONTENTS

ABBREVIATIONS

1DMe	[D-Tyr^1, (NMe)Phe^3] neuropeptide FF
3V	third ventricle
ACTH	adrenocorticotrophic hormone
AgRP	agouti-related peptide
Akt	protein kinase B
ANOVA	analysis of variance
AP	area postrema
AP-1	activator protein 1
ARC	arcuate nucleus
AS160	Akt substrate of 160 kDa
BAT	brown adipose tissue
B_{max}	total number of receptors/receptor density
cAMP	cyclic adenosine monophosphate
CART	cocaine- and amphetamine-regulated transcript
CCK	cholecystokinin
Cha	cyclohexylalanine
CHO	Chinese hamster ovary cells
CNS	central nervous system
CREB	cAMP response element-binding protein
CRF	corticotropin-releasing factor
CRH	corticotropin-releasing hormone
CSF	cerebrospinal fluid
DIO	diet-induced obesity
dKO	double knock-out mice
DMN	dorsomedial nucleus
Dodec	dodecanoyl
DOR	δ-opioid receptor
EC_{50}	50% maximal effect
EDTA	ethylenediaminetetraacetic acid
EPM	elevated plus maze
EPM	elevated plus maze
ERK	extracellular signal-regulated kinase
fa/fa	obese Zucker fatty rats with a mutated leptin receptor

FFA	free fatty acids
FRET	fluorescence resonance energy transfer
FSH	follicle-stimulating hormone
GABA	gamma-aminobutyric acid
GAPDH	glyceraldehyde-3-phosphate dehydrogenase
GHSR	ghrelin receptor, growth hormone secretagogue receptor
GLP-1	glucagon-like peptide 1
GPCR	G-protein coupled receptors
GPR10	G-protein coupled receptor 10, PrRP receptor
gRNA	guide RNA
GSK-3β	glycogen-synthase kinase-3beta
gWAT	gonadal white adipose tissue
HDL	high density lipoprotein
HEPES	4-(2-hydroxyethyl)-1-piperazineethanesulfonic acid
HFD	high-fat diet
HPA	hypothalamic-pituitary-adrenal
i.c.v.	intracerebroventricular
IC_{50}	half-inhibitory concentration
i.p.	intraperitoneal
IC_{50}	half-inhibitory concentration
JNK	c-Jun N-terminal protein kinase
K_d	dissociation constant
K_i	inhibition constant
KO	knock-out
KOR	κ-opioid receptor
LDL	low density lipoprotein
LH	luteinizing hormone
LHA	lateral hypothalamic area
MAPK	mitogen-activated protein kinase
MC3R	melanocortin 3 receptor
MC4R	melanocortin 4 receptor
ME	median eminence
MOR	μ- opioid receptor
MS	mass spectrometry

Myr	myristoyl
N-Ac	N-acetylated
Nal	napthylalanine
NPAF	neuropeptide AF
NPFF	neuropeptide FF
NPFFR1 (GPR147)	Neuropeptide FF receptor type 1, G-protein coupled receptor 147
NPFFR2 (GPR74)	Neuropeptide FF receptor type 2, G-protein coupled receptor 74
NPY	neuropeptide Y
NTS	nucleus tractus solitarii
ob	recessive mutation in *ob* gene coding hormone leptin
OF	open field
OGTT	oral glucose tolerance test
OLETF	otsuka long-evans tokushima fatty
ORL-1	opioid receptor-like 1
Palm	palmitoyl
Palm-COOH	hexadecanedioic acid
PBS	phosphate-buffered saline
PDK	phosphoinositide-dependent kinase
PEI	polyethylenimine
PerVN	periventricular hypothalamic nucleus
PFA	paraformaldehyde
$PheCl_2$	(3,4-dichloro)phenylalanine
$PheF_5$	pentafluoro-phenylalanine
$PheNO_2$	(4-nitro)phenylalanine
Phg	phenylglycine
PI3K	phosphoinositide 3-kinase
PKA	cAMP-dependent protein kinase, protein kinase A
PKC	protein kinase C
POMC	pro-opiomelanocortin
PrRP	prolactin-releasing peptide
PTX	pertussis toxin
PVN	paraventricular nucleus
PYY	peptide YY
QRFP	pyroglutamylated RF-amide peptide

Q-TOF	quadrupole-time of flight
RF9	N-adamantane-carbonyl-Arg-Phe-NH_2 trifluoroacetat
RFRP	RF-amide-related peptide
RT	room temperature
s.c.	subcutaneous
scWAT	subcutaneous white adipose tissues
SDS	sodium dodecyl sulfate
SEM	standard error of the mean
SOCS3	suppressor of cytokine signaling 3
STD	standard diet
subAP	area subpostrema
TAG	triacylglycerol
TBS	tris buffered saline
TH	tyrosine hydroxylase
Tris	tris-(hydroxymethyl)aminomethane
TTDS	1,13-diamino-4,7,10-trioxatridecan-succinamic acid
U2OS	human bone osteosarcoma epithelial cells
UHR-1	unknown hypothalamic receptor
VMN	ventromedial nucleus
WT	wild-type
Y1	neuropeptide Y receptor type 1
Y2	neuropeptide Y receptor type 2
Y4	neuropeptide Y receptor type 4
Y5	neuropeptide Y receptor type 5
α-MSH	α-Melanocyte stimulating hormone
γE	gamma-glutamic

1. INTRODUCTION

1.1 Obesity

One of the most widespread civilization diseases is obesity. Normal regulation of body weight occurs when food intake and energy expenditure are in balance. Obesity can be caused by a range of factors, including dysregulation of energy metabolism, but there are other factors to consider such as genetics, environment, lifestyle, and medication use. The amount of energy expended per unit of weight in a specific period is called the metabolic rate, which is known to be decreased as people gain weight (Ravussin and Bogardus, 1989).

Obesity is defined as an abnormal or excessive accumulation of fat. Currently, is obesity considered to be one of the most prevalent diseases in civilization and is reaching epidemic proportions all over the world. Several diseases are associated with obesity among them inflammation, endothelial dysfunction, insulin resistance, hypertension, dyslipidemia, and atherosclerosis (WHO European Regional Obesity Report, 2022).

The central nervous system (CNS) is responsible for closely monitoring and controlling the body's energy balance to maintain energy homeostasis. To regulate the balance between energy intake and energy expenditure, the CNS coordinates with various peripheral factors, and sensory nerve fibers and carries information to the brain (Schwartz and Porte, 2005).

1.1.1 Regulation of Food Intake and Energy Homeostasis

The most important part of the CNS involved in the regulation of feeding and energy expenditure is the hypothalamus, specifically the arcuate nucleus (ARC). The ARC is an area with a relatively porous blood-brain barrier containing fenestrated capillaries and is situated near the third ventricle and the circumventricular organ median eminence (ME) (Myers and Olson, 2012).

There are two distinct neuronal populations located in the ARC of the hypothalamus, the anorexigenic (suppressing food intake) pro-opiomelanocortin (POMC) and cocaine- and amphetamine-regulated transcript (CART) expressing neurons, and the orexigenic (promoting food intake) neuropeptide Y (NPY) and agouti-related peptide (AgRP) expressing neurons (Fig.1) (Timper and Bruning, 2017; Yu and Kim, 2012). They are the primary point of transfer for various metabolic signals coming from the periphery, including leptin, insulin, ghrelin, and some nutrients (Yu and Kim, 2012).

α-Melanocyte stimulating hormone (α-MSH) is released by POMC/ CART neurons, leading to binding and activating melanocortin receptors and subsequent inhibition of food intake (Fan et al., 1997). On the other hand, when orexigenic signals are accepted in the ARC, the antagonist of the melanocortin receptors (MC3R and MC4R) AgRP is released by NPY/AgRP expressing neurons and competes with α-MSH. Moreover, NPY/AgRP neurons inhibit POMC/CART neurons by releasing a neurotransmitter gamma-aminobutyric acid (GABA) (Blouet and Schwartz, 2010; Yu and Kim, 2012). Together, NPY, AgPR and GABA mediate orexigenic effect by activation of NPY/AgPR neurons. The NPY receptors are found throughout the CNS. The receptors known as Y1, Y2 and Y5 are present in high concentrations especially in the ARC, the paraventricular nucleus (PVN), and the ventromedial nucleus (VMN) hypothalamic regions (Blouet and Schwartz, 2010). Additionally, receptors for peripheral hormones such as insulin and leptin are also expressed by POMC/CART and AgRP/NPY neurons. Leptin and insulin exert an anorexigenic effect by stimulating *Pomc* and inhibiting *Agpr* expression (Timper and Bruning, 2017). Conversely, ghrelin is mainly produced in the stomach during periods of food deprivation and it strongly induces hunger by activating AgRP/NPY neurons (Timper and Bruning, 2017).

The POMC/CART and NPY/AgRP expressing neurons project signals to other areas of the hypothalamus that are closely involved in controlling hunger, such as PVN, VMN, the dorsomedial nucleus (DMN), and the lateral hypothalamic area (LHA) (Fig.1) (Morton et al., 2006; Timper and Bruning, 2017).

The vagus nerve is a crucial link between the gut and the brain and carries satiety signals from the gastrointestinal tract to the nucleus tractus solitarii (NTS), which is in the brainstem in close proximity to the circumventricular organ area postrema (AP). Moreover, NTS receives and transmits neural signals to the hypothalamic PVN and ensures a connection between the hypothalamus and the brainstem. A hunger suppressor cholecystokinin (CCK), produced by cells of the small intestine, is known to play a role in the central regulation of energy homeostasis by transmitting satiety signals to the brain via afferent fibers of the vagus nerve and synapses to the NTS (Fig.1) (Morton et al., 2014; Yu and Kim, 2012). Like CCK, another peptide released by the digestive system in response to food ingestion that transmits satiety signals via the vagus nerve is glucagon-like peptide 1 (GLP-1) (Fig.1). Stable synthetic GLP-1 analogs, such as liraglutide (recently at the market for treatment of type 2 diabetes and obesity), have previously been found to have the ability to reverse both obesity and diabetes, as they can enhance insulin

secretion, decrease glucagon secretion, reduce gastric emptying, and promote satiety (Maselli and Camilleri, 2021). Intestinal hormone peptide YY (PYY) is released postprandially in proportion to meal size and by signaling feelings of fullness and satiety to the brain (Fig.1), it reduces food intake (Cummings and Overduin, 2007).

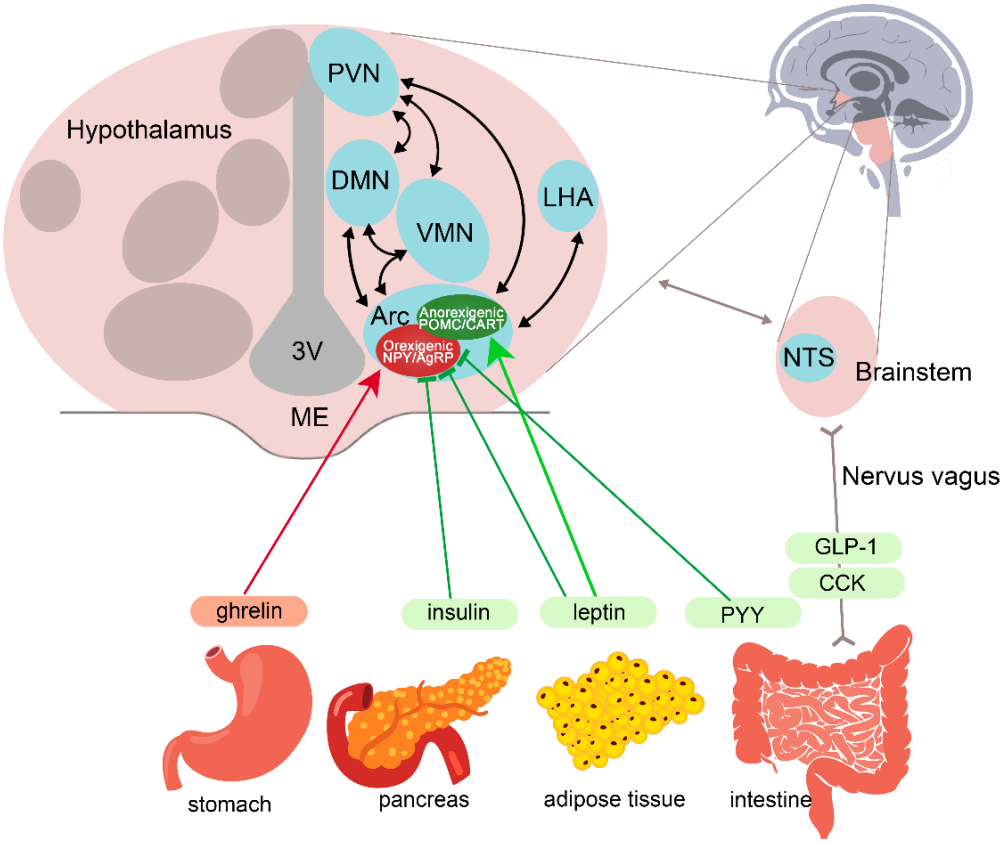

Fig. 1: Hormonal regulation of food intake.
The median eminence (ME), adjacent to the third ventricle (3V), facilitates the transport of peripheral hormones to the arcuate nucleus (ARC). Leptin, insulin, and peptide YY (PYY), decrease food intake by inhibiting neurons in the ARC producing neuropeptide Y (NPY) and agouti-related peptide (AgRP). Ghrelin increases food intake by activating NPY/AgRP-expressing neurons. The ARC project signals to other hypothalamic nuclei, the paraventricular nucleus (PVN), lateral hypothalamus (LHA), and dorsomedial (DMN) and ventromedial nuclei (VMN). Through direct inputs via nervus vagus to the nucleus tractus solitarii (NTS) and indirect inputs to the hypothalamus, the NTS responds to satiety signals. Cholecystokinin (CCK) and glucagon-like peptide 1 (GLP-1) modulate the NTS pathway via the vagus nerve.

1.2 RF-amide Neuropeptides

The neuropeptides of the RF-amide peptide family contain the typical carboxy-terminal amino acid sequence Arg-Phe-NH2 (RF-NH_2), which is essential for binding to their receptors. These neuropeptides exhibit N-terminal variation, which results in a wide range of biological actions. The first RF-amide peptide discovered and isolated was tetrapeptide Phe-Met-Arg-Phe-NH_2 (FMRF-NH_2) from the nervous system of the clam *Macrocallista nimbosa* in 1977 (Price and Greenberg, 1977) and a few years later in order to identify

structurally-similar peptides across species, antibodies against FMRF-NH_2 peptides were used. RF-amide peptides' C-terminal amide sequence was then also found in the neural systems of numerous additional taxa, including insects, fish, and mammals (Boer et al., 1980). The first RF-amide peptide discovered in a vertebrate, found in a chicken, was pentapeptide Leu-Pro-Leu-Arg-Phe-NH_2 (Dockray et al., 1983). Neuropeptides FF (NPFF) and AF (NPAF) purified from bovine brain were the first two discovered mammalian RF-amide peptides (Yang et al., 1985).

Mammalian RF-amide peptides family could be subdivided into five groups encoded by five genes: NPFF group, the RF-amide-related peptide (RFRP) group, the prolactin-releasing peptide (PrRP) group, the kisspeptin group and finally the pyroglutamylated RF-amide peptide (QRFP) group (Fukusumi et al., 2006). These peptides exert their effects via G-protein coupled receptors (GPCR) which are encoded by five genes. Four of the neuropeptide groups (RFRP, NPFF, QRFP, and PrRP) act through receptors that belong to the rhodopsin-β-type GPCR and kisspeptins act through receptors which belong into rhodopsin-γ-type GPCRs. Rhodopsin β-type receptors of RF-amide peptides are clustered in one the same region of the phylogenetic tree which suggest that RF-amide neuropeptide signaling system share common ancestor which evolved independently in the history at least three times (reviewed in (Elphick and Mirabeau, 2014)). However, PrRP receptor (GPR10) is phylogenetically more distant from NPFF and QRFPs receptors and appears to be closely related to neuropeptide Y (NPY) receptors. This suggest PrRP system importance in the regulation of feeding behavior (Yun et al., 2014).

1.3 Neuropeptide FF

NPFF was discovered and subsequently isolated from the bovine brain in 1985 using antibodies against FMRF-NH_2. Neuropeptide AF (NPAF) together with NPFF are encoded by a single *Npff* gene and they are created from the NPA-NPFF precursor by post-translational modifications. Human NPFF has 8 amino acids and NPAF has 18 amino acids (Yang et al., 1985). The overall sequence identity of the highly conserved precursors is 40%, with rat and mouse homology at 88% and bovine and human homology at 71% (Vilim et al., 1999). They were initially recognized for their ability to increase hyperalgesia and attenuate antinociception induced by opioids (Yang et al., 1985). NPFF family's peptide sequences are summarized in Table 1.

NPFF receptors defined as NPFFR1 (GPR147) and NPFFR2 (GPR74) belong to the GPCR family. NPFF specifically binds to both receptors with K_i (inhibition constant) at nanomolar concentrations (Bonini et al., 2000). However, it displayed higher affinity towards NPFFR2 compared to NPFFR1 (Liu et al., 2001).

Structure-activity studies of NPFF revealed that C-terminal Arg-Phe-NH_2 is essential for receptor activation. Positively charged Arg at position 7 was found to be crucial for the biological function of NPFF (Findeisen et al., 2011; Payza et al., 1993). Moreover, deletion of the two N-terminal amino acids did not significantly change the peptide affinity, but when the three N-terminal residues were removed, it resulted in a lower affinity towards NPFF receptor (Payza et al., 1993).

The protease degradation-resistant analog of NPFF 1DMe ([D-Tyr1, (NMe)Phe^3] neuropeptide FF) (see the Fig 6 for the peptide structure) was synthesized by Gicquel *et al*. The affinity towards NPFF receptors remained similar to natural peptide NPFF but it showed 3 times lower degradation rate (Gicquel et al., 1992). 1DMe analog is used in our *in vitro* competitive binding studies as an agonist of receptors NPFFR1 and NPFFR2.

Simonin *et al*. prepared compound RF9 (N-adamantane-carbonyl-Arg-Phe-NH_2 trifluoroacetat) with potent NPFFR1/NPFFR2 antagonist activity. When administered in conjunction with an opioid receptor agonist, RF9 has been shown to mitigate tolerance to analgesics and hyperalgesia caused by repeated use of opiates (Simonin et al., 2006). However, our subsequent research questioned the antagonistic activity of RF9 compound towards NPFFR1/NPFF2 receptor in food intake test in mice (Maletinska et al., 2013).

Table 1: Peptide sequences of human and mouse NPFF and PrRP.

	Peptide	Species	Peptide sequence	Receptors
NPFF group	**NPFF**	human	FLFQPQ**RF–NH$_2$**	**NPFFR1**
		mouse	FLFQPQ**RF–NH$_2$**	(GPR147),
	NPAF	human	AGEGLNSQFWSLAAPQ**RF–NH$_2$**	**NPFFR2**
		mouse	QFWSLAAPQ**RF–NH$_2$**	(GPR74)
PrRP group	**PrRP20**	human	TPDINPAWYASRGIRPVG**RF–NH$_2$**	**GPR10** **NPFFR2** (GPR74)
		mouse	TPDINPAWYTSRGIRPVG**RF–NH$_2$**	
	PrRP31	human	SRTHRHSMEIRTPDINPAWYASRGIRPVG**RF–NH$_2$**	
		mouse	SRAHQHSMEIRTPDINPAWYTSRGIRPVG**RF–NH$_2$**	

1.3.1 Expression of NPFF in the Brain and Periphery

In situ hybridization was used to characterize the expression of NPFF mRNA in rat (Goncharuk et al., 2006; Vilim et al., 1999) and mouse (Nystedt et al., 2006) brain. Moderate NPFF expression levels were found in PVN, VMN, DMN, LHA, ARC, and supraoptic nucleus in the hypothalamus. In particular, the lateral part of NTS showed a very strong NPFF expression. NPFF mRNA was discovered also in the amygdala or hippocampus. Moreover, a strong signal was revealed also in the AP, the area subpostrema (subAP), spinal trigeminal nucleus located in the lateral medulla of the brainstem. Another strong mRNA expression of NPFF was found in the superficial layers of the spinal cord. The spinal cord, along with the brainstem, plays an important role in the transmission of pain and temperature perceptions (Goncharuk et al., 2006; Lin et al., 2016b; Nystedt et al., 2006; Vilim et al., 1999; Zhang et al., 2018). Furthermore, Zhang *et al*. showed decreased NPFF mRNA expression in the subAP and brainstem when mice fed with a high-fat diet (HFD), which indicates that NPFF system is involved in the regulation of energy balance (Zhang et al., 2018).

Interestingly, precursor NPA-NPFF is twenty times more abundant than NPFF in the spinal cord (Bonnard et al., 2001), where a number of enzymes cleaving neuropeptide precursors is expressed (Schafer et al., 1993). This explains the finding of Roumy *et al*. that NPA-NPFF has a stronger potency to inhibit nociception activity than NPFF (Roumy et al., 2000).

NPFF mRNA was not detected in the anterior pituitary or the periphery in the adrenal gland, pancreas, epididymis (Nieminen et al., 2000). A weak signal was also observed in the mouse heart, spleen, and embryo (Nystedt et al., 2006).

NPFF was previously identified in human plasma (Sundblom et al., 1995), mouse plasma (Waqas et al., 2017), and in human cerebrospinal fluid (CSF) (Sundblom et al., 1997).

1.3.2 Discovery and Distribution of NPFF Receptors

The NPFF receptors were identified in 2000 by three studies, according to publications by Elshourbagy *et al.* (Elshourbagy et al., 2000), Bonini *et al*. (Bonini et al., 2000), and Hinuma *et al.* (Hinuma et al., 2000). As was previously mentioned, NPFF signals via receptors NPFFR1 and NPFFR2.

The human NPFFR1 and NPFFR2 exhibit a sequence homology of 59% and display conserved amino acid sequence domains in rodents and humans. In comparison

with other human GPCR receptors human NPFFR1 showed high sequence similarity with orexin receptors (35-37%), NPY receptors (Y1 32%, Y2 34%, Y4 31%), CCK receptor (34%) and GPR10 receptor (32%) (Bonini et al., 2000; Hinuma et al., 2000). NPFF peptide is less potent than other members of the RF-amide peptide group, specifically the RFRP family group, such as peptides RFRP-1 (also known as neuropeptide SF, NPSF) and RFRP-3 (also known as neuropeptide VF, NPVF, or Gonadotropin-inhibitory hormone, GnIH), in activating NPFFR1 signaling (Mollereau et al., 2002). NPFFR1 is also known as RFRPR (RFRP receptor) since RFRP peptides are the preferred ligands of NPFFR1 (Pineda et al., 2010).

The human NPFFR2 gene is located nearby the gene cluster of Y5, Y1, and Y2 receptors on chromosome 4q3. Therefore, NPFFR2 also shares a high sequence identity with NPY receptors (Bonini et al., 2000), especially with the Y2 subtype (33%), and the NPFFR2 receptor was considered to be a possible candidate to join the Y receptor family (Parker et al., 2000). Moreover, NPFFR2 was found to share 37% amino acid identity with orexin receptor 1 (Elshourbagy et al., 2000).

1.3.2.1 Distribution of NPFFR1

The distribution of NPFFR1 was examined by the reverse transcription polymerase chain reaction (RT-PCR) and *in situ* hybridization in rats (Bonini et al., 2000; Hinuma et al., 2000; Liu et al., 2001) and humans (Bonini et al., 2000). Rats and humans both have a high levels of NPFFR1 expression predominantly in their CNS and are more widely distributed there than NPFFR2 (Liu et al., 2001).

In rats, NPFFR1 is highly expressed in the amygdala and hypothalamus. In the hypothalamus NPFFR1 can be found specifically in the PVN, DMN, VMN, ARC, periventricular nucleus, anterior hypothalamic nucleus, supraoptic nucleus and medial preoptic nucleus (Bonini et al., 2000; Higo et al., 2021; Hinuma et al., 2000; Liu et al., 2001). Receptors were also found along the wall of the 3V in the anteroventral periventricular nucleus in the females, but not in the male mice, and those NPFFR1 receptors were colocalized with kisspeptin-positive neurons (Higo et al., 2021). Moreover, other CNS regions that contain NPFFR1 are the thalamus, NTS, septal nuclei (also termed the medial olfactory area), cerebral cortex, choroid plexus, olfactory bulb, and the AP of the medulla oblongata (Bonini et al., 2000; Higo et al., 2021; Hinuma et al., 2000; Liu et al., 2001). However, in humans, the highest level of NPFFR1 expression was found in the spinal cord, hippocampus, and thalamus (Bonini et al., 2000).

The higher levels of NPFFR1 expression in peripheral tissues of rat were discovered in the ovaries, testicles, placenta, and eye, while very low levels were found in the liver, lung, kidney, adrenal gland, pituitary gland, or heart (Bonini et al., 2000; Hinuma et al., 2000).

1.3.2.2 Distribution of NPFFR2

In situ hybridization and RT-PCR analyses were used to determine the distribution of NPFFR2 in rodents (Anko et al., 2006; Bonini et al., 2000; Higo et al., 2021; Waqas et al., 2017) and humans (Bonini et al., 2000; Elshourbagy et al., 2000; Parker et al., 2000).

NPFFR2 is generally expressed in ascending tracts, and is less abundant in the CNS than NPFFR1. The NPFFR2 expression in the rat hypothalamus was detected in PVN, DMN, LHA, medial preoptic nucleus, and suprachiasmatic nucleus. Moreover, the ARC showed high expression of NPFFR2, which is predominantly expressed on NPY-positive or GABA-positive neuronal cells (Anko et al., 2006; Higo et al., 2021; Liu et al., 2001; Torz et al., 2022). The highest expression level of NPFFR2 in the rodents was detected in the olfactory bulb, NTS, thalamus, and amygdala (Anko et al., 2006; Goncharuk and Jhamandas, 2008). The lateral reticular nucleus, which is crucial for transmitting information from the spinal cord to the brain, was also shown to express NPFFR2 (Higo et al., 2021). Moreover, NPFFR2 is also highly expressed in the spinal cord. Lower expression levels of NPFFR2 were identified in the AP, choroid plexus, hippocampus, or cerebral cortex (Bonini et al., 2000; Higo et al., 2021; Parker et al., 2000). Even though rodents NPFFR2 mRNA is mostly expressed in the CNS, higher levels of NPFFR2 expression were also discovered in the heart and pituitary gland. Lower expression was then found in lungs, testes, salivary gland urinary bladder, stomach or adipose tissue (Bonini et al., 2000; Waqas et al., 2017).

NPFFR2 mRNA expression in the human CNS was found to be high in the amygdala and lesser levels in the hippocampus, hypothalamus, medulla oblongata, and the part of the limbic system cingulate gyrus (Bonini et al., 2000; Elshourbagy et al., 2000). The immunostaining of the human hypothalamus displayed neurons expressing NPFFR2 in clusters in DMN and VMN (Goncharuk and Jhamandas, 2008). In the human periphery, low expression of NPFFR2 was observed in the lung, adipose tissue, liver, kidney, spleen, pituitary gland and pancreas (Bonini et al., 2000; Elshourbagy et al., 2000; Parker et al., 2000). The placenta, on the other hand, exhibited the highest expression level (Bonini et al., 2000; Elshourbagy et al., 2000).

1.3.3 Physiological Properties of NPFF

NPFF is believed to be involved in the pain regulation, the development of tolerance to opioid drugs, as well as other physiological functions. As indicated earlier, NPFF was discovered by Yang et al. to have antinociception-modulating properties after it was centrally co-administered with morphine (Yang et al., 1985).

1.3.3.1 NPFF in Modulation of Nociception and Cardiovascular Regulation

The intracerebroventricular (i.c.v.) administration of antibodies against NPFF and NPAF increased latency to pain stimuli and enhanced the pain-relieving effects of morphine (Kavaliers and Yang, 1989). Additionally, intrathecal administration of NPFF or stable analog of NPFF 1DMe into spinal canal showed dose-related anti-nociceptive effects induced by morphine or [D-Ala^2]deltorphin I (agonist of the δ-opioid receptor, DOR) without signs of motor impairment (Gouarderes et al., 1993; Gouarderes et al., 1996). Moreover, naloxone, which has the ability to counteract opioid effects, was able to partially but significantly block the antinociception of NPFF (Gouarderes et al., 1993; Kavaliers and Yang, 1989).

Even though these studies show that NPFF has a pro-opioid effect, a few other investigations have found the opposite. Hyperalgic properties were observed after i.c.v. co-administration of morphine and NPFF or 1DMe into the mouse brain (Gicquel et al., 1992). Study by Desprat and Zajac indicated that NPFF and 1DMe is able to reverse opioid analgesia induced by μ-receptors (MOR) (Desprat and Zajac, 1997). Deletion of genes coding proteins for μ-δ-κ-opioid (MOR, DOR, KOR) receptors resulted in significant changes in NPFF receptors density which suggested a connection between the opioid and NPFF systems (Gouarderes et al., 2004).

Transgenic mice over-expressing NPFFR2 used in the study by Lin et al. displayed reduced nociceptive response compared to their wild-type (WT) littermates and no difference was observed after injection of morphine (Lin et al., 2016a). On the other hand, in the different study mice over-expressing NPFFR2 showed increased neural activity in the brain after hind paw electric pain stimuli (Lin et al., 2017a).

NPFF system was also found to regulate cardiovascular actions. Previous studies showed that intravenous administration of NPFF into rats caused an increase in blood pressure and heart rate (Allard et al., 1995; Prokai et al., 2006). The same effect was observed after i.c.v. administration of NPFF, but only in high doses (Jhamandas and Mactavish, 2002). Moreover, the antagonist of the α1-adrenergic receptor was found to

diminish this effect of NPFF. Interestingly, no altering of the amount of noradrenaline and adrenaline in the blood was observed (Allard et al., 1995). Furthermore, the injection of 1DMe into commissural NTS increased blood pressure and heart rate and inhibited components of the baroreceptor reflex (Laguzzi et al., 1996).

1.3.3.2 Role of NPFF in the Control of Energy Homeostasis and Food Intake

Due to the localization of NPFF and its receptors in the hypothalamus, it is likely that NPFF directly affects the hypothalamic neurons that regulate appetite and energy metabolism. Multiple studies previously showed anorexigenic effect of NPFF after i.c.v administration in rats (Murase et al., 1996; Sunter et al., 2001), and chicks (Cline et al., 2007). Additionally, decreased food intake was also observed after i.c.v. administration of NPFF in GPR10 knock-out (KO) mice (Bechtold and Luckman, 2006). Moreover, central i.c.v administration of NPFF was observed to stimulate water intake in rats (Sunter et al., 2001). On the other hand, the infusion of NPFF into the parabrachial nucleus of the brainstem resulted in an increase of food intake, albeit only at higher doses (Nicklous and Simansky, 2003).

Npff was discovered to be expressed in the pancreas, as indicated earlier (Nieminen et al., 2000). The secretion of insulin from isolated rat's pancreas was found to be inhibited by NPFF and NPAF, suggesting endocrine actions of these peptides (Fehmann et al., 1990). NPFF and NPAF contain specific cleavage sites of insulin-degrading enzyme. Therefore, in the presence of insulin their degradation is attenuated, and *vice versa* (Waclawczyk et al., 2021). When mice were fed HFD they showed decreased *Npff* expression in the pancreas, but the expression in the hypothalamus was unchanged. Moreover, chronic intraperitoneal (i.p.) administration of NPFF increased adipose tissue insulin sensitivity together with glucose tolerance, but no changes in food consumption were observed (Waqas et al., 2017). Interestingly, NPFF deletion showed improvement of glucose tolerance in mice. In addition, in the subAP, NPFF-positive neurons were discovered to have high colocalization with insulin receptors and it is possible that they are able to directly accept peripheral input to control glucose and energy homeostasis (Zhang et al., 2022b).

NPFF signaling has been suggested to play role in the regulation of energy metabolism. NPFF-deficient mice fed standard diet (STD) showed increased energy expenditure in thermoneutral environment (at 28 $^{\circ}$C). Moreover, they displayed higher basal brown adipose tissue (BAT) thermogenic activity (Zhang et al., 2022a). Higher basal

thermogenic activity was previously showed also in NPFFR2 KO mice (Zhang et al., 2018). NPFFR2 was found to regulate the diet-induced adaptive thermogenesis through a pathway that is dependent on hypothalamic NPY which suggests that NPFFR2 may have a significant impact on energy balance and body weight regulation (Zhang et al., 2018). When NPFF KO and NPFFR2 KO mice fed HFD they revealed higher fat mass and lower lean mass comparing to WT mice in thermoneutral environment (Zhang et al., 2018; Zhang et al., 2022a). NPFFR2 KO female mice also showed significantly increased leptin levels when fed HFD comparing to their WT controls (Zhang et al., 2018).

NPFF KO male mice under negative energy balance conditions (24 hours fasting and subsequent 48 hours refeeding) showed a significantly decreased respiratory exchange quotient during the last 6 h of fasting (which indicates a higher usage of lipids) and subsequent significant increase during refeeding (which indicates a higher usage of carbohydrates) comparing to WT controls. Moreover, *Npff* expression was found to be increased after fasting. These findings imply that NPFF signaling is up-regulated in energy deficiency situations (Zhang et al., 2021).

1.3.3.3 Other Physiological Roles of NPFF

Since NPFF receptors are particularly abundant in the PVN it is possible that the NPFF system has a role in the regulation of the hypothalamic-pituitary-adrenal (HPA) axis, which is known to mediate physiological stress responses, but is also able to regulate food intake, immune system, cardiovascular system, and reproductive systems (Lin and Chen, 2019). The HPA axis is regulated by the effects of GABA and previously it was shown that NPFF is able to disinhibit the activity of GABAergic neurons in the PVN (Jhamandas et al., 2007).

In reaction to changes in blood pressure, blood volume, and osmolarity, the hormones vasopressin and oxytocin are released. According to a prior study the i.c.v. administration of NPFF resulted in increased activation of vasopressin, oxytocin, tyrosine hydroxylase (TH), and corticotropin-releasing factor (CRF) synthesizing neurons (Jhamandas and MacTavish, 2003). Moreover, vasopressin released in response to hyperosmolarity was found to be reduced after i.c.v. administration of NPFF in rats (Arima et al., 1996).

Previous research has indicated that the NPFF system may have an impact on the depressive and anxiety-like behaviors. NPFF-deficient mice of both sexes reduced anxiety-like behavior and increased exploration in behavioral experiments and no changes

in corticosterone levels were observed (Zhang et al., 2021). On the other hand, non-peptidic agonist of NPFFR2 AC-263093 was shown to increase corticosterone levels in serum after i.p. administration in mice (Lin et al., 2017b). Furthermore, mice that over-expressed NPFFR2 not only had higher corticosterone levels but also showed apparent depression-like or anxiety-like behavior in the elevated plus maze test. Interestingly, mice over-expressing NPFFR2 showed decreased neural stem cells neurogenesis in the hippocampal dentate gyrus, which was likely caused by dysregulation of the HPA axis induced by chronic stress (Lin et al., 2016b). NPFFR2 KO mice displayed decreased behavioral responses and reduced anxiety-like behaviors compared to WT mice after exposure to a single prolonged stress caused by a forced swimming test (Lin et al., 2020).

1.4 Prolactin-Releasing Peptide

PrRP was discovered in 1998 as a hormone potentially stimulating prolactin release in mammals from anterior pituitary cells (Hinuma et al., 1998). However, the role of PrRP in the physiological regulation of prolactin secretion has been questioned and it was later discovered that i.c.v administration of PrRP reduces food intake and increases energy expenditure in rodents (Lawrence et al., 2000; Lawrence et al., 2002). PrRP has been identified as ligand to the orphan hGR3 receptor, later referred to as GPR10 receptor (Hinuma et al., 1998). Later it was discovered that PrRP has a high binding affinity also towards the NPFFR2 (Engstrom et al., 2003; Maletinska et al., 2015).

The prepropeptide of PrRP has two cleavage sites from which two peptides, PrRP31 and PrRP20 (Table 1), with identical C-terminal sequences, are produced. These peptides include either 31 (PrRP31) or 20 (PrRP20) amino acids with highly conserved amino acid structure. In mammals, rat and mouse, PrRP are identical and show high homology to human PrRP (Table 1) (Hinuma et al., 1998).

1.4.1 Expression of PrRP in the Brain and Periphery

Localization of PrRP-synthesizing neurons in the rat brain was previously determined using *in situ* hybridization and immunocytochemistry. PrRP mRNA signals were detected in neurons, the NTS, thalamus, caudal medulla oblongata, and in the hypothalamus in caudal portion of the DMH, VMN nuclei, medial preoptic area, PVN, or periventricular hypothalamic nucleus (PerVN). The strongest signal in the CNS was observed in the NTS (Iijima et al., 1999; Minami et al., 1999; Yano et al., 2001). Moreover, immunohistochemistry staining showed PrRP-positive neurons in close contact with CSF in the ependymal zone of the lateral ventricle and ependymal 3V of the hypothalamus.

Therefore, PrRP might act through the hypothalamus/portal vessel/pituitary axis suggesting its neuromodulatory function (Hinuma et al., 1998; Iijima et al., 1999). When mice were fed HFD, there was a significant increase in PrRP expression observed in the NTS region, but it was not affected in the hypothalamus. Conversely, PrRP expression was lower in leptin-deficient, or fasted mice (Zhang et al., 2018).

PrRP has been also detected in adrenal glands and plasma in the rat (Matsumoto et al., 1999) and it was reported that PrRP plays role in stress responses as a mediator of the HPA axis (Maruyama et al., 2001). Moreover, PrRP was also found in the human placenta and in the lining of the uterus in decidua (Lin, 2008). In addition, PrRP was also discovered in the spinal cord, lungs, thyroid gland, digestive system, pancreas and testis in the rat (Fujii et al., 1999).

1.4.2 Discovery and Distribution of Receptor GPR10

The rat orphan receptor UHR-1 (Unknown Hypothalamic Receptor) was originally isolated from hypothalamus in 1995 (Welch et al., 1995). In the same year, the receptor was first mentioned as the human GPR10 receptor in a study by Marchese *et al*. (Marchese et al., 1995). The sequence of the human GPR10 receptor is 369 amino acids long and the gene is located on chromosome 10 (locus10q26.13). Moreover human, rat and mouse GPR10 share over 90% sequence identity (Gu et al., 2004; Marchese et al., 1995).

GPR10 displays a low level of sequence homology with other known GPCRs. The GPR10 was found to be closely related to neuropeptide Y receptors family. It shares 31% overall amino acid sequence identity with neuropeptide Y1 receptor and 46% identity in transmembrane domains (Marchese et al., 1995).

The mRNA of receptor GPR10 is widely distributed throughout the brain. The highest mRNA levels of GPR10 were detected in several parts of the rat brain, mainly in the reticular nucleus of the thalamus, PVN, PerVN and DMN, NTS and in the medulla oblongata. A moderate expression levels of GPR10 were detected in the anterior pituitary and VMN. In the periphery, the GPR10 receptor was found in the adrenal gland, femur and stomach (Fujii et al., 1999; Ibata et al., 2000; Roland et al., 1999).

1.4.3 Physiological Properties of PrRP

As previously mentioned, PrRP was identified and named as a result of its ability to stimulate prolactin secretion in adenohypophysis cells RC-4B/C (Hinuma et al., 1998). Despite the fact that a later study showed PrRP's ability to stimulate prolactin *in vivo*, Spuch *et al*. confirmed that it is not a typical hypothalamic factor releasing prolactin

(Spuch et al., 2007). This was also supported by findings that PrRP is not present in the hypothalamic ME (Iijima et al., 1999). Therefore, PrRP's ability in relation to prolactin secretion was controversial. Other studies did not observe any effect of PrRP on prolactin release and concluded that it is not factor controlling prolactin release from the pituitary (Samson et al., 2003; Seal et al., 2000).

1.4.3.1 PrRP in the Regulation of Food Intake

PrRP's role in the release of prolactin during lactation was investigated by Lawrence *et al*. in fasting and lactating female rats. They observed significantly reduced PrRP neurons in DMN and NTS in fasted and lactated rats which led them to suggestion that PrRP neuron population is involved in energy homeostasis regulation and questioned importance of PrRP in the release of prolactin during lactation (Lawrence et al., 2000). I.c.v administration of PrRP in male rats caused decreased food intake which subsequently led to reduction in body weight gain (Lawrence et al., 2000; Lawrence et al., 2002). Moreover, a later study showed immediate early gene c-Fos neuronal activation in areas associated with feeding behavior after i.c.v administration of PrRP in male mice (Bechtold and Luckman, 2006).

The activation of PrRP neurons in the NTS and ventrolateral medulla oblongata through i.p. injection of CCK indicates that the PrRP neurons may mediate the central effects of CCK on satiety (Lawrence et al., 2002). Moreover, no effect on food intake was observed after subcutaneous (s.c.) administration of CCK into GPR10 KO mice. Therefore, the PrRP receptor possibly plays an important role in mediating the anorexigenic effects of CCK (Bechtold and Luckman, 2006). In addition, higher food consumption of PrRP KO mice was caused by eating bigger meal sizes rather than meal frequency. Similar findings were observed also in CCK_A receptor KO mice (Bi et al., 2004). On the other hand, another study of Ellacott *et al.*, suggested interaction between PrRP and anorexigenic peptide leptin. Coadministration of these two peptides led to an additive effect of PrRP in the reduction of food intake, body weight, and increased energy expenditure compared to peptides administered alone. Moreover, the leptin receptor was found to be colocalized in DMH, NTS or VLM with neurons expressing PrRP (Ellacott et al., 2002). It is clear, that both anorexigenic peptides CCK and leptin cooperate with PrRP in regulating food intake. In contrast to leptin, repeated injection of PrRP was found to affect energy homeostasis on a short-term level similarly to CCK (Ellacott et al., 2003).

1.4.3.2 The Regulation of Food Intake in GPR10- and PrRP-Deficient Mice

As described above, PrRP and its receptor GPR10 were found in multiple hypothalamic nuclei and in the brainstem, indicating their involvement in the regulation of body weight and food intake (Prazienkova et al., 2019; Roland et al., 1999).

PrRP KO mice showed significantly higher food intake than WT mice, more body fat, reduced glucose tolerance and increased insulin resistance (Takayanagi et al., 2008). Although i.c.v. administration of PrRP was found to increase body temperature, deficiency of PrRP did not affect energy expenditure (Ellacott et al., 2002; Takayanagi et al., 2008). These findings imply that hyperphagia, rather than a decrease in energy expenditure, was fundamental for the obesity driven by PrRP-deficiency (Takayanagi et al., 2008).

Our previous study with GPR10 KO mice revealed significantly increased food intake of GPR10-deficient male and female mice especially when fed HFD (Prazienkova et al., 2021). Moreover, multiple studies demonstrated increased body weight in older age of GPR10 KO mice compared to their WT controls (Bjursell et al., 2007; Gu et al., 2004; Prazienkova et al., 2021). Interestingly, when GPR10 KO mice were fed HFD, no difference in body weight compared to HFD-fed WT control mice was observed (Prazienkova et al., 2021). GPR10 KO mice revealed elevated insulin levels and impaired glucose tolerance. In addition, GPR10 KO mice showed significantly elevated plasma leptin followed by increased adipose tissue and liver weight with higher fat accumulation in the liver (Gu et al., 2004; Prazienkova et al., 2021). GPR10 KO mice also displayed elevated cholesterol, low density lipoprotein (LDL), and high density lipoprotein (HDL) levels, and liver fat accumulation subsequently caused severe hepatic steatosis (Bjursell et al., 2007). Study by Prazienkova *et al.* showed that GPR10 receptor deletion led to changes in the expression of genes involved in the regulation of lipid metabolism (Prazienkova et al., 2021). Moreover, the energy expenditure (Bjursell et al., 2007) and respiratory quotient (Prazienkova et al., 2021) were dramatically decreased in GPR10 KO female mice but not males. These results show importance of GPR10 receptor signaling in maintaining glucose and lipid homeostasis.

Study by Bechtold and Luckman showed that centrally administered PrRP into GPR10-deficient mice had no anorexigenic effect (Bechtold and Luckman, 2006). Additionally, PrRP given centrally to rats with mutant GPR10 was also ineffective to decrease food intake (Watanabe et al., 2005). This indicates that PrRP requires GPR10 to its acute anorexigenic effect.

1.4.3.3 Other Physiological Functions of PrRP

Another study confirming that PrRP i.c.v. administration has no effect on prolactin release also displayed that, PrRP caused an increase of luteinizing hormone (LH), and follicle-stimulating hormone (FSH), followed by the rise of testosterone in the plasma of male Wistar rats. Moreover, stimulation of rat hypothalamic explants *in vitro* with PrRP showed increase of galanin and vasoactive intestinal peptide. This work proposed that PrRP plays a role in control of the hypothalamic-pituitary-gonadal axis (Seal et al., 2000).

Moreover, Samson *et al.* suggested PrRP is important for the stimulation of corticotropin-releasing hormone (CRH) release into the area of hypophyseal portal vessels in the ME after they observed a significant increase in CRH levels in serum after administration of PrRP31 into the ventricular cavity of male rats (Samson et al., 2003). In addition, another study found that i.c.v. administration of PrRP31 (10 nmol) led to an increase in adrenocorticotrophic hormone (ACTH) level in plasma, which was mediated by elevated CRH. This finding was also supported by immunohistochemical staining of c-Fos induced by i.c.v. injection of PrRP31 which showed direct contact of PrRP neurons with CRH-expressing neurons in the PVN (Matsumoto et al., 2000). Even though, i.c.v. administration either low concentration (1 nmol) of PrRP or noradrenalin did not increase ACTH plasma levels, coadministration of PrRP (1 nmol) with noradrenalin caused induction of plasma ACTH elevation. Together, these results show a synergistic effect of noradrenalin and PrRP on the HPA axis and suggest that PrRP is a stress mediator (Maruyama et al., 2001; Matsumoto et al., 2000).

It has been previously proposed that PrRP may function as a co-transmitter or a neuromodulator in the medullary noradrenergic neurons because PrRP-positive neurons were found to be expressed together with TH-positive neurons in the caudal A1 and A2 regions of the brainstem (Maruyama et al., 2001; Uchida et al., 2010). Moreover, co-administration of PrRP with noradrenalin caused an immediate synergistic effect in the increase of vasopressin, which was not observed when PrRP or noradrenalin was injected separately. Therefore, PrRP could have a function in the release of vasopressin, which is induced by noradrenalin (Uchida et al., 2010).

Under chronic stress, the HPA axis is known to induce an increase in food intake which can lead to obesity. Using PrRP KO mice Mochiduki *et al.* confirmed the role of PrRP in the response to stressful stimuli and hypothesized that PrRP might control glucose metabolism via corticosterone secretion or the adrenal glands' production of catecholamines. PrRP KO mice not only displayed increased body weight when fed a STD

or HFD and elevated corticosterone secretion and catecholamine content after stress exposure (Mochiduki et al., 2010).

The presence of PrRP in brainstem and noradrenergic neurons of the caudal medulla led to the hypothesis that PrRP affects the cardiovascular system. Later, it was discovered that central PrRP administration increased arterial blood pressure in rats (Samson et al., 2000; Yamada et al., 2009). The study of Yamada et al. suggested that regulation of the cardiovascular system after PrRP administration could act through CRH in the PVN via the sympathetic nervous system (Yamada et al., 2009). According to a different study, i.c.v coadministration of PrRP with an antagonist of the NPFF receptors reduces the impact of PrRP on blood pressure increase. Moreover, PrRP was found to increase blood pressure in OLETF (Otsuka Long-Evans Tokushima Fatty) rat strain, which lacks functional GRP10 receptor. Therefore, PrRP's responses to cardiovascular system appear to be mediated via NPFF receptors. It was shown that PrRP significantly increased blood pressure in rats and this increase was blocked by an antagonist of NPFF receptors, RF9 (Ma et al., 2009). These findings show that PrRP's cardiovascular effects were exhibited through NPFFR2 due to its increased activity and binding affinity for NPFFR2 (Engstrom et al., 2003).

1.4.4 Structure-Activity Relationship Studies

Peptides are generally defined as physiologically active compounds that play a significant role in the control of physiological processes and have great potential in the treatment of a wide range of diseases. Unfortunately, the obstacle to their use is insufficient availability and low stability under physiological conditions. Therefore, peptide modification is an important strategy for improving availability or stability.

In order to find the bioactive part of PrRP and improve stability of PrRP many studies were performed (Boyle et al., 2005; Deluca et al., 2013; Maixnerova et al., 2011; Maletinska et al., 2011; Roland et al., 1999). The last seven amino acids at the C-terminal end are essential for PrRP peptide biological function. On the other hand, the Arg amino acids at positions 23 and 26 may be replaced without dramatically diminishing the affinity towards GPR10 (Boyle et al., 2005). A different study showed that the last 13 amino acids of PrRP20 at C-terminal part are the last amino acids that can still form a geometrical α-helix character. Losing this helical structure leads to a decrease in biological activity of the peptide (Deluca et al., 2013). Our previous *in vivo* study demonstrated that PrRP20

and PrRP31, but not PrRP13 (Fig. 2), exhibit anorexigenic effects following i.c.v. administration to fasting mice (Maixnerova et al., 2011).

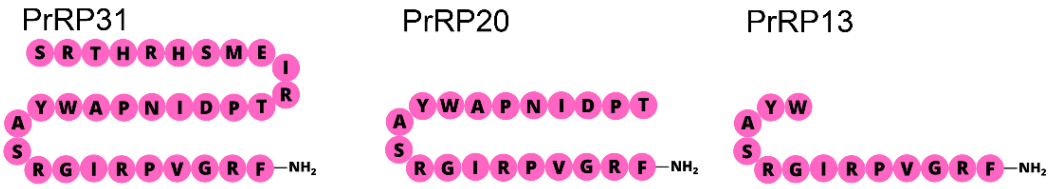

Fig. 2: Structure of human PrRP31, PrRP20, and PrRP13.

It was found that the ability of the peptide to bind to its receptor was completely lost when the PrRP-(1-31) C-terminal amide was changed to an carboxyl (Roland et al., 1999). The C-terminal Phe^{31}-NH_2 is crucial in providing a backbone and blocking the hydrophobic side chain in the L-configuration. Phe has a hydrophobic side chain, which helps to block water molecules from interacting with the peptide chain. It is important in maintaining the stability of the peptide (Boyle et al., 2005). Previously we made changes aiming to design a stable analog of PrRP20 with high anorexigenic potency (Maletinska et al., 2011). Therefore, (3,4-dichloro)phenylalanine ($PheCl_2$), (4-nitro)phenylalanine ($PheNO_2$), pentafluoro-phenylalanine ($PheF_5$), napthylalanine (1-Nal, 2-Nal), tyrosine (Tyr), cyclohexylalanine (Cha), or phenylglycine (Phg), were used to replace aromatic amino acid Phe^{31}. The binding affinity to GPR10 receptors were preserved except of analogs containing Cha^{31} and Phg^{31}. Moreover, after i.c.v administration, a stronger and longer-lasting anorexigenic effect compared to natural PrRP20 was observed for analogs [$PheNO_2^{31}$]PrRP20, [Tyr^{31}]PrRP20, [1-Nal^{31}]PrRP20, and [2-Nal^{31}]PrRP20 in fasting mice (Maletinska et al., 2011).

1.4.4.1 Lipidized PrRP Analogs

One of the strategies in designing new peptide analogs with improved availability, increased stability, and prolonged half-life in an organism, is lipidization (linking fatty acids to esters or amide bonds of peptides). Previously myristic and palmitic acids were added to Lys via an amide bond to insulin analog detemir (Havelund et al., 2004) or GLP-1 analog liraglutide (Gault et al., 2011), respectively.

Even though, centrally administered natural PrRP showed anorexigenic properties (Lawrence et al., 2002; Maletinska et al., 2011), no food intake lowering effect was observed after peripheral administration. The linear arrangement of the chain in this molecule makes it highly suitable for lipidization, and increasing the lipophilicity of PrRP facilitates its diffusion into the brain. By lipidization at Ser at position 1 or through linkers attached to Lys at positions 11 were designed new PrRP analogs (Fig. 3). All PrRP20 and

PrRP31 analogs lipidized with octanoic, decanoic, dodecanoic, myristic, palmitic, and stearic acid showed high binding affinity to receptor GPR10 and increased affinity towards NPFFR2 (Maletinska et al., 2015). Likewise, PrRP31 analogs myristoylated or palmitoylated on the N-terminus with replacement of aromatic amino acid Phe^{31} at the C-terminus with noncoded amino acids 1-Nal, $PheCl_2$, $PheNO_2$, $PheF_5$, or Tyr, also revealed high binding affinities to GPR10 (Prazienkova et al., 2016). However, only myristoylated PrRP20, and palmitoylated, or stearoylated PrRP31 analogs showed significant decrease in food intake in mice after acute peripheral administration (Maletinska et al., 2015; Prazienkova et al., 2017). Moreover, significant increase of c-Fos in the PVN, NTS, DMN, or ARC after acute s.c. administration of palm-PrRP31 or $palm^{11}$-PrRP31 was observed which confirm that lipidization of PrRP helps its central effect (Pirnik et al., 2015; Pirnik et al., 2018; Prazienkova et al., 2017).

Chronic studies with diet-induced obesity (DIO) mice treated with palm-PrRP31 (Fig. 3A) and $palm^{11}$-PrRP31 (Fig. 3B) for two weeks significantly decreased cumulative food intake and body weight which was followed by reduction of the fat mass and a decrease of plasma leptin levels (Maletinska et al., 2015; Prazienkova et al., 2017). Therefore, these two structures (Fig. 3) were used as lead structures in other studies (Korinkova et al., 2020; Mrazikova et al., 2021; Mrazikova et al., 2022; Pirnik et al., 2021).

Previously we showed that the combined treatment of leptin and $palm^{11}$-PrRP31 had a synergistic effect on reducing body weight and increased rectal temperature in mice with a recessive mutation in *ob* gene (*ob/ob*) which codes hormone leptin (Korinkova et al. 2020). Another our study using Zucker fatty (*fa/fa*) rats which are genetically predisposed to develop obesity due to a recessive mutation in the leptin receptor gene showed no significant changes in body weight or glucose tolerance after treatment with $palm^{11}$-PrRP31 (Mrazikova et al., 2022). These studies suggested that the action of $palm^{11}$-PrRP31 in regulating food intake and body weight is dependent on leptin signaling.

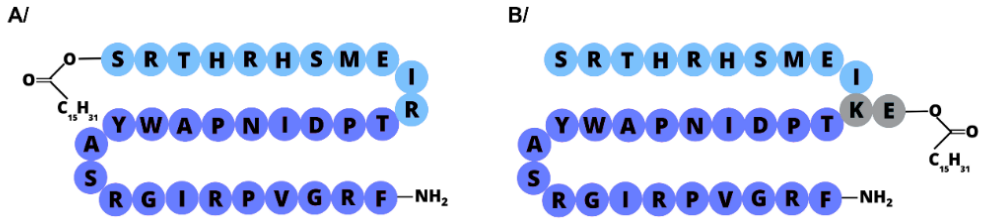

Fig. 3: Structure of lipidized analogs of PrRP31 with marked human PrRP31 (purple and blue) and PrRP20 (purple). Palm-PrRP31 palmitoylated at position 1 (A), and $palm^{11}$-PrRP31 palmitoylated at position 11 on lysine though γ-glutamic acid - E linker (B).

1.4.4.2 Intracellular Signaling Pathways of PrRP

As previously mentioned PrRP exerts strong dual-agonist activity towards GPR10 and NPFFR2 receptors (Alexopoulou et al., 2022; Engstrom et al., 2003), which was confirmed also by our studies (Maletinska et al., 2015; Prazienkova et al., 2017).

Incubation of GH3 cells with PrRP stimulated activation of the extracellular signal-regulated kinase (ERK). Even though GPR10 signaling was noted to be mediated through the Gi/o subunit. ERK could be activated either through Gi or Gq alpha subunits. The activation of ERK was almost completely prevented by preincubation with pertussis toxin (PTX), which inactivates the Gi and Go protein (Kimura et al., 2000). In contrast to this study, it was also reported that GPR10 signals through the Gq alpha subunit. PrRP stimulated Ca^{2+} release in HEK293 cells stably transfected with GPR10 and the release was found to be blocked by the inhibitor thapsigargin, which targets the Sarco/endoplasmic reticulum Ca^{2+} ATPase (Langmead et al., 2000). These results are in agreement with the study by Hinuma *et. al* who found PrRP causes partial inhibition of cyclic adenosine monophosphate (cAMP) production and triggers Ca^{2+} influx (Hinuma et al., 1998). Different studies also found PrRP to stimulate cAMP and suggested that GPR10 signals through Gs alpha subunit in PC12 cells (Nanmoku et al., 2003; Samson and Taylor, 2006). In this study, GPR10 signaling was further investigated.

PrRP was reported to activate in GH3 cells also another member of the mitogen-activated protein kinase (MAPK) family, c-Jun N-terminal protein kinase (JNK) (Kimura et al., 2000). Additionally, it was discovered that PrRP stimulation activated Akt in GH3 cells. This activation was entirely diminished by preincubation with the phosphoinositide 3-kinase (PI3K) inhibitor wortmannin which suggest activation of Akt via PI3K-dependent mechanism. Moreover, Hayakawa et. al proposed that Act activation was mediated by Gβγ subunits (Hayakawa et al., 2002). Our previous studies also reported PrRP ability to stimulate ERK phosphorylation in RC/4BC cells (Maixnerova et al., 2011) or CHO-K1 cells transfected with GPR10 (Maletinska et al., 2015) and activation of cAMP response element-binding protein (CREB) in RC/4BC (Maixnerova et al., 2011). The design of signal transduction through GPR10 is summarized in Fig.4.

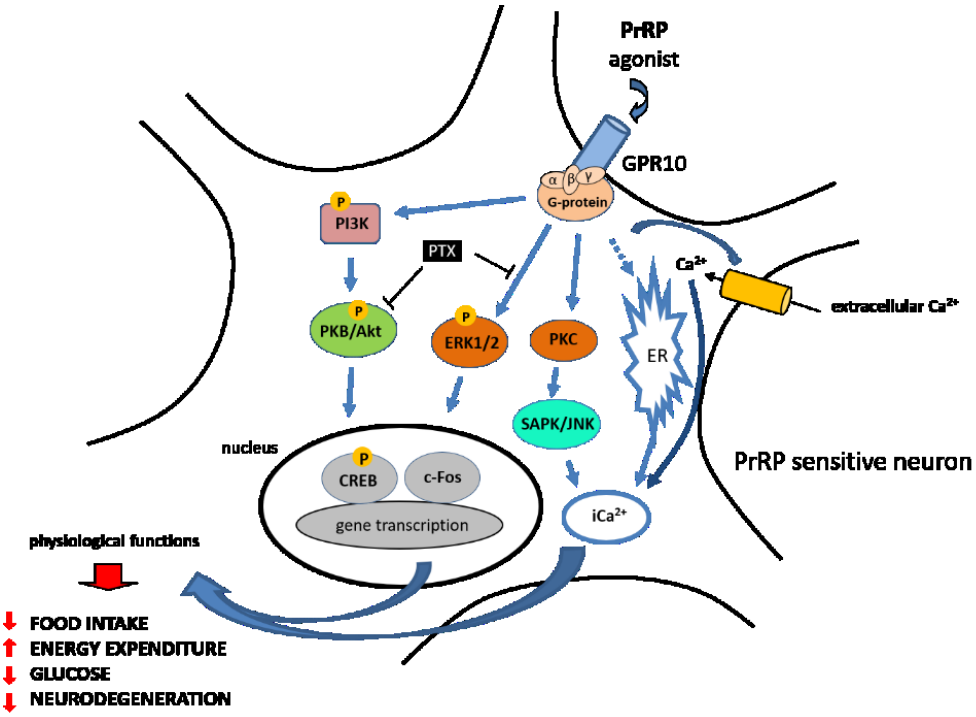

Figure 4: **Summary of transduction pathways of PrRP mediated through GPR10 receptor** (from (Prazienkova et al., 2019)).
ERK, extracellular signal-regulated protein kinase; JNK, c-Jun N-terminal protein kinase; CREB, cAMP response element-binding protein; Akt, protein kinase B; PTX, Pertussis toxin; PKA, protein kinase A; PKC, protein kinase C.

CHO-K1 cells with transfected NPFFR2 previously showed that PTX pretreatment completely abolished cAMP induced by forskolin after stimulation with NPFF (Kotani et al., 2001; Mollereau et al., 2002; Talmont et al., 2010). Moreover, no Ca^{2+} release was detected after incubation with NPFF (Kotani et al., 2001). These results clearly demonstrated that NPFFR2 signals through the Gi/o protein. On the other hand, transduction pathways mediated by NPFFR2 after stimulation with PrRP have not been characterized yet.

Previously, we demonstrated that palm^{11}-PrRP31 had an effect on both body weight and leptin levels in the blood, as well as on the insulin and leptin signaling pathways in the hypothalamus of DIO mice. This effect was observed after the mice were treated with palm^{11}-PrRP31 for either 28 days or 14 days followed by a switch to saline for another 14 days. Significant increase of total protein levels of the p85 regulatory subunit of PI3K as well as increased phosphorylation of Akt at Ser473 was observed after the treatment with palm^{11}-PrRP31. Treatment also caused increase of ERK phosphorylation and decrease of protein level of the suppressor of cytokine signaling 3 (SOCS3). Moreover, total protein levels of JNK and c-Jun were found to be increased after the treatment (Holubova et al., 2018).

2. AIMS OF THE THESIS

The first part of this thesis was dedicated to *in vitro* experiments where the goal was to specify the biological activity of lipidized PrRP31 analogs.

1. To compare the affinity of lipidized PrRP31 analogs and the natural PrRP31 peptide in cells transfected with GPR10 and NPFFR2.
2. To test and compare agonist properties of selected lipidized PrRP31 analogs at GPR10 or NPFFR2 receptors.
3. To test and compare signaling transduction pathways of natural PrRP31 and its selected lipidized PrRP31 analogs in cells expressing GPR10 and NPFFR2.
4. To test the affinity of natural PrRP31 and its selected lipidized PrRP31 analogs for potential off-target receptors in cells transfected with these receptors.

The second part of this thesis was dedicated to *in vivo* experiments.

1. Metabolic phenotyping of NPFFR2-deficient mice of both sexes fed either STD or HFD and comparing them to age-matched WT control mice.
2. Metabolic phenotyping of GPR10/NPFFR2-deficient mice of both sexes fed either STD or HFD and comparing them to age-matched WT control mice.

3. METHODS

3.1 Peptides Synthesis

All PrRP31 analogs (Fig. 5), NPFF, and 1DMe (Fig. 6), were synthesized at the IOCB, Prague, at the peptide synthesis department by Ing. Blechová, using the solid phase synthesis method according to previous studies (Maletínská et al., 2015). Lipidation was the last step of the synthesis. Peptide purification and identification were determined by analytical high-performance liquid chromatography and by using a Q-TOF (quadrupole-time of flight) micro MS (mass spectrometry) technique (Waters, MA, USA). And purity of the synthesized peptides was greater than 95%.

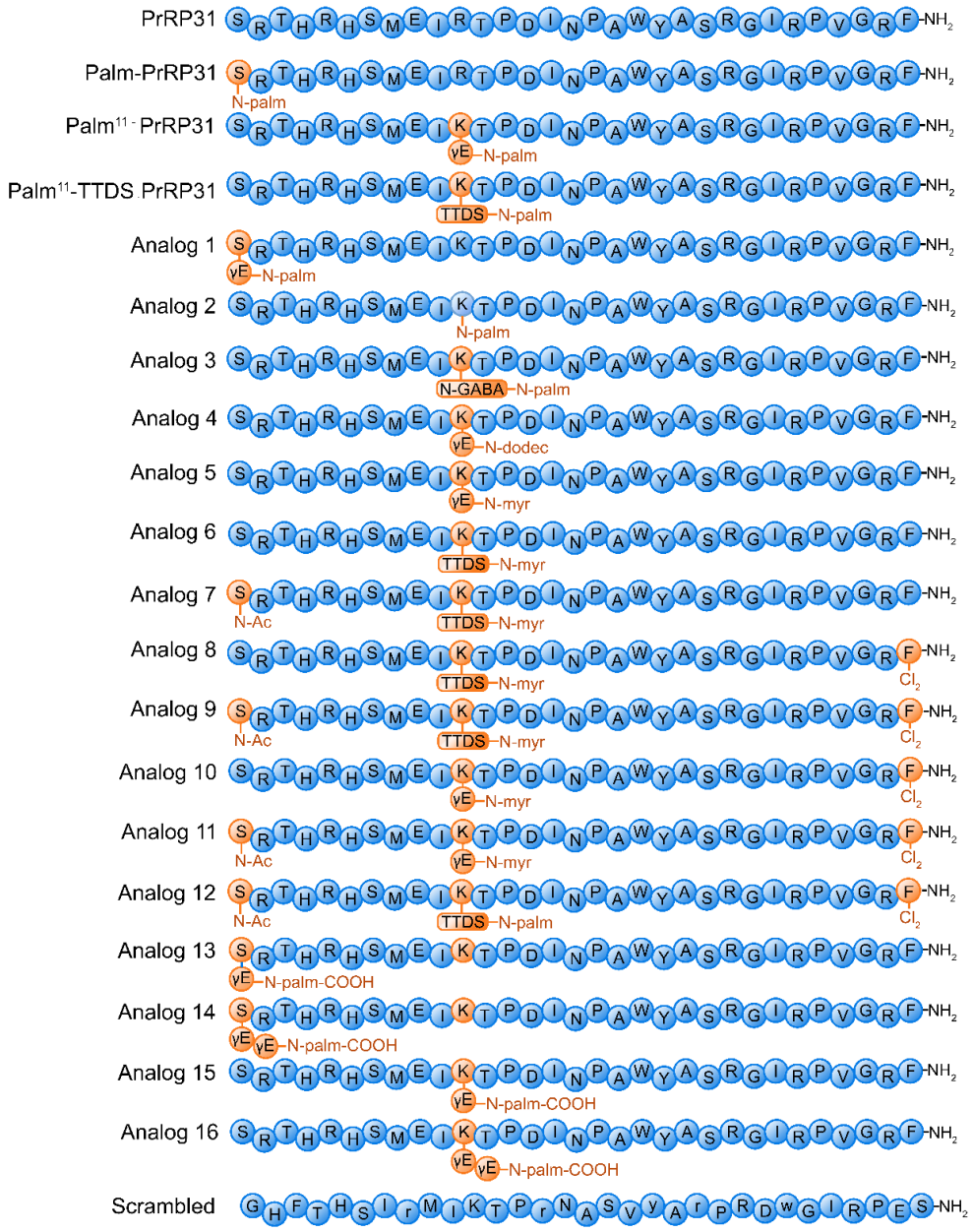

Figure 5: Overview of peptide sequences of tested PrRP31 peptide analogs.

palm: palmitoyl (C16), dodec: dodecanoyl (C12), myr: myristoyl (C14), palm-COOH: hexadecanedioic acid, γE: gamma-glutamic acid, TTDS: 1,13-diamino-4,7,10-trioxatridecan-succinamic acid, GABA: gamma-aminobutyric acid, N-Ac: N-acetylated at the N-terminus, $PheCl_2$: dichlorophenylalanine, scrambled peptide has randomly shuffled amino-acid sequence.

Human PYY (#SC319) was obtained from the PolyPeptide Group (Strasbourg, France). The selective KOR agonist (±)-trans-U-50488 methanesulfonate salt was purchased from Sigma-Aldrich (St. Louis, MO, USA) and [D-Pro10]-dynorphin A, which used as an agonist of KOR in binding experiments, was purchased from Phoenix Pharmaceuticals (Burlingame, CA, USA). All selective agonists of MOR DAMGO and agonist of the opioid receptor-like 1 (ORL-1) and DOR [D-Ala2]-deltorphin II were obtained from Tocris (Bristol, UK).

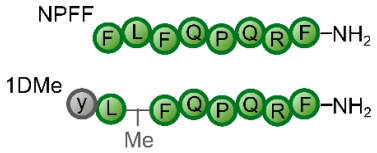

Figure 6: Overview peptide of sequences of human NPFF and 1DMe.
Me: methyl.

3.2 *In Vitro* Experiments

3.2.1 Cell Cultures

All cells (Table 2) were maintained at 37 °C in a humified incubator with 5% CO_2. Growth and assay media were prepared according to manufacturer protocols. Medium was changed every 2-3 days and cells were cultured as required.

Table 2: Tested cell lines with stably transfected receptors

Cell line	Receptor	Cat. Number	Brand
CHO-K1	GPR10	#K1732	Thermo Fisher Scientific Inc.
CHO-K1	NPFFR2	#ES-490-A	Perkin Elmer
CHO-K1	NPFFR1	#ES-491-C	Perkin Elmer
CHO-K1	KOR	#K1533	Thermo Fisher Scientific Inc.
U2OS	MOR	#K1523	Thermo Fisher Scientific Inc.
U2OS	DOR	#K1778	Thermo Fisher Scientific Inc.
U2OS	ORL-1	#K1786	Thermo Fisher Scientific Inc.
U2OS	Y1	#K1803	Thermo Fisher Scientific Inc.
U2OS	Y2	#K149	Thermo Fisher Scientific Inc.
U2OS	Y5	#K1782	Thermo Fisher Scientific Inc.
U2OS	GHSR	#K1819	Thermo Fisher Scientific Inc.

*Chinese hamster ovary cells (CHO-K1) and human bone osteosarcoma epithelial cells (U2OS).

3.2.2 Peptide Iodination

Competitive binding experiments were carried out using human PrRP31 and 1DMe iodinated by team of Ing. Aleš Marek Ph.D. at IOCB Prague with Na[^{125}I] purchased from

Izotop (Budapest, Hungary) using IODO-GEN (Pierce, Rockford, IL, USA) at Tyr20 and D-Tyr1, respectively, as described previously (Maletinska et al., 2012). Radioligands [^{125}I]-dynorphin A, [^{125}I]-PYY, and [^{125}I]-ghrelin were iodinated at Tyr1, Tyr20 (Tyr27), and His9, respectively. The identity of peptides was determined by a MALDI-TOF Reflex IV mass spectrometer (Bruker Daltonics, Billerica, MA, USA). The specific activity of all ^{125}I-labeled peptides was approximately 2100 Ci/mmol. The radiolabeled peptides were kept in aliquots at -20 °C and used within 1 month.

3.2.3 Cell Membrane Isolation

CHO-K1 cells expressing NPFFR2, NPFFR1 and KOR receptors were centrifuged and pellets collected and stored in -80°C. Pellets were homogenized using a DIAX 100 Homogenizer (Heidolph Instruments, Schwabach, DE) in ice-cold homogenizing buffer (20 mM HEPES pH 7.1, 5 mM $MgCl_2$, 0,7 mM bacitracin) and subsequently centrifuged in an ultracentrifuge (Beckman Coulter, Fullerton, CA, USA) at 26 000 x g for 15 minutes at 4°C. Supernatant was discarded and the previous steps were repeated 2 more times. Pellets were resuspended in ice-cold storage buffer (50 mM Tris-Cl pH 7.4, 0.5 mM EDTA, 10 mM $MgCl_2$, 10% sucrose), and concentration of isolated membrane proteins was determined by a Pierce™ BCA Protein Assay Kit (Pierce, Rock-ford, IL). Aliquots were stored at -80°C.

3.2.4 Saturation and Competitive Binding Experiments

CHO-K1 cell line transfected with GPR10 were seeded in polyethylenimine (PEI)-coated 24-well plates at a density of 30,000 cells/well. U2OS cells expressing Y1, Y2, Y5 or GHSR (ghrelin receptor; growth hormone secretagogue receptor) receptors were seeded in PEI precoated 24-well plates at a density 40,000 cells/well for NPY receptors and 20,000 cells/well for GHSR receptor. The cells were allowed to grow for 3 days. At the day of experiment cells were incubated for 60 minutes at room temperature (RT) with 200 ul binding buffer (Table 3). Competitive binding experiments with 25 µl 0.1 nM [^{125}I]-Peptide (Table 3) and 25 ul peptide or analog at final concentrations from 10^{-12} to 10^{-5} M and for saturation experiments with increasing concentration of [^{125}I]-peptide from 0.05 to 2 nM and nonlabled peptide at concentration 10^{-6} M. The cells were rinsed with wash buffer (20 mM Tris pH 7.4,118mM NaCl, 4.7 mM KCl, and 5 mM $MgCl_2$) and subsequently lysed in 0.1 M NaOH.

Cell membranes isolated from CHO-K1 cells overexpressing receptors NPFFR2, NPFFR1 and KOR were used at a concentration of 5 µg of protein/tube diluted with ice-

cold 200 ul/tube binding buffer. Diluted membranes were incubated for 60 minutes at RT; competitive binding experiments with 25 µl 0.1 nM [^{125}I]-Peptide (Table 3) and 25 µl peptide or analog at final concentrations from 10^{-12} to 10^{-5} M and for saturation experiments with increasing concentrations of radioligands in final concentrations of 0.05-2 nM just concentration 10^{-6} M. After incubation were tubes subsequently filtered in a Brandel cell harvester (Biochemical and Development Laboratories, Gaithersburg, MD, USA) using Whatman GF/B filters which were preincubated in 0.3% PEI in wash buffer (50 mM Tris pH 7.4 + 60 mM NaCl).

Radioactivity was determined by a γ-counter Wizard 1470 Automatic Gamma Counter (Perkin Elmer, Waltham, MA, USA). Experiments were carried out in duplicates at least three times.

Table 3: The binding buffers composition and radioligands used for individual transfected cell lines.

Receptor	[^{125}I]-Peptide	Binding buffer
GPR10	[^{125}I]-hPrRP31	25 mM HEPES pH 7.4, 120 mM NaCl, 10 mM $MgCl_2$, 1 mM $CaCl_2 \cdot 2H_2O$, 0.5% BSA, 2 g/l glucose
NPFFR1 NPFFR2	[^{125}I]-1DMe	50 mM Tris-HCl pH 7.4 + 60 mM NaCl + 1 mM $MgCl_2$ + 0.5% BSA
KOR	[^{125}I]-dynorphin A	50 mM Tris-HCl pH 7.4 + 60 mM NaCl + 1 mM $MgCl_2$ + 0.5% BSA
Y1, Y2 Y5	[^{125}I]-PYY	25 mM HEPES, 120 mM NaCl, 5 mM MgCl2, 4.7 mM KCl, 1 mM $CaCl_2$, 0.5% BSA, 2 g/l glucose
GHSR	[^{125}I]-ghrelin	50 mM Tris-Cl pH 7.4, 118 mM NaCl, 5 mM $MgCl_2$, 4.7 mM KCl, 0.1% BSA, 2 g/l glucose

3.2.5 Binding Experiments Evaluation

Both saturation and competitive binding experiments were performed according to the principles of Motulsky and Neubig (Motulsky and Neubig, 2002). The dissociation constant (K_d) values were determined using GraphPad Prism from saturation binding experiments along with the total number of receptors (B_{max}) [number of binding sites/cell (membrane)].

$$K_d = \frac{[\text{ligand}] \times [\text{receptor}]}{[\text{ligand-receptor}]}$$

The half-inhibitory concentration IC_{50} was determined from the competitive binding curves. Binding curves were evaluated with GraphPad Prism using a single binding site model and the non-linear regression method. The K_i was determined from the IC_{50} value using the Cheng and Prusoff equation (Cheng and Prusoff, 1973).

$$K_i = \frac{IC_{50}}{1 + \frac{[\text{radioligand}]}{Kd}}$$

3.2.6 Receptor Activation Determined by Beta-Lactamase-Dependent Fluorescence Resonance Energy Transfer (FRET) Assay

The agonist/antagonist properties of PrRP31 and lipidized PrRP31 analogs were studied using cell lines stably expressing receptors GPR10, Y5, GHSR, and opioid receptors and containing beta-lactamase reporter genes to monitor β-arrestin recruitment. Cells were seeded at 10 000 cells/well in a 384-well plate in assay medium, and the assay was performed according to Thermo Fisher's protocol. Receptor agonists were tested at final concentrations from 10^{-12} to 10^{-5} M. The concentration of the agonist in antagonist assay mode ranged from 10^{-12} to 10^{-5} M, and the potential antagonists PrRP31 and palm^{11}-PrRP31 were tested at final concentrations from 10^{-7} or 10^{-6} to 10^{-5} M. Fluorescence was detected at 409 nm excitation wavelength and 460 and 530 nm emissions wavelengths using the FlexStation 3 fluorescent plate reader (Molecular Devices, Sunnyvale, CA, USA).

Data were evaluated using GraphPad Prism software (San Diego, CA, USA). 50% maximal effect (EC_{50}) values were determined by non-linear regression as the log agonist versus response. Data are representative of at least two experiments, each performed in duplicate.

3.2.7 Receptor Activation Determined by Calcium Mobilization Assay

The intracellular Ca^{2+} level was measured using the AequoScreen CHO-K1 cell line expressing aequorin and NPFFR2 according to the Perkin Elmer's manufacturer protocol (Waltham, MA, USA). Cells were cultured in media without selective antibiotics till 80-90% confluence and were subsequently detached (PBS pH 7.4 + 0.5 mM EDTA) and subsequently centrifuged. Cells were resuspended in phenol red-free DMEM with 0.1% protease-free BSA and 5 μM coelenterazine h (Thermo Fisher Scientific Inc. Brand) and seeded at 50 000 cells/well in 96-well plates and incubated in the dark at RT with gentle agitation for 4 hours. Peptides were tested at concentrations from 10^{-12} to 10^{-5} M. Luminescent light emission was recorded using a FlexStation 3 plate reader (Molecular Devices).

Data were analyzed by nonlinear regression as log agonist versus response using GraphPad software. Data are representative of at least three experiments, each performed in duplicate.

3.2.8 Cell Signaling in the CHO-K1 Cells with GPR10, NPFFR1 and NPFFR2

Activation of signaling pathways was studied in the CHO-K1 cell lines expressing GPR10, NPFFR2 and NPFFR1. Seeded cells were incubated with PrRP31, lipidized PrRP31 analogs, NPFF or 1DMe at final concentration 10^{-6} M for 5 minutes or 60 minutes at 37°C and subsequently washed with ice-cold phosphate-buffered saline (PBS) pH 7.4. In experiments with inhibitor PTX was PTX added 16 hours before stimulation with peptide into cells in final concentrations of 10^{-7} M. Cells were lysed with Laemmli sample buffer (62.5 mM Tris-HCl at pH 6.8, 2% SDS, 10% glycerol, 0.01% bromophenol blue, 5% β-mercaptoethanol, 50 mM NaF, and 1 mM Na_3VO_4).

Electrophoresis and immunoblotting were performed as described previously (Spolcova et al., 2015). Nitrocellulose membranes were blocked in 5% nonfat dried milk dissolved in TBS/Tween-20 buffer (20 mM Tris, 136 mM NaCl, 0.1% Tween-20) for 1 h and incubated overnight in primary antibody at 4°C. List of primary monoclonal antibodies used for detection of cell signaling pathways purchased from Cell Signaling Technology (Danvers, MA, USA) is in the Table 4. Using ChemiDoc™ system Chemiluminescence was detected, and bands were subsequently quantified using Image Lab Software. Both were obtained from Bio-Rad (Hercules, CA, USA). The protein level was normalized to the loading control protein, glyceraldehyde-3-phosphate dehydrogenase (GAPDH).

The obtained data from cell signaling were statistically processed using the GraphPad Prism program (GraphPad Software, Inc., San Diego, CA, USA) and are presented as the mean ± SEM, and statistics were performed by One-Way analysis of variance (ANOVA). Differences were considered statistically significant when $p < 0.05$.

Table 4: Primary antibodies used for cell immunoblotting and their dilutions.

Antibody against	Cat. number	Source	Dilution
Phospho-Akt (Thr308)	#2965	Rabbit	1:1000, 5% BSA, TBS/T-20
Phospho-Akt (Ser473)	#4060	Rabbit	1:1000, 5% BSA, TBS/T-20
Akt	#4691S	Rabbit	1:1000, 5% BSA, TBS/T-20
Phospho-CREB (Ser133)	#9196	Mouse	1:1000, 5% BSA, TBS/T-20
CREB	#9104S	Mouse	1:1000, 5% milk, TBS/T-20
Phospho-p44/42 MAPK (Erk1/2) (Thr202/Tyr204)	#4370S	Rabbit	1:2000, 5% BSA, TBS/T-20
p44/42 MAPK (Erk1/2)	#9107S	Mouse	1:2000, 5% milk, TBS/T-20
Phospho-SAPK/JNK (Thr183/Tyr185)	#4668	Rabbit	1:1000, 5% BSA, TBS/T-20
SAPK/JNK	#9252	Rabbit	1:1000, 5% BSA, TBS/T-20
Phospho-p38 MAPK (Thr180/Tyr182)	#4511	Rabbit	1:1000, 5% BSA, TBS/T-20
p38 MAPK	#9212	Rabbit	1:1000, 5% BSA, TBS/T-20
Phospho-PKA C (Thr197)	#5661	Rabbit	1:1000, 5% BSA, TBS/T-20
c-Fos	#2250	Rabbit	1:1000, 5% BSA, TBS/T-20
c-Jun	#9165	Rabbit	1:1000, 5% BSA, TBS/T-20
GAPDH	#97166	Mouse	1:1000, 5% milk, TBS/T-20

3.3 *In Vivo* Experiments

3.3.1 Experimental Animals

All animal experiments followed the ethical guidelines of the EU (86/609/EU) for work with animals, and the Act of the Czech Republic law 246/1992, and were approved by the Committee for Experiments with Laboratory Animals of the CAS.

The animals were housed in the animal facility under standard conditions (12/12 light-dark cycle, temperature 22 ± 2°C). Mice had free access to water and either STD (Ssniff R/M-H diet; 8% kcal from fat, 21% kcal from protein, 71% kcal from carbohydrate; Ssniff Spezialdieten GmbH, Soest, Germany) or HFD (60% kcal from fats, 13% kcal from proteins and 27% kcal).

3.3.2 Acute Food Intake After Administration of PrRP31 Analogs

Up until the age of twelve to fourteen weeks, Charles River Laboratories (Sulzfeld, Germany) male C57BL/6J mice (n = 5–6) were used to study acute food intake. The day before the experiment, the mice were fasted overnight (16 h). PrRP31 analogs were dissolved in saline to a final dose of 5 mg/kg were dissolved in saline. Saline, which was used as a control, or PrRP31 analogs were administered s. c. and fifteen minutes after the injection, the mice were given a weighed pellet. Subsequently was monitored food intake and the maximal effect was observed 45 minutes after the injection.

Two-way ANOVA followed by Dunnett's post-hoc test was used to analyze acute food intake in fasted mice. Differences were statistically significant when $p < 0.05$.

3.3.3 Effects of Chronic Administration of Lipidized PrRP Analogs

C57BL/6J mice were fed from 4 weeks of age with HFD and given water *ad libitum* for 16 weeks. At the age of 20 weeks and the mice were divided into groups of 10 animals and placed into the separate cages.

Groups were injected s.c. either with saline, palm^{11}-PrRP31 or with analog 12 dissolved in saline at a dose of 5 mg/kg twice a day for 21 days and body weights of the mice were monitored. At the end of the experiment, overnight-fasted mice were sacrificed by decapitation and the gonadal white adipose tissue (gWAT) and subcutaneous white adipose tissue (scWAT) was dissected and weighed.

Body, gWAT, and scWAT weights in DIO mice were evaluated by one-way ANOVA followed by Bonfferoni's post-hoc test and differences were statistically significant when $p < 0.05$.

3.3.4 NPFFR2 KO Characterization Study

Mice with a genetic change that eliminates the functional *Npffr2* gene were created using the CRISPR genome-editing system. The CRISPOR online design tool was used to create specific guide RNAs (gRNAs) that recognize exon 2 of the *Npffr2* gene (5′-CCAGTAAATCACTTATGGCA -3′ and 5′-ATGAAGACAGCTGCCACTTG -3′). For the zygote, electroporation was used spCas9 protein (500 ng/µl) and gRNAs (50 ng/µl each) according to a protocol previously described in (Jenickova et al., 2021).

NPFFR2 KO mice were exposed to an STD or an HFD starting at the age of 9 weeks. Food intake and body weight were monitored weekly. Behavioral experiments (described in the chapter 3.3.6) and oral glucose tolerance test (OGTT) (described in the chapter 3.3.7) were performed at the age of 24 weeks, and fasted blood from the tail was taken before the OGTT was performed. At the end of the experiment at 26 weeks of age, blood of mice in a randomly fed state was collected for plasma leptin detection, and mice were subsequently perfused with heparinized saline (20 U/ml) under pentobarbital anesthesia and mice were subsequently dissected. For experimental design see the Fig. 7.

The liver, hypothalamus, brainstem, gWAT, and subcutaneous white adipose tissues were dissected and weighted and were subsequently frozen in liquid nitrogen and then stored at -80°C before morphometric and biochemical analyses, liver histology, immunoblotting, and mRNA analyses of tissues were performed.

Results were evaluated by one-way ANOVA followed by Bonfferoni post-hoc test and differences were considered to be statistically significant when $p < 0.05$.

Figure 7.: Experimental design of NPFFR2 KO characterization study

3.3.5 GPR10/NPFFR2 KO Characterization Study

C57BL/6J *Gpr10*$^{-/-}$ (Prazienkova et al., 2021) and C57BL/6n *Npffr2*$^{-/-}$ mice, described in previous chapter, were crossbred to generate double knock-out mice (dKO) of both sexes.

Mice were exposed to either STD or HFD beginning at 8 weeks of age (Fig.8). Their body weight and food intake were tracked weekly. At the age of 21 weeks and 24 weeks, behavioral experiments (described in the chapter 3.3.6) and OGTT (described in the chapter 3.3.7) were performed, respectively. Before the OGTT, fasted blood from the tail was taken. At the end of the experiment, at 25 weeks of age, blood of mice in a randomly fed state was collected for plasma leptin and ghrelin detection and the mice were subsequently euthanized under pentobarbital anesthesia and perfused with heparinized saline (20 U/ml). For experimental design see the Fig. 8.

The organs were dissected and weighted and subsequently frozen in liquid nitrogen and then stored at -80°C. Afterward, morphometric, biochemical analyses, liver histology, and immunoblotting were performed.

Results were evaluated by one-way ANOVA followed by Bonfferoni post-hoc test and differences were statistically significant when $p < 0.05$.

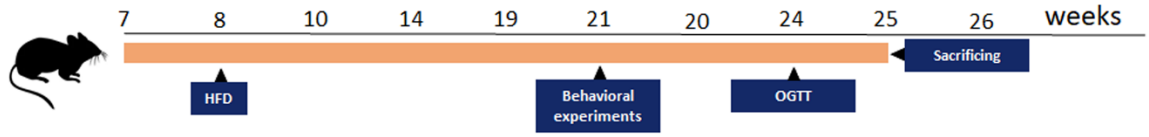

Figure 8.: Experimental design of GPR10/NPFFR2 KO characterization study

3.3.6 Behavioral and Nociception Experiments

Mice fed STD or HFD were put through behavioral experiments specifically, elevated plus maze (EPM) and open field (OF), to measure locomotor activity, curiosity about a new environment, and anxiety-like behavior at 24 and 21 weeks of age of NPFFR2 KO and dKO mice, respectively. Nociception (pain sensitivity) was determined by hot plate (HP) test. All results were analyzed using Graph Pad Prism 8 by one-way ANOVA

followed by Bonferroni post-hoc test and differences were statistically significant when $p < 0.05$.

OF test: The locomotor activity of each mouse was monitored for 10 minutes after they were deposited into the square arena (50x50 cm). To evaluate anxiety-like behavior and the mice's desire to explore open areas, we defined a central area square (25x25) and the duration and frequency of visits to the central area were monitored. EthoVision XT (Noldus, Wageningen, Netherlands) was used to evaluate the obtained record.

EPM test: Mice were positioned individually in the middle of the maze 50 cm above the ground with two arms open and two arms closed, and their activity was monitored for 10 minutes. After that, time spent in arms and the number of visits of open or closed arms were determined using EthoVision XT.

HP test: The HP apparatus (TSE Systems, Bad Homburg, Germany) with a 53°C setting was used to test the pain threshold to heat stimulation. The time between placing the animal on the hot plate surface and the onset of nociceptive behavior (front paw licking) was recorded.

3.3.7 Oral Glucose Tolerance Test

After 6 h of fasting, mice from NPFFR2 KO and dKO characterization experiments were submitted to an OGTT. Before gavage at time 0, blood was taken from the tail vessels to measure levels of insulin, glucagon, triacylglycerol (TAG), free fatty acids (FFA), cholesterol. Mice were then given an oral dose of 2 g/kg of glucose through gavage, and their blood glucose levels were measured using a glucometer (LifeScan, Inc., Milpitas, CA, USA) at 15, 30, 60, 90, 120, and 180 minutes post-gavage.

3.3.8 Hematoxylin and Eosin Liver Staining

Following an overnight fixation in 4% paraformaldehyde (PFA), the right lobe of the liver was embedded in paraffin blocks. The livers were cut to 5 µm thick slices and were processed as previously described (Prazienkova et al., 2021). Subsequently were samples covered with the DPX mounting medium (MilliporeSigma) and cover glass. The photomicrographs of liver sections were taken with an Olympus IX83 microscope (Olympus Europa SE & Co. KG, Hamburg, Germany).

3.3.9 Biochemical Parametres in Blood Plasma

Glucose levels in the whole blood were measured in male DIO mice, and NPFFR2 KO and dKO mice with the Glucocard glucometer (Arkray, Kyoto, Japon). Fasted plasma was

used to detect insulin and glucagon using radioimmunoassay (MilliporeSigma), FFA (Roche, Mannheim, Germany), cholesterol with TAG (Erba Lachema, Brno, Czech Republic). Plasma from *ad libitum* fed anesthetized mice was collected to measure leptin (Millipore Sigma) and ghrelin (Millipore Sigma) levels. The manufacturer's instructions were followed for all measures.

3.3.10 Immunoblot Analysis of Tissue Samples

The hypothalamus, brainstem, liver, adipose tissue and gastrocnemius samples were prepared as previously described in (Spolcova et al., 2015) and kept at -20 °C. Proteins were separated using precast gradient 4–15% Criterion™ TGX™ gels (Bio-Rad) and transferred into nitrocellulose membranes using the Criterion™ blotter (Bio-Rad). Nitrocellulose membranes were blocked for 1 h in 5% milk and then incubated with primary antibodies (Table 5) overnight at 4 °C. Using ChemiDoc™ system Chemiluminescence was detected, and bands were subsequently quantified using Image Lab Software obtained from Bio-Rad. The protein level was normalized to GAPDH.

The obtained data from *in vivo* immunoblots were statistically processed using the GraphPad Prism program and are presented as the mean value ± SEM, and statistics were performed by One-Way ANOVA with Bonferroni post hoc test. Differences were considered statistically significant when $p < 0.05$.

Table 5: List of used primary antibodies

Abbreviation	Antibody	MW kDa	Dilution	Provider
p-Akt S473	Phospho-Akt (Ser473) (D9E) XP® Rabbit mAb #4060	60	1:1000	Cell Signaling Technology
Akt	Akt (pan) (C67E7) Rabbit mAb #4691	60	1:1000	Cell Signaling Technology
p-AS160 S588	Phospho-AS160 (Ser588) (D8E4) Rabbit mAb #8730	160	1:1000	Cell Signaling Technology
AS160	AS160 (C69A7) Rabbit mAb #2670	160	1:1000	Cell Signaling Technology
GAPDH	GAPDH (D4C6R) Mouse mAb #97166	37	1:1000	Cell Signaling Technology
GSK-3β	GSK-3β (27C10) Rabbit mAb #9315	46	1:1000	Cell Signaling Technology
p-PDK	Phospho-PDK1 (Ser241) (C49H2) Rabbit mAb #3438	58-68	1:0000	Cell Signaling Technology
PDK	PDK1 Antibody Rabbit Ab #3062	58-68	1:0000	Cell Signaling Technology
PI3K p85	PI3 Kinase p85 (19H8) Rabbit mAb #4257	85	1:1000	Cell Signaling Technology
PI3K p110α	PI3 Kinase p110α (C73F8) Rabbit mAb #4249	110	1:1000	Cell Signaling Technology

3.3.11 Determination of the mRNA Expression

The samples for mRNA determination were processed by Miloslava Čechová at the Institute for Clinical and Experimental Medicine (IKEM).

The mRNA expression of the genes of interest was determined in samples from the NPFFR2 KO experiment. Samples were homogenized using MagNA Lyser Instrument using MagNA Lyser Green Beads (Roche Diagnostics GmbH, Mannheim, Germany) and total RNA was extracted with MagNA Pure Compact RNA Isolation (Tissue) kit (Roche Diagnostics GmbH, Mannheim, Germany).

In the NPFFR2 KO characterization experiment the level of reference gene beta2-microglobulin (B2m) was measured and used to normalize and quantify the RT-PCR of the gene for mRNA expression of genes of interest which was determined using an ABI PRISM 7500 instrument (Applied Biosystems, Foster City, CA, USA).

4. RESULTS

4.1 Structure-Activity Study

The results in this chapter were published in (Strnadova et al., 2023). *In vivo* experiments were performed by RNDr. Strnadová Veronika Ph.D., RNDr. Lenka Maletínská, CSc., and Mgr. Barbora Neprašová Ph.D. *In vitro* experiments were performed by RNDr. Strnadová Veronika Ph.D and Ing. Alena Karnošová. Competitive binding experiments using isolated cell membranes from cells expressing NPFFR1 and NPFFR2 and cell signaling using immunoblots were performed by Ing. Alena Karnošová.

4.1.1 Binding Affinities of Lipidized PrRP31 Analogs for Receptors GPR10, NPFFR2, and NPFFR1

We designed and characterized new series of lipidized PrRP31 analogs (for structures see Fig. 5) to find the best anorexigenic analog with strong dual GPR10-NPFFR2 agonist properties.

First, we performed saturation binding experiment to determine K_d values of radioligands were determined using Graph Pad Prism for CHO-K1 cell line expressing GPR10, NPFFR1, and NPFFR2 (Table 6). K_i values for each analog were computed using K_d values obtained from saturation experiments and IC_{50} values obtained from competitive binding experiments using Cheng and Prusoff equation (Cheng and Prusoff, 1973).

Table 6: K_d values determined for receptors GPR10 NPFFR2 and NPFFR1.

GPR10	**NPFFR2**	**NPFFR1**
^{125}I-PrRP31	^{125}I-DMe	^{125}I-DMe
	K_d [n M]	
1.06 ± 0.36	0.72 ± 0.12	0.94 ± 0.06

Data are presented as the mean values ± SEM and performed in 2-3 independent experiments in duplicates.

Palm^{11}-PrRP31, palm-PrRP31, and palm^{11}-TTDS-PrRP31 analogs demonstrated a higher binding affinity for GPR10 and NPFFR2 compared to natural PrRP31. Moreover, palm^{11}-PrRP31 demonstrated a greater affinity for the GPR10 than for the NPFFR2 receptor. Palm-PrRP31 and palm^{11}-TTDS-PrRP31, on the other hand, displayed a higher affinity towards NPFFR2.

The possible target or off-target properties of another NPFF receptor, NPFFR1, were examined. Palmitoylation increased the binding affinities of analogs palm^{11}-PrRP31 and palm-PrRP31 for NPFFR1 and palm-PrRP31 displayed higher binding affinity then palm^{11}-PrRP31 not only towards NPFFR2 but also towards NPFFR1 receptor (Table 7).

Lower affinity than natural PrRP31 displayed analogs 1, 2, and 3 for the GPR10, and the affinity toward receptors NPFFR2 and NPFFR1 were 3 to 4-fold higher. Additionally, analog 5 with myristoyl at the Lys^{11}, which is structurally similar as $palm^{11}$-PrRP31, demonstrated increased affinity for GPR10 and NPFFR2, and decreased for NPFFR1. Analog 4 containing dodecanoic fatty acid revealed a lower binding affinity to NPFFR2, which is important for analog's anorexigenic function. Analogs 6-12 retained a strong binding affinity in a nanomolar range for the GPR10 receptor even had a stronger affinity for the NPFFR2 receptor than the natural PrRP31. Additionally, Analogs 9 and 12 had binding abilities towards the NPFFR1 receptor similar as natural PrRP31 (Table 7).

Analogs 13-16 with hexadecanedioic acid displayed a lower binding affinity than other analogs by up to two orders for both GPR10 and NPFFR2, and they also had a low binding affinity for NPFFR1. This suggests that hexadecanedioic acid is not a feasible alternative for lipidization of PrRP31. The scrambled peptide displayed no affinity towards tested receptors (Table 7).

The affinity of NPFF and its stable analog 1DMe towards their receptor NPFFR2 was found to be in the nanomolar range. Moreover, NPFF and 1DMe exert negligible affinities for the GPR10 receptor (Table 7). NPFF,1DMe and analogs $palm^{11}$-PrRP31 and palm-PrRP31 (In Table 7 tested peptides are highlighted gray) were further investigated in following chapter 4.2.

Table 7: Binding affinities to CHO-K1 cell line expressing GPR10, NPFFR2, and NPFFR1.

	GPR10		NPFFR2		NPFFR1	
	^{125}I-PrRP31	% of PrRP31	^{125}I-1DMe	% of PrRP31	^{125}I-1DMe	% of PrRP31
Analog	**K_i [n M]**		**K_i [n M]**		**K_i [n M]**	
PrRP31	4.58 ± 0.66	**100**	18.82 ± 2.28	**100**	40.39 ± 4.20	**100**
Palm-PrRP31	4.04 ± 0.01	**113**	0.45 ± 0.04	**4182**	0.78 ± 0.11	**5178**
Palm^{11}-PrRP31	3.52 ± 0.71	**130**	9.08 ± 1.14	**207**	21.04 ± 2.87	**192**
Palm^{11}-TTDS-PrRP31	3.79 ± 0.46	**121**	2.09 ± 0.15	**900**	16.98 ± 2.53	**238**
analog 1	6.90 ± 1.00	**66**	2.89 ± 0.34	**651**	10.20 ± 1.46	**396**
analog 2	6.20 ± 0.76	**74**	6.26 ± 0.51	**301**	13.46 ± 0.28	**300**
analog 3	6.59 ± 1.36	**69**	3.55 ± 0.24	**530**	9.13 ± 0.91	**442**
analog 4	1.99 ± 0.41	**230**	27.55 ± 3.54	**68**	63.04 ± 4.35	**64**
analog 5	1.86 ± 0.07	**246**	1.61 ± 0.15	**1169**	72.71 ± 7.01	**56**
analog 6	1.78 ± 0.40	**257**	4.20 ± 0.46	**448**	10.59 ± 1.12	**381**
analog 7	2.10 ± 0.97	**218**	10.35 ± 0.31	**182**	15.13 ± 0.82	**267**
analog 8	1.65 ± 0.67	**278**	3.58 ± 0.33	**526**	60.55 ± 4.90	**67**
analog 9	1.81 ± 0.72	**253**	11.73 ± 1.02	**160**	35.84 ± 2.78	**113**
analog 10	3.15 ± 1.09	**145**	19.16 ± 2.58	**98**	149.10 ± 16.85	**27**
analog 11	3.14 ± 1.03	**146**	17.37 ± 1.92	**108**	157.07 ± 12.19	**26**
analog 12	1.48 ± 0.58	**309**	2.93 ± 0.37	**642**	28.38 ± 3.93	**142**
analog 13	30.67 ± 5.04	**15**	129.95 ± 9.16	**14**	780.17 ± 74.65	**5**
analog 14	27.90 ± 4.89	**16**	139.57 ± 19.92	**13**	522.88 ± 66.02	**8**
analog 15	23.41 ± 5.44	**20**	313.38 ± 45.76	**6**	932.47 ± 110.21	**4**
analog 16	15.40 ± 2.76	**30**	320.34 ± 25.44	**6**	2158 ± 81	**2**
scrambled	>10 000	**-**	>10 000	**-**	>10 000	**-**
NPFF	>10 000	**-**	0.28 ± 0.06	**6721**	1.08 ± 0.09	**3740**
1DMe	>10 000	**-**	1.03 ± 0.23	**1827**	0.79 ± 0.06	**5113**

Data are presented as the mean ± SEM, performed in 2–5 independent experiments in duplicates, and analyzed in Graph-Pad Software. K_i values determined using Cheng and Prusoff equation (Cheng and Prusoff, 1973).

4.1.2 Agonist Properties of Lipidized PrRP31 Analogs at GPR10 Receptor

To determine the agonist characteristics of natural PrRP31 and lipidized PrRP31 analogs, receptor activation was investigated using the beta-lactamase reporter gene assay.

Lipidization increased the agonist properties of all tested analogs. The strongest agonist activity revealed palm^{11}-PrRP31. Lower but still very potent agonist activity at GPR10 was observed for palm-PrRP31, palm^{11}-TTDS-PrRP31, analogs 1–3, and analog 12 (Table 8).

Table 8: Agonist properties of PrRP31 analogs at the GPR10 receptor.

Analogs	EC_{50} [pM]	% of PrRP31	Analogs	EC_{50} [pM]	% of PrRP31
PrRP31	530 ± 70	**100**	**analog 7**	294 ± 37	**180**
palm-PrRP31	72 ± 6	**736**	**analog 8**	378 ± 60	**140**
palm^{11}-PrRP31	39 ± 5	**1359**	**analog 9**	338 ± 57	**157**
palm^{11}-TTDS-PrRP31	84 ± 18	**631**	**analog 10**	278 ± 26	**191**
analog 1	78 ± 19	**679**	**analog 11**	300 ± 37	**177**
analog 2	77 ± 2	**688**	**analog 12**	109 ± 13	**486**
analog 3	81 ± 13	**654**	**analog 13**	336 ± 16	**158**
analog 4	332 ± 28	**160**	**analog 14**	316 ± 36	**168**
analog 5	213 ± 22	**249**	**analog 15**	262 ± 33	**202**
analog 6	401 ± 48	**132**	**analog 16**	343 ± 80	**155**

Data presented as the means EC_{50} values ± SEM and analyzed in Graph-Pad Prism and performed in 2–3 independent experiments.

4.1.3 Acute Injections of PrRP31 Analogs Strongly Reduced Food Intake

To evaluate the anorexigenic effect of PrRP31 analogs (structures in Fig. 5), food intake after a single s.c. injection was measured in fasted mice. The maximal effect was observed 45 min after the injection (Table 9). Analogs palm-PrRP31, and palm^{11}-TTDS-PrRP31, displayed the strongest anorexigenic effect from all tested analogs. Palm^{11}-PrRP31 also revealed strong reduction in food intake, but not as strong as analogs mentioned above. Very strong food intake lowering effect also showed analogs 2 and 9 which are both lipidized at position 11. A substantial anorexigenic effect was also seen in analog 1 that was lipidized at position 1 (Table 9).

Analog 12 has very similar structure as analog 9 and displayed strong anorexigenic effect. Moreover, analog 12 displayed overall better *in vitro* properties compared to analogs 1, 2, and 9 from previous *in vitro* experiments (Table 7 and 8). Therefore, analog 12 was chosen for further chronic treatment study.

Analogs 13 – 16 showed the lowest food intake lowering effect from all tested analogs. They also had the worst binding affinities from all tested analogs, therefore, hexadecanedioic acid is not an appropriate option to use for lipidized PrRP31 (Table 9).

Table 9. Acute food intake in fasted lean mice 45 min. after s.c. administration of PrRP31 analogs.

Analogs	Acute food intake [g]	% of Saline	Analogs	Acute food intake [g]	% of Saline
Saline	0.43 ± 0.01	**100**			
PrRP31	0.41 ± 0.04	**95**	**analog 7**	0.26 ± 0.04	**60**
palm-PrRP31	0.05 ± 0.02	**12**	**analog 8**	0.13 ± 0.04	**30**
palm^{11}-PrRP31	0.13 ± 0.02	**30**	**analog 9**	0.06 ± 0.02	**14**
palm^{11}-TTDS-PrRP31	0.05 ± 0.02	**12**	**analog 10**	0.21 ± 0.04	**49**
analog 1	0.08 ± 0.04	**19**	**analog 11**	0.18 ± 0.04	**42**
analog 2	0.06 ± 0.03	**14**	**analog 12**	0.10 ± 0.04	**23**
analog 3	0.16 ± 0.04	**37**	**analog 13**	0.44 ± 0.03	**102**
analog 4	0.33 ± 0.03	**77**	**analog 14**	0.41 ± 0.04	**95**
analog 5	0.35 ± 0.04	**81**	**analog 15**	0.37 ± 0.04	**86**
analog 6	0.23 ± 0.03	**53**	**analog 16**	0.45 ± 0.04	**105**

Data are presented as the mean ± SEM and expressed as the weight of consumed food intake (n = 5–6) and percentage of food intake of the saline-treated group.

4.1.4 Chronic Treatment of Lipidized PrRP31 Analogs Decreased Body Weight and Adiposity

Analog 12, which was determined to be one of the most effective PrRP31 analog in experiments *in vitro* (Table 7 and 8) and *in vivo* (Table 9), was used for long-term administration in the DIO mice model. It was compared to palm^{11}-PrRP31, which had previously been shown to have a strong impact on reducing food intake and body weight (Prazienkova et al., 2017). Saline or peptide analogs at a dose of 5 mg/kg were injected twice daily for 21 days.

The results showed that both palm^{11}-PrRP31 and analog 12 were effective in reducing body weight (Fig.9A) and the weight of white adipose tissues (gWAT and scWAT) (Fig.9B) in the DIO mice. Analog 12 proved to be even more potent than analog palm^{11}-PrRP31.

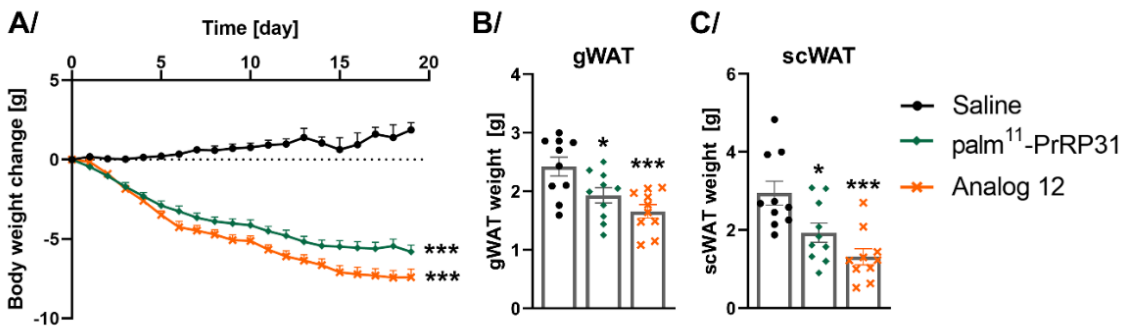

Figure 9: Palm^{11}-PrRP31 and analog 12 decreased body weight and adiposity in DIO mice.

Body weight change were monitored during the experiment and final body weight was compared and statistically analyzed (**A**). Weight of gonadal white adipose tissue (gWAT) (**B**) and subcutaneous white adipose tissue (scWAT) (**C**) at the end of experiment. Data are expressed as the mean ± SEM (n = 10) and determined by one-way ANOVA with Bonferroni post hoc test. *p < 0.05 and ***p < 0.001 for saline vs. PrRP31 analogs.

4.2 Search for Mechanism of Action of lipidized PrRP31 *In Vitro*

The results in this chapter were published in (Karnosova et al., 2021). Experiments were performed by Ing. Alena Karnošová, RNDr. Veronika Strnadová, Ph.D., and Ing. Lucie Holá.

4.2.1 The Affinity of Natural PrRP31 and Its Two Most Potent Analogs for Other Potential Off-target Receptors

The binding affinities of natural PrRP31, palm^{11}-PrRP31, and palm-PrRP31 towards other potential off-target receptors Y1, Y2, and Y5, ghrelin receptor GHSR and KOR were evaluated. The K_d values for each receptor were determined from saturation experiments (Table 10).

Table10: K_d values determined for other potential off-target receptors.

Y1	**Y2**	**Y5**	**KOR**	**GHSR**
^{125}I-PYY	^{125}I-PYY	^{125}I-PYY	^{125}I-Dynorphin	^{125}I-ghrelin
		K_d [n M]		
1.53 ± 0.08	2.18 ± 0.85	1.01 ± 0.27	2.38	0.44 ± 0.12

Data are presented as the mean values ± SEM and performed in 1–2 independent experiments in duplicates.

The natural ligand for Y receptors PYY bound to Y1, Y2, and Y5 receptors in the nanomolar concentrations. Natural PrRP31 did not bind to Y1 and Y2 receptors, and also both tested palmitoylated analogs, palm-PrRP31 and palm^{11}-PrRP31, bound to Y1 and Y2 with a negligible affinity. Interestingly, natural PrPR31 and palm^{11}-PrRP31 displayed a negligible affinity for the Y5 receptor, but palm-PrRP31 exhibited a relatively high affinity for this receptor (Table 11).

Dynorphin showed a very high affinity for the receptor KOR. No binding was observed in the case of natural PrRP31, but the affinity was increased after its palmitoylation. Palm-PrRP31 displayed higher binding affinity towards KOR than palm^{11}-PrRP31 (Table 11).

The receptor GHSR was also evaluated as a potential off-target receptor. Natural PrRP31 was found to have no binding towards GHSR, but palmitoylated analogs of this peptide exhibited a low binding affinity for this receptor. Among these analogs, palm-PrRP31 demonstrated a stronger binding to GHSR than palm^{11}-PrRP31 (Table 11).

Table 11: Binding affinities of natural PrRP31and its palmitoylated analogs towards potential off-target receptors.

Analog	Y1 ^{125}I-PYY	Y2 ^{125}I-PYY	Y5 ^{125}I-PYY	GHSR ^{125}I-Ghrelin	KOR ^{125}I-Dynorphin
			K_i [n M]		
PrRP31	>10 000	>10 000	2863 ± 43	>10 000	>10 000
Palm^{11}-PrRP31	>10 000	>10 000	362 ± 96	2800 ± 466	4278 ± 866
Palm-PrRP31	3147 ± 31	>10 000	32.62 ± 6.16	160 ± 16	106 ± 15
PYY	2.92 ± 0.28	6.51 ± 0.71	3.06 ± 0.49		
Ghrelin				4.59 ± 0.41	
Dynorphin					0.36 ± 0.03

Data are presented as the mean ± SEM, performed in 2–5 independent experiments in duplicates, and analyzed in Graph-Pad Software. K_i values determined using Cheng and Prusoff equation (Cheng and Prusoff, 1973).

4.2.2 Agonist Properties of Natural PrRP31 and its Two Most Potent Analogs at NPFFR2 Receptor

The agonist effects of PrRP31, its palmitoylated analogs, palm-PrRP31 and palm^{11}-PrRP31, NPFF, and 1DMe, were investigated using the CHO-K1 cell line with NPFFR2 transfected with aequorin, and intracellular Ca^{2+} release was detected. Both palmitoylated analogs showed increased agonist activity compared to natural PrRP31 at the NPFFR2 receptor, but agonists of NPFFR2 receptor NPFF and 1DMe promoted intracellular Ca^{2+} release at substantially lower concentrations (Table 12).

Table 12: Agonist properties of PrRP31 and its palmitoylated analogs at the NPFFR2 receptor.

Analogs	EC_{50} [n M]	% of PrRP31
PrRP31	89.33 ± 0.84	**100**
palm-PrRP31	14.16 ± 1.52	**631**
palm^{11}-PrRP31	18.71 ± 1.31	**477**
NPFF	0.24 ± 0.02	**37221**
1DMe	0.82 ± 0.15	**10894**

Data are presented as the mean ± SEM, performed in 3 independent experiments in duplicates, and analyzed in Graph-Pad Software.

4.2.3 Agonist and Antagonist Properties of Natural PrRP31 and Its Two Most Potent Analogs at Other Potential Off-target Receptors

The activation of potential off-target receptors was studied to establish agonist properties of natural PrRP31 and its two palmitoylated analogs, palm^{11}-PrRP31 and palm-PrRP31. Natural PrRP31 displayed no agonist effect at Y5, GHSR, KOR and other opioid receptors (Table 13). Moreover, for neither palm^{11}-PrRP31 or palm-PrRP31was not observed agonist activity at the DOR, MOR, and ORL-1 opioid receptors. Interestingly, they exert

very weak agonist activity at the KOR. Additionally, modest agonist effects of both palmitoylated analogs were shown at the GHSR. Moreover, palm-PrRP31 demonstrated a more potent agonist effect at the Y5 receptor compared to palm^{11}-PrRP31 (Table 13).

Table 13: Agonist properties of natural PrRP31 and its palmitoylated analogs at potential off-target receptors.

Receptor	Y5	GHSR	KOR	DOR	MOR	ORL-1
			EC_{50} [n M]			
PYY	19.4 ± 2.5					
Ghrelin		2.8 ± 2.5				
U-50488			1.4 ± 1.0			
Deltorphin II				5.6 ± 9.9		
DAMGO					14.7 ± 1.9	
Nociceptin						3.8 ± 0.6
PrRP31	N	N	N	N	N	N
Palm^{11}-PrRP31	583.3 ± 121.1	1068.1 ± 272.2	>10 000	N	N	N
Palm-PrRP31	56.5 ± 18.4	1273.5 ± 167.9	>10 000	N	N	N

Data are presented as the mean ± SEM, performed in 2–3 independent experiments in duplicates, and analyzed in Graph-Pad Software. N = no agonist properties.

Because palm^{11}-PrRP31 displayed lower agonist activity at the potential off-target receptor Y5, the antagonist activity at the Y5, GHSR, and opioid receptors, was tested only with this analog. There were not observed antagonistic effects of either PrRP31 or palm^{11}-PrRP31 at the Y5, GHSR, or opioid receptors (KOR, DOR, MOR, ORL-1). Interestingly, palm^{11}-PrRP31 demonstrated to increase PYY activity and has the potential to be a positive allosteric modulator of the Y5 receptor (Fig. 10).

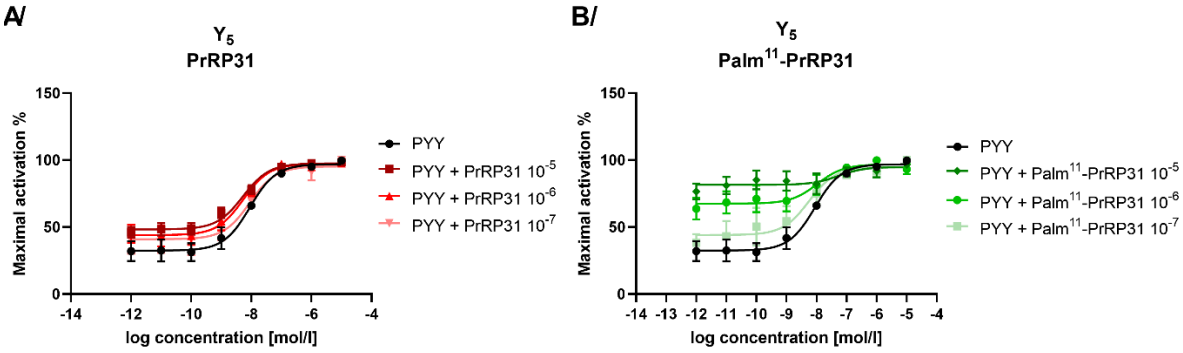

Figure 10: The Y5 receptor's response to the PYY agonist in an antagonist mode experiment. PrRP31 (**A**) or palm^{11}-PrRP31 (**B**) used as antagonist of Y5 receptor competing with PYY. Data are presented as mean ± SEM, the experiments were performed in duplicates and were repeated at least two times and analyzed using nonlinear regression.

4.2.4 Palmitoylated PrRP31 Analogs Activate Various Intracellular Signaling Pathways in Cells Expressing GPR10, NPFFR2, or NPFFR1

To understand the mechanism of action of PrRP31 and its selected palmitoylated analogs to intracellular signaling pathways, CHO-K1 cells that stably express GPR10, NPFFR2,

and NPFFR1 receptors were used. NPFF and 1DMe were employed as reference compounds to activate NPFFR1 and NPFFR2

To clarify whether GPR10 signals through Gq or Gi/o proteins, CHO-K1 cells with transfected GPR10 were preincubated with PTX (Fig 11). PTX completely blocked phosphorylation of Akt at Ser473 (Fig. 11A). However, phosphorylation of ERK (Fig. 11B) and activation of c-Fos (Fig. 11C) were inhibited only partially. Therefore, there is possibility that GPR10 is coupled with both Gq and Gi/o proteins simultaneously and the stimulus of GPR10 can lead to diverse cellular signaling.

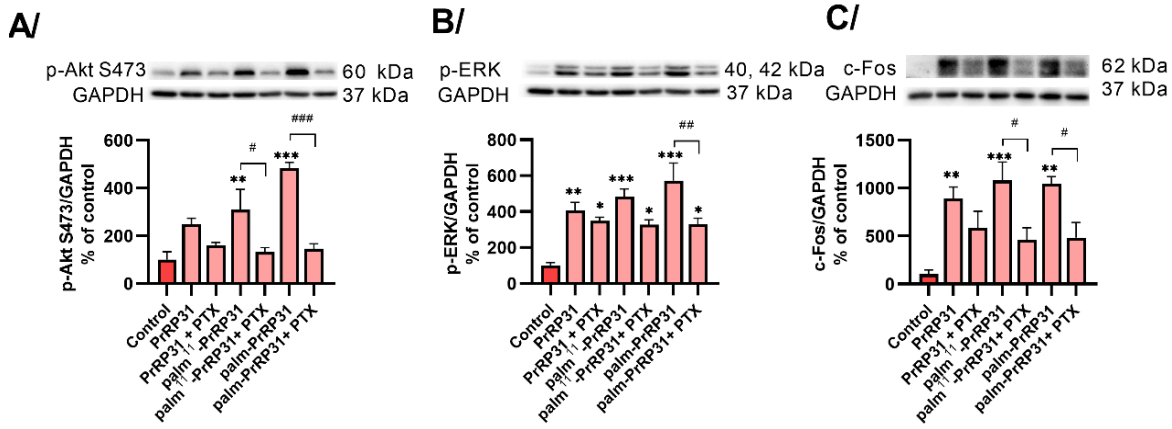

Figure 11: Inhibition of Akt and ERK induction and activation of c-Fos by PTX in CHO-K1 cells expressing GPR10 receptor.
Phosphorylation of Akt (S473) (**A**) and ERK (**B**) after 5 minutes and activation of c-Fos (**C**) after 60 minutes incubation and at 37°C with peptides at final concentrations of 10^{-6} M. Cells preincubated with pertussis toxin (PTX) for 16 hours at final concentrations of 10^{-7} M. Densitometric quantification of immunoblots normalized to GAPDH and the phosphorylation level in the untreated control was standardized as 100%. Experiments were performed independently at least three times. Data are expressed as the mean ± SEM and were determined by one-way ANOVA with Bonferroni post hoc test *p < 0.05, **p < 0.01, ***p < 0.001 for control vs stimulated cells and #p < 0.05, ##p < 0.01, ###p < 0.001 for stimulated cells vs. PTX preincubated stimulated cells.

The activation of the cAMP-dependent protein kinase (PKA) was examined to assess the possibility of GPR10 coupling with the Gs protein. However, no changes were observed in the cells expressing GPR10, NPFFR2 and NPFFR1 after incubation with PrRP31, palmitoylated PrRP31 analogs, NPFF or 1DMe (Fig. 12).

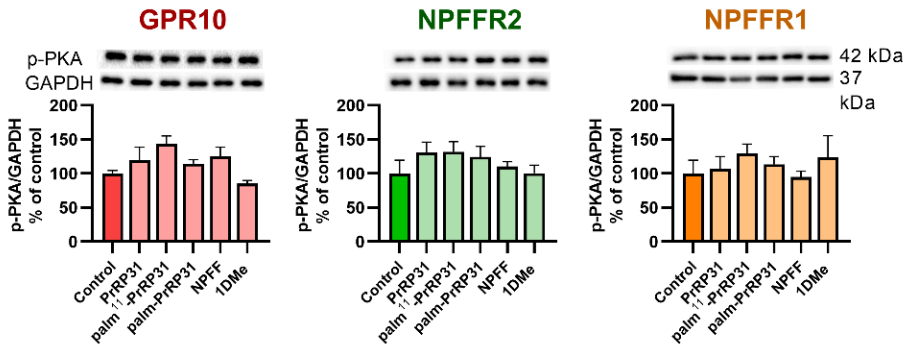

Figure 12: Induction of PKA activation by PrRP31 and its palmitoylated analogs in CHO-K1 cells expressing GPR10, NPFFR2, and NPFFR1 receptors.
Phosphorylation of PKA after 5 minutes incubation at 37°C with peptides at final concentrations of 10^{-6} M. Densitometric quantification of immunoblots normalized to GAPDH and the phosphorylation level in the untreated control was standardized as 100%. Experiments were performed independently at least three times. Data are expressed as the mean ± SEM and were determined by one-way ANOVA with Dunnett's post hoc test.

The phosphorylation of Akt at Ser473 and Thr308 was measured in order to investigate the activation of Akt pathway. Natural PrRP31 significantly increased phosphorylation of Akt at both Ser473 (Fig. 13A) and Thr308 (Fig. 13B) in cells expressing NPFFR2. However, no activation was observed in cells with NPFFR1. The phosphorylation of Akt at Ser473 and Thr308 was shown to be significantly increased by palm^{11}-PrRP31 and palm-PrRP31 in cells expressing GPR10 and NPFFR2, as well as in cells expressing NPFFR1 (Fig. 13).

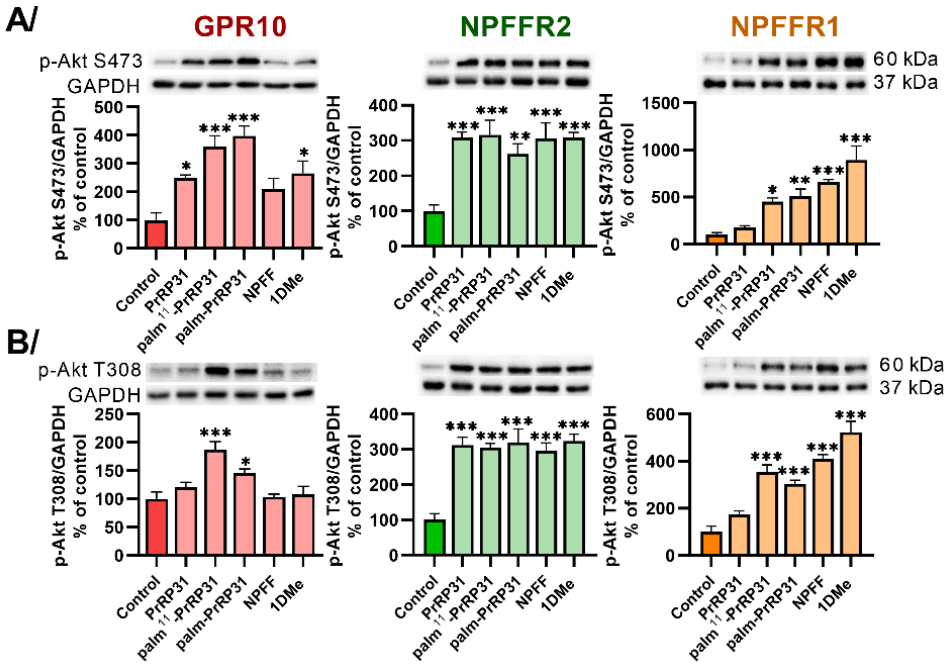

Figure 13: Akt activation by PrRP31 and its palmitoylated analogs in CHO-K1 cells expressing GPR10, NPFFR2, and NPFFR1 receptors.
Phosphorylation of Akt (Ser473) (**A**) and Akt (Thr308) (**B**) after 5 minutes incubation at 37°C with peptides at final concentrations of 10^{-6} M. Densitometric quantification of immunoblots

normalized to GAPDH and the phosphorylation level in the untreated control was standardized as 100%. Experiments were performed independently at least three times. Data are expressed as the mean ± SEM and were determined by one-way ANOVA with Dunnett's post hoc test *p < 0.05, **p < 0.01, ***p < 0.001 for control vs stimulated cells.

The effects of PrRP31 and palmitoylated PrRP31 analogs on the activation of the MAPK pathway were investigated. Natural PrRP31 was able to activate MAPK intracellular signaling pathways in cells expressing GPR10 and NPFFR2, but it failed to do so in cells that express NPFFR1 receptor. Stimulation with palm-PrRP31 in cells expressing GPR10, NPFFR2, and NPFFR1 receptors significantly increased the phosphorylation of MAPKs ERK (Fig. 14A), JNK (Fig. 14B), and p38 (Fig. 14C). Additionally, palm^{11}-PrRP31 significantly increased the phosphorylation of ERK, JNK, and p38 in cells expressing GPR10 and NPFFR2, but significant effect was not observed in cells with NPFFR1 (Fig. 14).

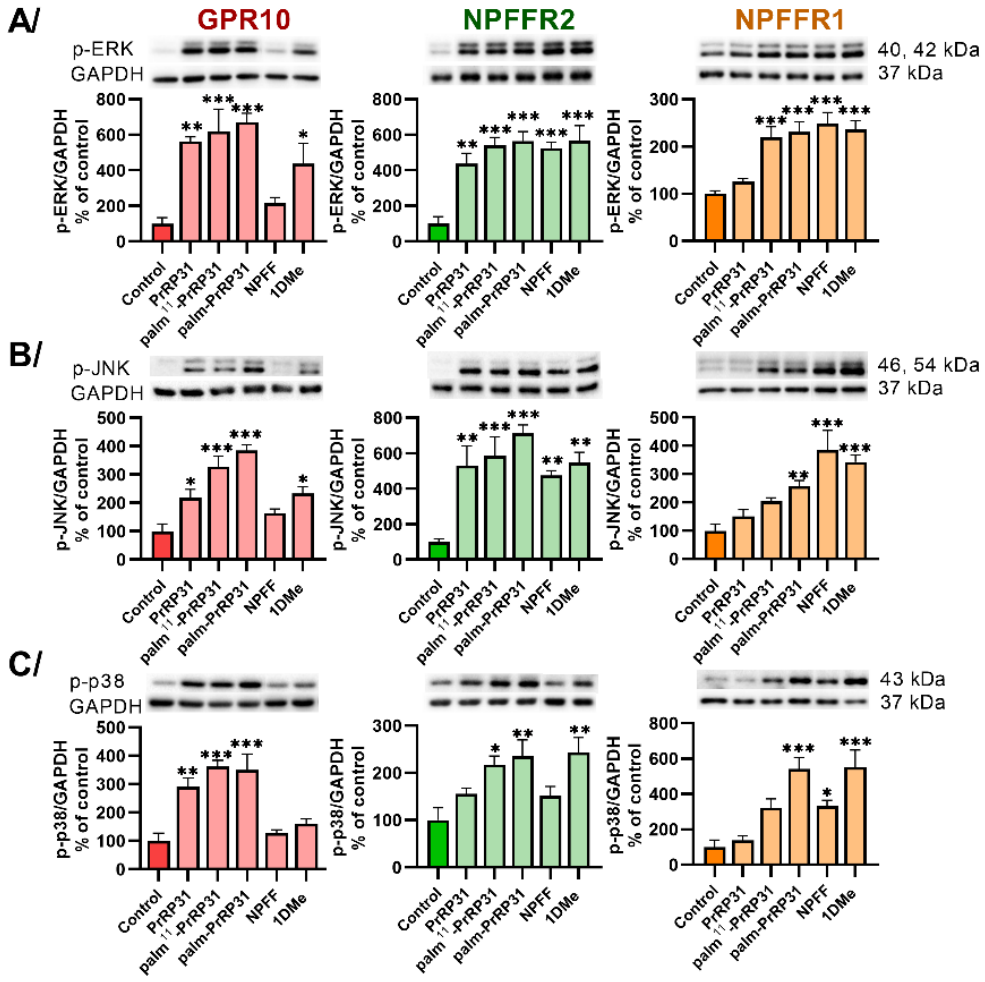

Figure 14: Activation of MAPK pathway by PrRP31 and its palmitoylated analogs in CHO-K1 cells expressing GPR10, NPFFR2, and NPFFR1 receptors.
Phosphorylation of ERK (**A**) and JNK (**B**) after 5 minutes and p38 (**C**) after 60 minutes incubation at 37°C with peptides at final concentrations of 10^{-6} M. Densitometric quantification of immunoblots normalized to GAPDH and the phosphorylation level in the untreated control was standardized as 100%. Experiments were performed independently at least three times. Data are

expressed as the mean ± SEM and were determined by one-way ANOVA with Dunnett's post hoc test *p < 0.05, **p < 0.01, ***p < 0.001 for control vs stimulated cells.

Three DNA-binding proteins, CREB, c-Jun, and c-Fos protein, were examined for their potential to regulate the expression of other genes regulating cell proliferation, differentiation, and apoptosis. The results revealed that natural PrRP31 and palm^{11}-PrRP31 showed significant activation of c-Jun (Fig. 15A), c-Fos (Fig. 15B) and increased phosphorylation of CREB (Fig. 15C) in cells with GPR10 and NPFFR2, but no differences were observed in cells with NPFFR1. Palm-PrRP31 significantly activated c-Jun and c-Fos, as well as phosphorylation of CREB, in cells expressing GPR10, NPFFR2, and NPFFR1 receptors (Fig. 15).

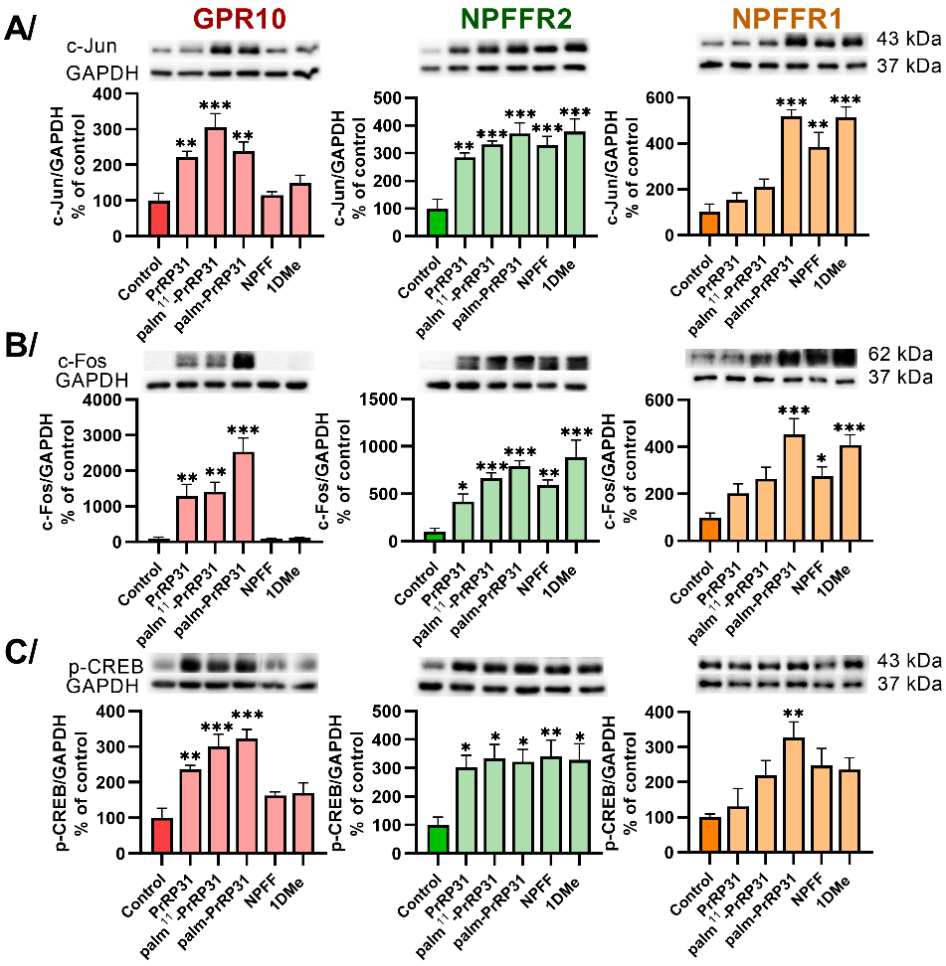

Figure 15: Induction of CREB and activation of c-Fos and c-Jun by PrRP31 and its palmitoylated analogs in CHO-K1 cells expressing GPR10, NPFFR2, and NPFFR1 receptors.
Activation of c-Jun (**A**) and c-Fos (**B**) after 60 minutes and phosphorylation of CREB (**C**) after 5 minutes incubation at 37°C with peptides at final concentrations of 10^{-6} M. Densitometric quantification of immunoblots normalized to GAPDH and the phosphorylation level in the untreated control was standardized as 100%. Experiments were performed independently at least three times. Data are expressed as the mean ± SEM and were determined by one-way ANOVA with Dunnett's post hoc test *p < 0.05, **p < 0.01, ***p < 0.001 for control vs stimulated cells.

4.3 NPFFR2 KO Characterization Study

The results obtained in this chapter are after major revision in Clinical Science. Experiments were performed and analyzed by Ing. Alena Karnošová and RNDr. Veronika Strnadová, Ph.D.

4.3.1 NPFFR2 Deletion Has No Impact on Behavior or Pain Perception

Behavioral experiments were carried out to detect potential anxiety-like behavior or exploratory alterations in the EPM and OF (Fig 16). In the OF arena, the track lengths of WT and NPFFR2 KO mice were comparable (Fig. 16A, C). Both NPFFR2 KO and WT on HFD displayed lower exploration behavior in the OF and enter less and spend less time in the center zone comparing mice on STD (Fig. 16B, D, E-H). NPFFR2 KO male mice showed no signs of anxiety-like behavior in the OF and EPM comparing to their WT controls, but females on HFD compared to those fed an STD, spent noticeably more time in the junction section of EPM (Fig. 16L). Moreover, NPFFR2 KO mice did not show any changes in pain sensitivity compared to WT mice measured by the HP test (Fig. 16N, P).

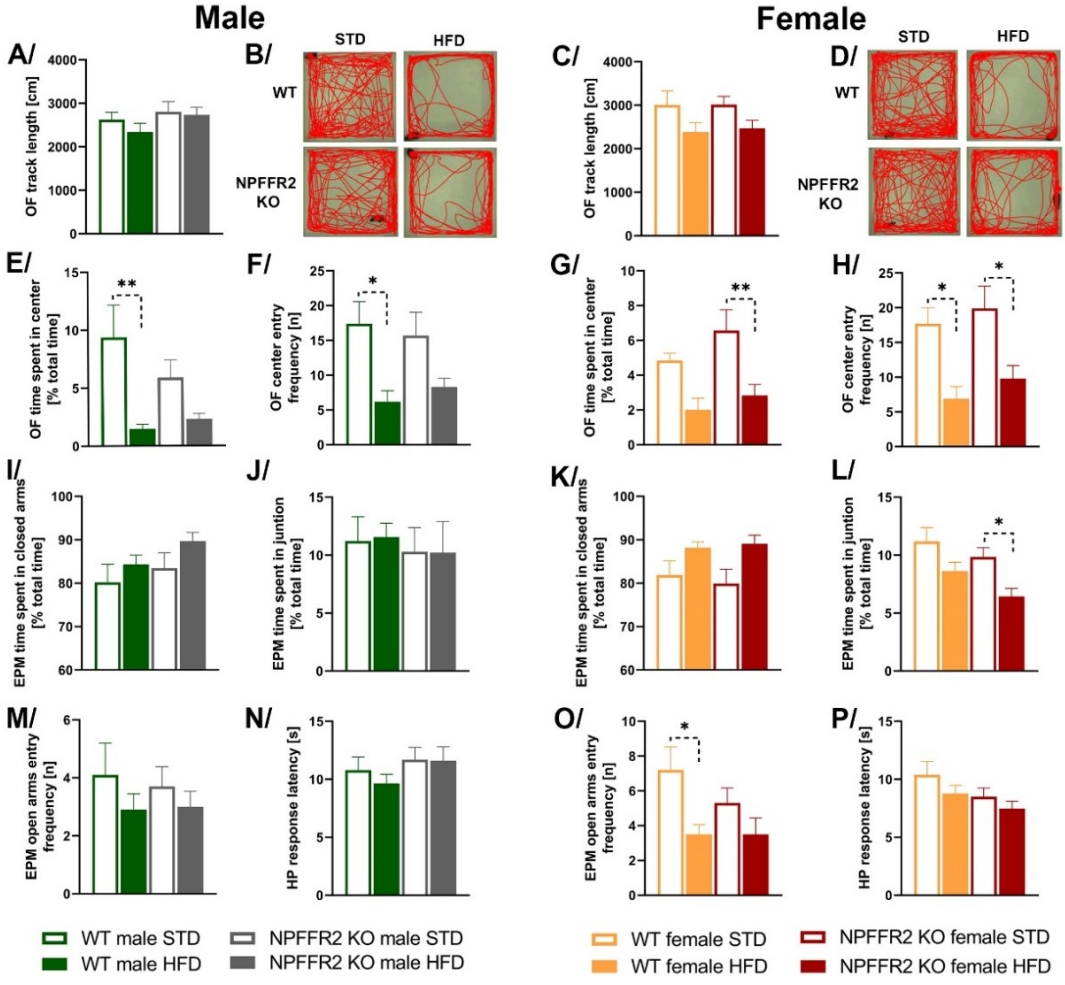

Figure 16. Behavioral experiments and pain perception experiments in NPFFR2 KO mice.

Track length in the open field (OF) test (**A**) males and (**C**) in females and track line of single representative animal for (**B**) males and (**D**) in females. Percentage (%) of total time (10 min) spent in the center zone for (**E**) males and (**G**) females, and the frequency of entries to the OF center zone for the (**F**) males and (**H**) females. Percentage (%) of total tested time (10 min) which animal spent in closed arms during the elevated plus maze (EPM), for (**I**) males and (**K**) females. Percentage (%) of total tested time which animal spent in the junction zone for (**J**) males and (**L**) females. Number of entries of open arms for (**M**) males and (**O**) females. For the hot plate (HP) test, latency to pain perception (paw licking) for (**N**) males and (**P**) females. Data are expressed as the mean ± SEM (n = 10) and determined by one-way ANOVA with Bonferroni post hoc test. *p < 0.05 and **p < 0.01 for STD vs. HFD mice of the same genotype.

4.3.2 NPFFR2 KO Mice Fed STD Displayed a Lean Phenotype, and NPFFR2 KO Males Fed HFD Gained Less Weight than WT Controls

NPFFR2 KO mice of both sexes fed STD showed a similar growth curve as their WT controls mice (Fig. 17A, G). When fed HFD at 9 weeks of age, male NPFFR2 KO mice showed significantly lower body weight than WT, whereas female body weight did not differ between HFD-fed genotypes (Fig. 17B, H). The energy intake of male NPFFR2 KO mice on STD was significantly increased comparing to WT controls (Fig. 17C).

At the end of the experiment, when the mice were 6 months old in a state of unrestricted feeding, the weight of the dissected organs were measured. The weight of the scWAT and gWAT correlated with the overall body weight of the mice in all groups (Fig. 17D, J). NPFFR2 KO male mice fed HFD had significantly lower weights of both adipose tissues compared to their WT controls (Fig. 17D). These differences were not observed in the female mice (Fig. 17J).

As anticipated, the HFD led to a significant increase in both plasma leptin levels (Fig. 17E, K) and *leptin* gene expression (Fig. 17F, L). However, the NPFFR2 KO mice that were fed HFD had a lower plasma leptin level than the WT control mice (Fig. 17E). This is consistent with the observed lower body weights and adipose tissue weights.

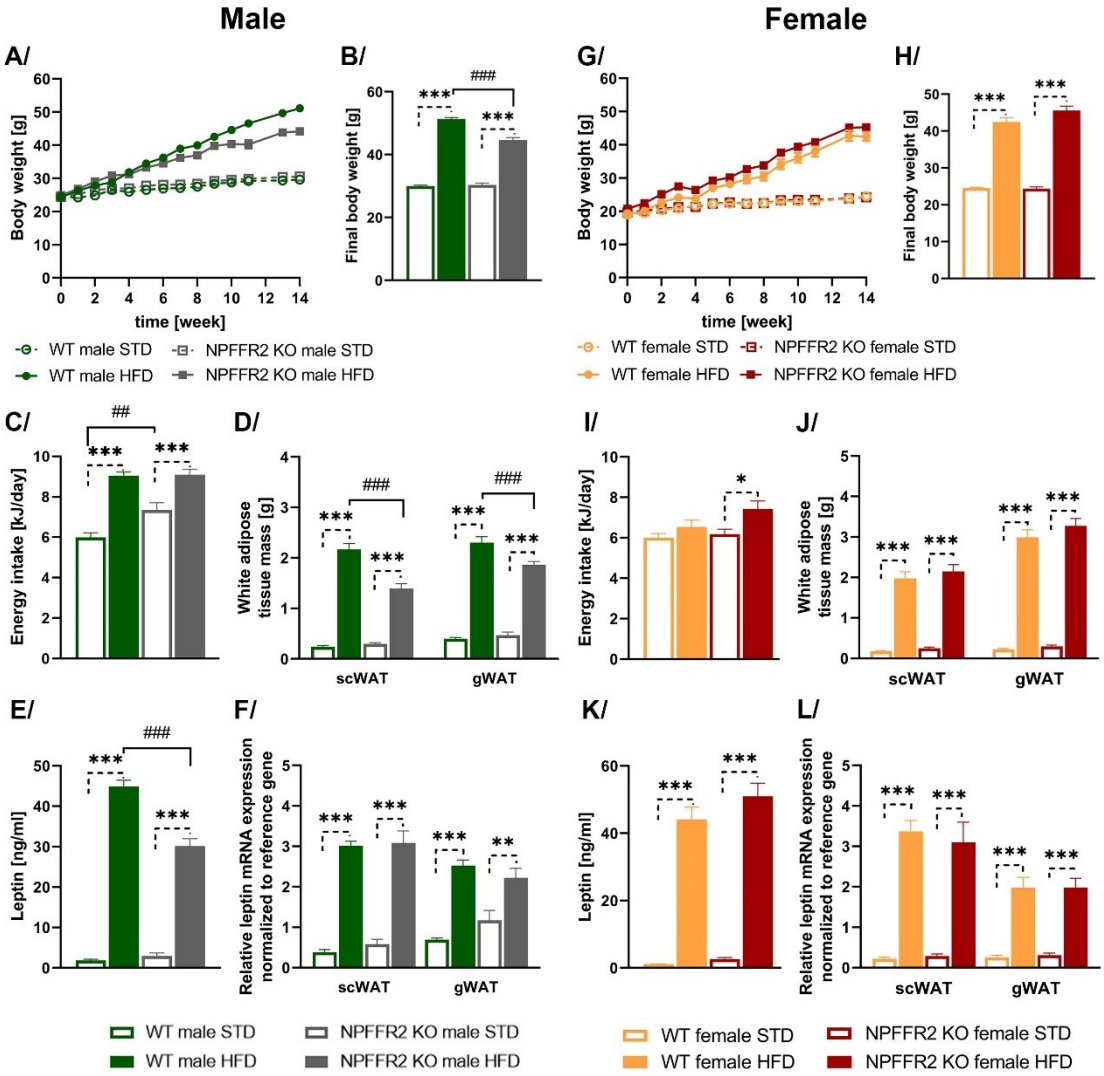

Figure 17: NPFFR2 KO male mice on HFD exhibit a reduced body weight compared to WT. Time course of body weight gain in (**A**) males and (**G**) females, final body weight (**B** and **H**), and average energy intake in (**C**) males and (**I**) females of NPFFR2 KO mice on a STD or HFD. Weights of dissected subcutaneous white adipose tissue (scWAT) and gonadal white adipose tissue (gWAT) in (**D**) males and (**J**) females. Serum leptin levels in (**E**) males and (**K**) females. All data are expressed as the mean ± SEM (n = 10). *Leptin* gene expression levels in white adipose tissues in (**F**) males and (**L**) females. Data are expressed as the mean ± SEM (n = 5). All Data were determined by one-way ANOVA with Bonferroni post hoc test. * $p < 0.05$, ** $p < 0.01$, and *** $p < 0.001$ for STD vs. HFD of the same genotype; ## $p < 0.01$ and ### $p < 0.001$ for NPFFR2 KO vs. WT mice on the same diet.

Both NPFFR2 KO and WT mice on the HFD displayed elevated plasma cholesterol and TAG levels. NPFFR2 KO females on the STD had lower cholesterol and TAG levels compared to their WT controls. There was no difference in plasma FFA levels among the groups (Table 14).

Table 14. Plasma metabolic profile of NPFFR2 KO and WT mice

Group	TAG [mmol/l]	FFA [mmol/l]	Cholesterol [mmol/l]
WT male STD	0.45 ± 0.02	0.73 ± 0.10	1.95 ± 0.12
WT male HFD	0.54 ± 0.04	0.60 ± 0.04	3.98 ± 0.07 ***
NPFFR2 KO male STD	0.43 ± 0.03	0.57 ± 0.06	1.89 ± 0.12
NPFFR2 KO male HFD	0.55 ± 0.04 *	0.61 ± 0.06	3.87 ± 0.18 ***
WT female STD	0.45 ± 0.03	0.47 ± 0.06	3.36 ± 0.21
WT female HFD	0.58 ± 0.02 **	0.39 ± 0.03	5.49 ± 0.23 ***
NPFFR2 KO female STD	0.35 ± 0.01 #	0.44 ± 0.04	2.17 ± 0.18 ##
NPFFR2 KO female HFD	0.51 ± 0.04 ***	0.38 ± 0.04	6.14 ± 0.28 ***

Triacylglycerol (TAG), free fatty acid (FFA). Data are expressed as the mean ± SEM (n = 8–10) and determined by one-way ANOVA with Bonferroni post hoc test. * $p < 0.05$, ** $p < 0.01$, and *** $p < 0.001$ for HFD vs. STD of the same genotype; # $p < 0.05$, ## $p < 0.01$, and ### $p < 0.001$ for NPFFR2 KO vs. WT mice on the same diet.

4.3.3 HFD-Fed NPFFR2 KO Mice Developed Severe Glucose Intolerance

Glucose tolerance was measured by OGTT in NPFFR2 KO and WT of both sexes fed either STD or HFD. The absence of the *Npffr2* gene led to significantly higher glucose levels after glucose gavage and higher AUC in both HFD- and STD-fed mice of both sexes (Fig. 18A, B, F, G). HFD-fed NPFFR2 KO mice showed significantly greater glucose excursions and AUC than their WT controls and NPFFR2 KO mice on STD (Fig. 18A, B, F, G). These results suggest that the absence of the *Npffr2* gene may cause severe glucose intolerance and potential insulin resistance.

The fasted glucose levels were increased in WT and NPFFR2 KO mice on HFD, but no differences were observed between genotypes (Fig. 18C, H). Additionally, the insulin levels were found to be increased in HFD-fed NPFFR2 KO and WT mice of both sexes than in their STD-fed controls (Fig. 18D, I). The levels of the glucagon hormone were found to be significantly lower in HFD-fed NPFFR2 KO females comparing to in their WT controls (Fig. 18J), however, no significant differences were observed among the male groups (Fig. 18E).

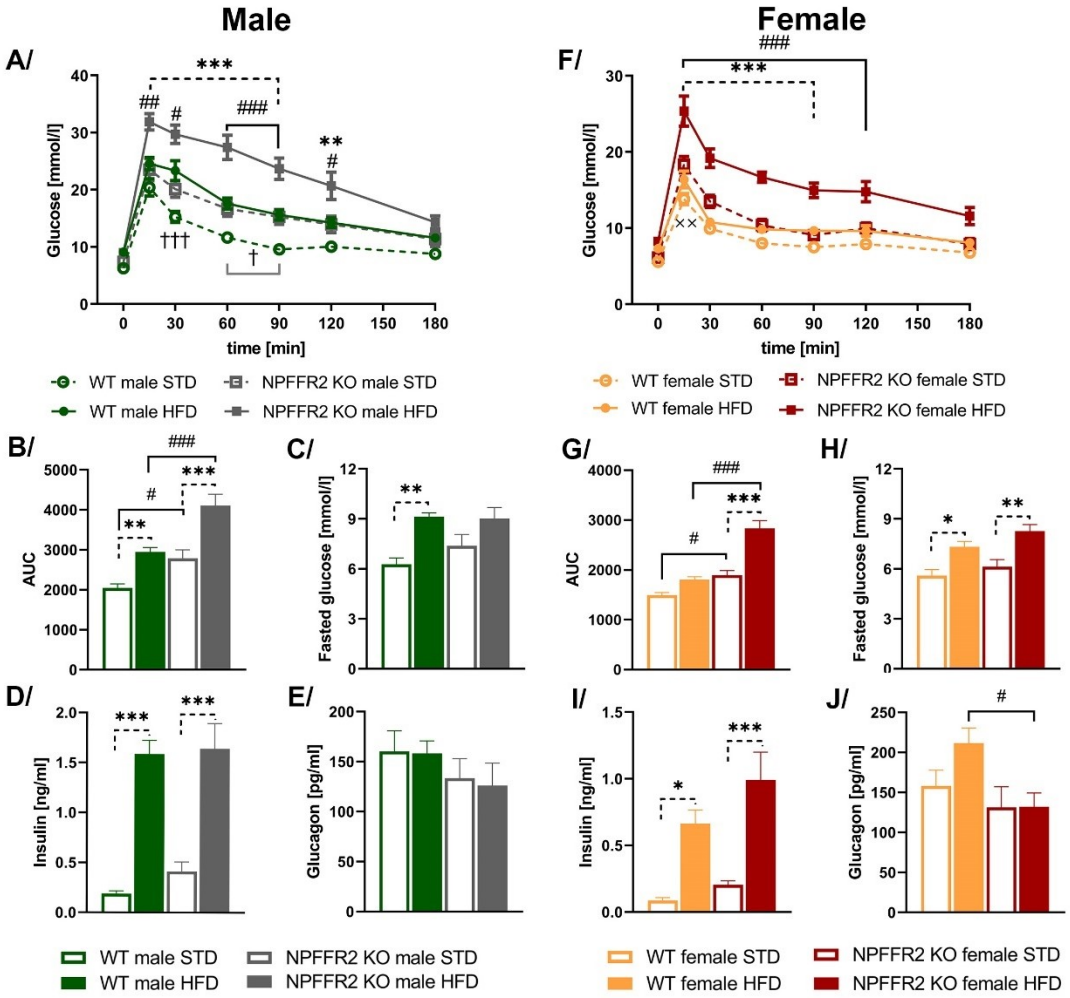

Figure 18: HFD-fed NPFFR2 KO mice exhibit severe glucose intolerance.
After oral glucose gavage (2 g/kg dosage), blood glucose excursions were seen in (**A**) males and (**F**) females. Data are expressed as the mean ± SEM (n = 10) and were determined by two-way ANOVA with Bonferroni post hoc test. † $p < 0.05$ and ††† $p < 0.001$ for WT mice fed a STD vs. HFD; ×× $p < 0.01$ for NPFFR2 KO vs. WT mice fed a STD; # $p < 0.05$, ## $p < 0.01$, and ### $p < 0.001$ for WT mice vs. NPFFR2 KO mice fed a HFD; ** $p < 0.01$ and *** $p < 0.001$ for NPFFR2 KO mice fed a HFD vs. NPFFR2 KO mice fed a STD. Area under the curve (AUC) from OGTT for (**B**) males and (**G**) females. Fasted glucose levels in (**C**) males and (**H**) females, insulin levels in (**D**) males and (**I**) females, and glucagon levels in (**E**) males and (**J**) females. Data are expressed as the mean ± SEM (n = 7–10) and were determined by one-way ANOVA with Bonferroni post hoc test. # $p < 0.05$, ## $p < 0.01$, and ### $p < 0.001$ for NPFFR2 KO vs. WT mice on the same diet; *$p < 0.05$, **$p < 0.01$, and ***$p < 0.001$ for STD vs. HFD mice of the same genotype.

4.3.4 NPFFR2 KO Mice on HFD Developed Disrupted Insulin Signaling in the Brain

HFD-fed NPFFR2 KO mice showed significantly decreased levels of important proteins involved in insulin signaling in the hypothalamus, such as PI3K regulatory subunit p85, PI3K regulatory subunit p110α, total Akt, and total AS160 (Akt substrate of 160 kDa) compared to their control WT mice (Fig. 19A, B). Additionally, the levels of p-AS160

(Ser588) in HFD-fed NPFFR2 KO males and p-Akt (Ser473) in HFD-fed NPFFR2 KO females were lower than those in their WT controls (Fig. 19A, B).

The same trend was observed in the brainstem of HFD-fed NPFFR2 KO males (Fig. 19C). Furthermore, it was found that in mice fed STD, but not HFD, the insulin signaling protein levels, such as PI3K regulatory subunit p85, p-Akt (Ser473), and p-AS160 (Ser588) were diminished in NPFFR2 KO females compared to WT (Fig. 19D). It is clear, that the glucose intolerance in NPFFR2 KO mice negatively impacted brain insulin signaling.

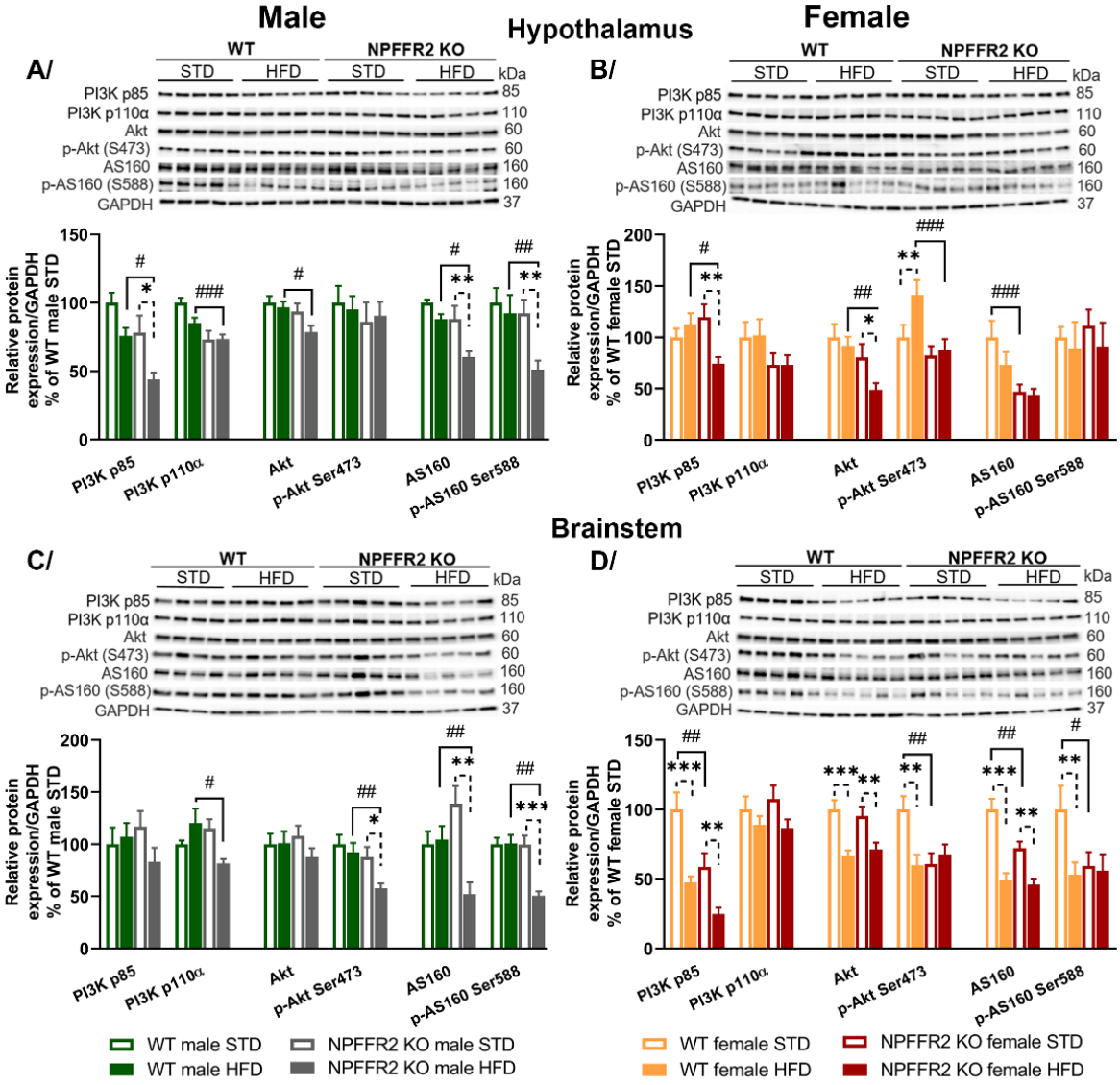

Figure 19: HFD-fed NPFFR2 KO mice have disrupted insulin signaling in the brain
Analysis of WB from hypothalamic (**A, B**) or brainstem (**C, D**) signaling. Densitometric quantification of immunoblots normalized to GAPDH. Data are expressed as the mean ± SEM (n = 4–5) and were determined by one-way ANOVA with Bonferroni post hoc test. # $p < 0.05$, ## $p < 0.01$, and ### $p < 0.001$ for NPFFR2 KO vs. WT mice on the same diet; *$p < 0.05$, **$p < 0.01$, and ***$p < 0.001$ for STD vs. HFD mice of the same genotype.

4.3.5 HFD-Fed NPFFR2 KO Mice did not Develop Fatty Liver but Show Worsened Hepatic Insulin Signaling

There was no difference in liver weight between NPFFR2 KO and WT mice on STD (Fig. 20A, D). NPFFR2 KO males on HFD had a lower liver weight compared to WT mice (Fig. 20A), which was in the line with their body weight (Fig. 17B). The HFD led to a significant increase in the liver weight in WT males and NPFFR2 KO females compared to their controls on STD (Fig. 20A, D).

Liver histology revealed no significant differences in the amount of fat in the livers of the NPFFR2 KO mice fed a STD compared to WT controls. Both WT and NPFFR2 KO mice of both sexes fed HFD showed an increase in fat in the livers compared to mice fed STD (Fig. 20B, C, E, F). In conclusion, the lack of the NPFFR2 gene did not affect the build-up of lipids in the liver.

Even though the *Npffr2* gene is not expressed in the liver of WT mouse, NPFFR2 deficiency in female mice indirectly impacted hepatic insulin signaling. Both male and female mice NPFFR2 KO fed HFD showed decreased insulin signaling when compared to WT mice but differences in female mice were more pronounced (Fig. 20G, H). NPFFR2 KO female fed a high-HFD displayed decreased levels of insulin signaling proteins, such as p85, phosphoinositide-dependent kinase (PDK), and total Akt, compared to WT female mice (Fig. 20H). There was also a similar trend in the levels of p-Akt, but the difference was not significant.

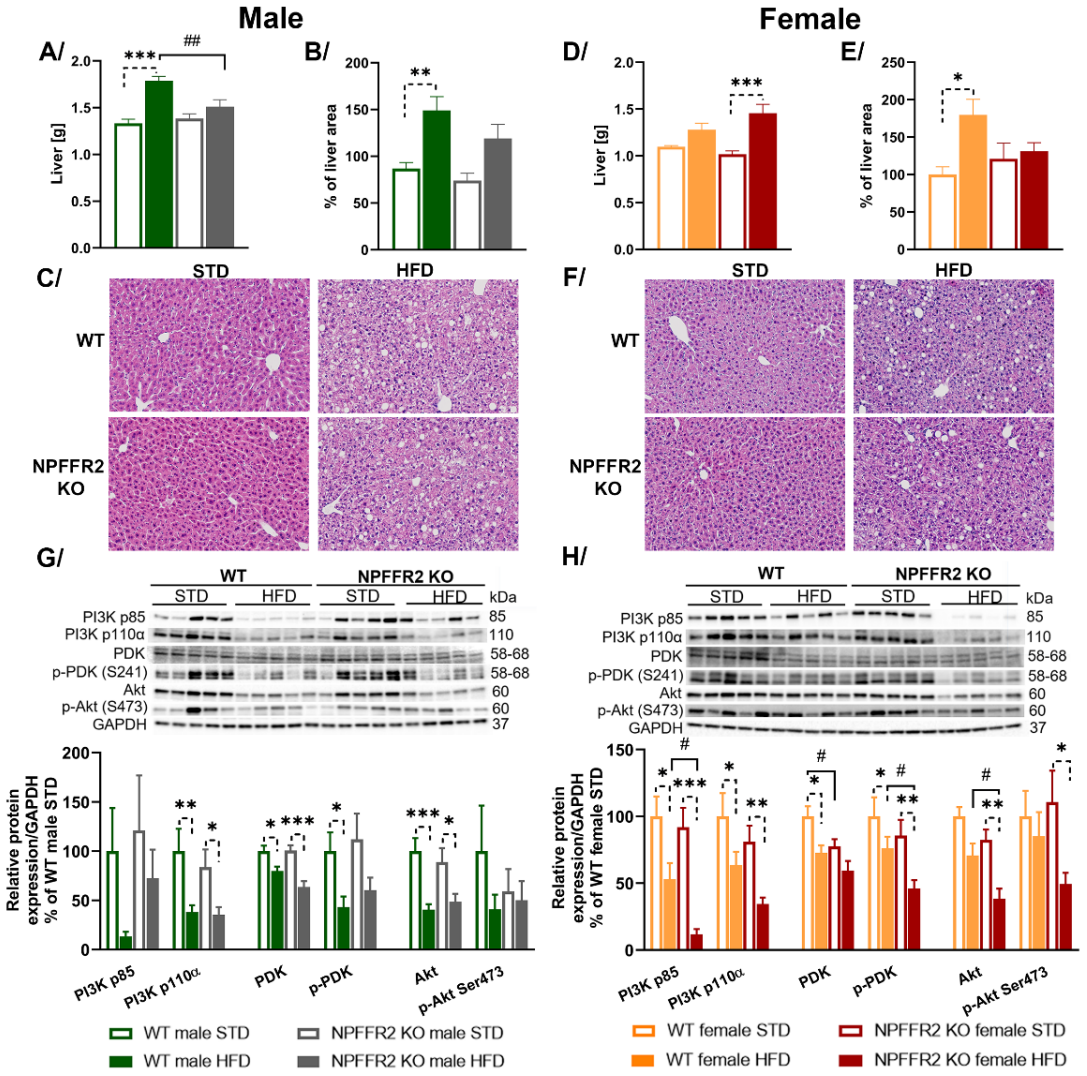

Figure 20: HFD-fed NPFFR2 KO mice exhibit impaired hepatic insulin signaling but no alterations in liver histology.
Liver weights in (**A**) males and (**D**) females. Data are expressed as the mean ± SEM (n = 10). Liver histology quantification in (B) males and (E) females as a percentage (%) of fat droplets in the liver area. Data are expressed as the mean ± SEM (n = 4–5). H&E staining of liver slices at a 200x magnification in representative photomicrographs of (**C**) men and (**F**) females. Hepatic insulin signal transduction pathway in (**G**) males and (**H**) females. Immunoblots have been quantified densitometrically and normalized to GAPDH. Data are expressed as the mean ± SEM (n = 5). All data were analyzed by one-way ANOVA with Bonferroni post hoc test. # $p < 0.05$, ## $p < 0.01$, and ### $p < 0.001$ for NPFFR2 KO vs. WT mice on the same diet; *$p < 0.05$, **$p < 0.01$, and ***$p < 0.001$ for STD vs. HFD mice of the same genotype.

4.4 GPR10/NPFFR2 KO Characterization Study

The results obtained in this chapter have not been published yet. The manuscript is in the preparation. Experiments were performed and analyzed by Ing. Alena Karnošová and RNDr. Veronika Strnadová, Ph.D.

4.4.1 GPR10/NPFFR2 Deletion Resulted in Anxiety-like Behavior in Female Mice fed HFD

PrRP has previously been recognized as a modulator of the HPA axis (Mochiduki et al., 2010). To identify any anxiety-like behavior or modifications in exploratory behavior the OF was conducted (Fig 21). Even though male WT mice on HFD showed a significant decrease in track lengths (Fig. 21B), no other significant changes were observed in the traveled distance. When compared to mice on STD, male dKO and WT mice on HFD showed lower exploratory behavior in the OF (Fig. 21A, C). Moreover, female dKO mice on either STD or HFD spent significantly less time in the center zone than WT controls (Fig. 21F, I). Female HFD-fed dKO mice displayed more pronounced anxiety-like behavior than mice fed STD (Fig. 21F, H, I).

Additionally, we performed the HP test and observed a similar nociceptive behavior latency (front paw licking) in both genotypes (Fig. 21I, J).

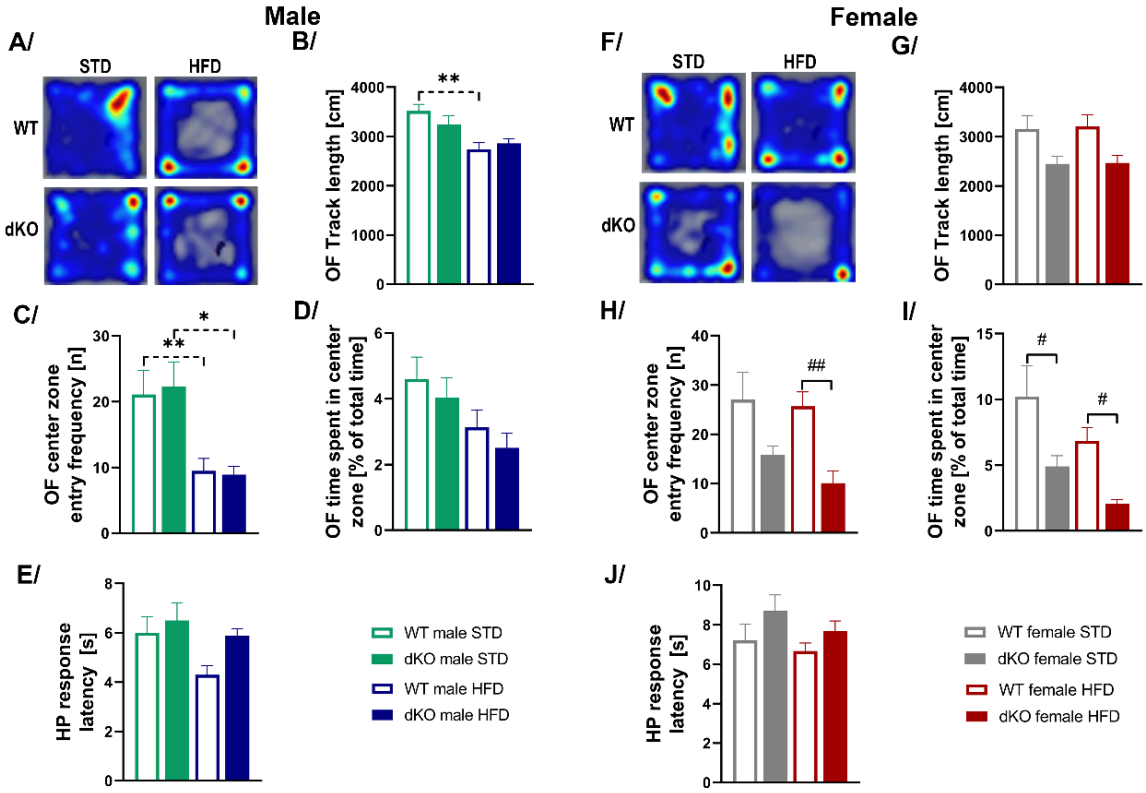

Figure 21: Behavioral experiments and pain perception experiments in dKO mice. Representative heat maps of WT and GPR10/NPFFR2 KO (dKO) mice showing time spent at different locations within the open field (OF) for (**A**) male and (**F**) female. Track length in the OF test for (**B**) males and (**G**) females, the frequency of entries to the OF center zone for (**C**) males and (**H**) females, % of total time (10 min) spent in the center zone in OF for (**D**) males and (**I**) females. Latency to pain perception (paw licking) in the hot plate (HP) test for (**E**) males and (**J**) females. Data are expressed as the mean ± SEM (n = 8-10) and determined by one-way ANOVA with Bonferroni post hoc test. *p < 0.05 and **p < 0.01 for STD vs. HFD mice of the same genotype and # p < 0.05, ## p < 0.01 for dKO vs. WT mice on the same diet.

4.4.2 GPR10/NPFFR2 Deletion Resulted in Late-onset Obesity in Male Mice fed STD and Female Mice fed HFD

The body weight was monitored during the whole experiment and at the end of the experiment, when the mice were 6 months old in a state of unrestricted feeding with STD or HFD, the weight of dissected organs, namely scWAT and gWAT, and liver was measured.

Male dKO mice fed STD had a considerably higher body weight than their WT controls (Fig. 22 A, B). When dKO male mice fed HFD, no changes in body weight were observed compared to their WT controls. Interestingly, dKO HFD-fed male mice exhibited significantly reduced white adipose tissue mass (Fig. 22C) and significantly decreased plasma leptin levels compared to HFD-fed WT mice (Fig. 22D).

Female dKO mice fed STD showed a growth curve and final body weight comparable to their WT control mice (Fig. 22 E, F). However, dKO female mice fed HFD showed significantly increased body weight compared to their WT controls on HFD (Fig. 22 E, F). Moreover, significantly increased scWAT and gWAT mass was observed in dKO female mice fed HFD (Fig. 22G) and as anticipated, they exhibited a significant increased plasma leptin level (Fig. 22H).

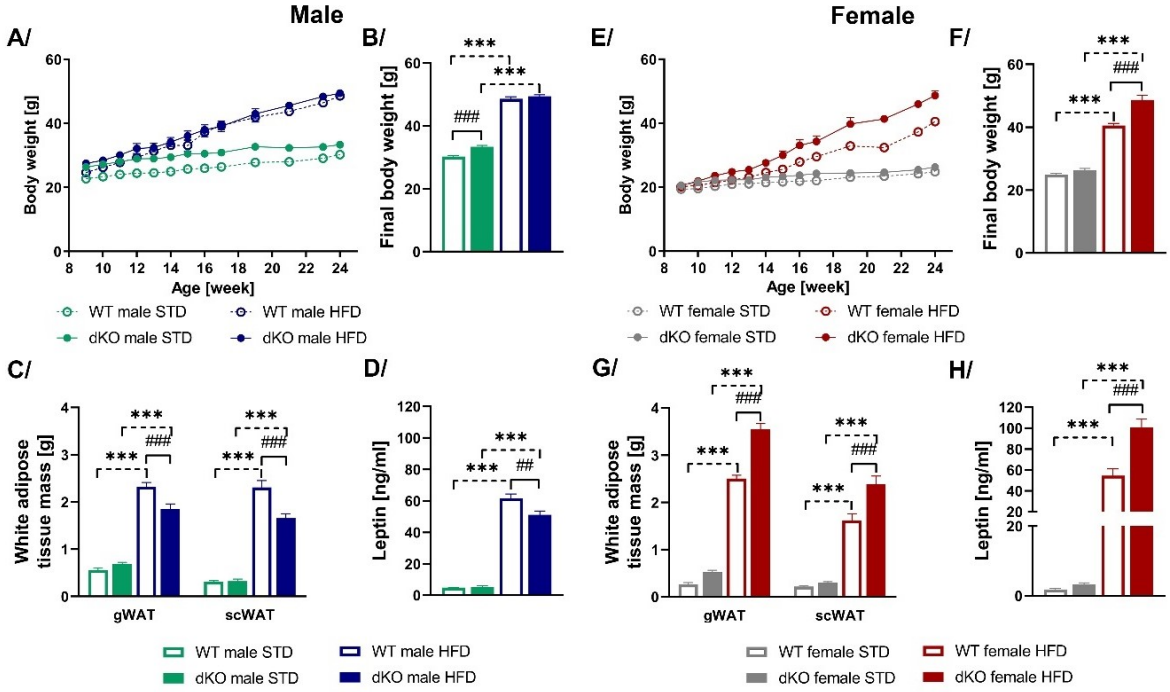

Figure 22: dKO female mice on HFD exhibit strong late-onset obesity.
Time course of body weight gain in (**A**) males and (**E**) females and final body weight in (**B**) males and (**F**) females of GPR10/NPFFR2 KO (dKO) mice on a STD or HFD. Weights of dissected subcutaneous white adipose tissue (scWAT) and gonadal white adipose tissue (gWAT) in (**C**) males and (**G**) females. Serum leptin levels in (**D**) males and (**H**) females. Data are expressed as

the mean ± SEM (n = 9-10) and determined by one-way ANOVA with Bonferroni post hoc test. *p < 0.05 and **p < 0.01 for STD vs. HFD mice of the same genotype and # p < 0.05, ## p < 0.01 for dKO vs. WT mice on the same diet.

The caloric intake between female groups fed either STD or HFD was not significantly different (Fig. 23B). Despite similar caloric intake dKO female mice fed HFD gained significantly more weight (Fig 22F). No changes between genotypes fed the same diet were also displayed in plasma total and active ghrelin levels in female mice (Fig. 23E, F).

Conversely, dKO male mice fed STD exhibited significantly increased caloric consumption (Fig. 23A), which is consistent with their higher end body weight (Fig. 22B). Moreover, significantly increased total and active ghrelin levels in plasma (Fig. 23C, D) in dKO male male fed STD suggest that dKO male mice have an increased motivation to eat.

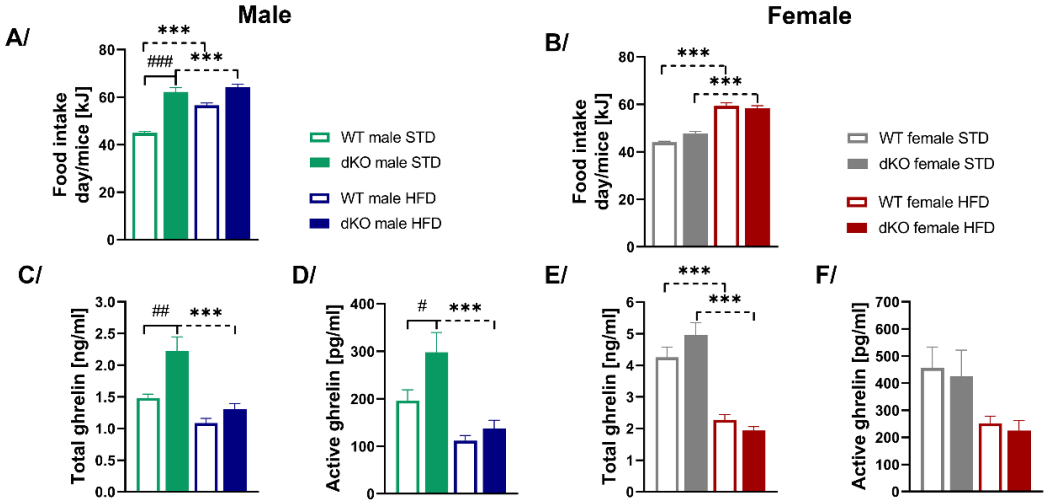

Figure 23: STD-fed dKO male mice displayed higher food caloric intake and ghrelin plasma levels.
Average daily caloric intake of WT and GPR10/NPFFR2 KO (dKO) (**A**) male and (**F**) female mice. Total ghrelin levels in (**C**) males and (**E**) females, and active ghrelin levels in (**D**) males and (**F**) females from plasma of free-fed mice. Data are expressed as the mean ± SEM (n = 8-10) and determined by one-way ANOVA with Bonferroni post hoc test. ***p < 0.001 for STD vs. HFD mice of the same genotype and # p < 0.05, ## p < 0.01 for dKO vs. WT mice on the same diet.

Metabolic parameters were determined from fasted blood plasma. Both dKO and WT mice on the HFD displayed elevated plasma cholesterol (Table 15). No significant changes between genotypes either on STD or HFD were observed in male mice. (Table 15). Female dKO mice on the STD had FFA levels compared to their WT controls. Moreover, dKO female mice fed HFD displayed significantly increased cholesterol levels in plasma (Table 15). This result is in line with increased final body weight and adipose tissue mass (Fig. 22 F-H).

Table 15. Plasma metabolic profile of dKO and WT mice

Group	TAG [mmol/l]	FFA [mmol/l]	Cholesterol [mmol/l]
WT male STD	0.80 ± 0.06	0.28 ± 0.01	2.80 ± 0.14
dKO male STD	0.74 ± 0.08	0.26 ± 0.02	3.07 ± 0.12
WT male HFD	0.82 ± 0.04	0.24 ± 0.02	6.67 ± 0.26 ***
dKO male HFD	0.80 ± 0.04	0.20 ± 0.01	6.82 ± 0.30 ***
WT female STD	0.61 ± 0.03	0.37 ± 0.05	2.63 ± 0.14
dKO female STD	0.60 ± 0.05	0.17 ± 0.02 ###	2.48 ± 0.16
WT female HFD	0.76 ± 0.04 *	0.19 ± 0.03 ***	4.46 ± 0.25 ***
dKO female HFD	0.74 ± 0.03 *	0.14 ± 0.01	6.41 ± 0.16 ***, ###

Triglyceride (TAG), free fatty acid (FFA). Data are expressed as the mean ± SEM (n = 6–10) and determined by one-way ANOVA with Bonferroni post hoc test. * $p < 0.05$, and *** $p < 0.001$ for STD vs. HFD of the same genotype; ### $p < 0.001$ for GPR10/NPFFR2 KO (dKO) vs. WT mice on the same diet.

4.4.3 Female HFD-fed GPR10/NPFFR2 Mice Showed Severe Glucose Intolerance

Since NPFFR2-deficient mice on HFD displayed severe glucose intolerance after glucose gavage, OGTT was tested as well in dKO mice. Interestingly, dKO male mice did not show significantly higher glucose excursion (Fig.24A) and AUC (Fig.24C) comparing to WT controls either on STD or HFD. On the contrary, female HFD-fed dKO mice revealed significantly elevated blood glucose during the OGTT (Fig.24B) and significantly higher AUC (Fig.24E) compared to WT mice. Moreover, dKO female mice fed HFD showed significantly increased glucose levels after 6 hours of fasting followed by glucose gavage (Fig.24F). This was not observed in dKO male mice (Fig.24D). Furthermore, dKO mice of both sexes of dKO mice fed the HFD showed significantly elevated insulin levels in fasted plasma (Fig.24G, H).

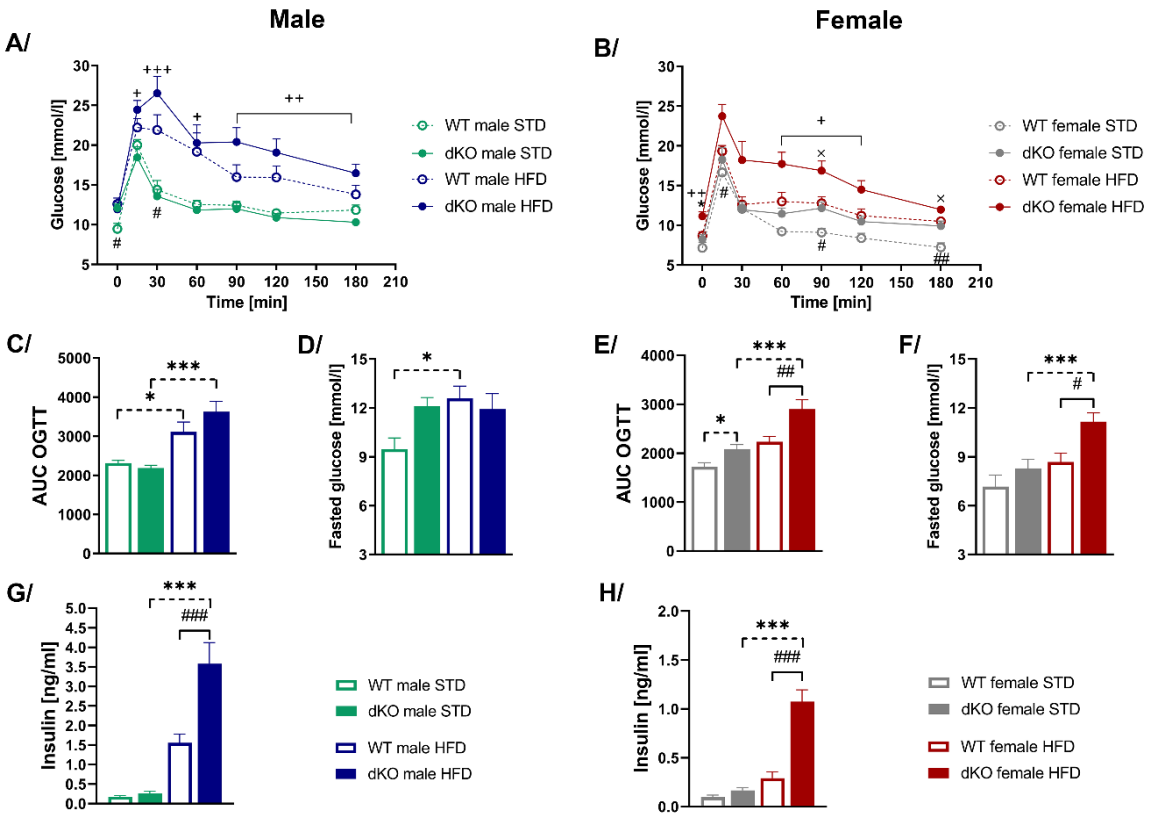

Figure 24: Female HFD-fed dKO mice exhibit severe glucose intolerance.
After oral glucose gavage (2 g/kg dosage) of WT and GPR10/NPFFR2 KO (dKO) mice, blood glucose excursions were seen in (**A**) males and (**B**) females. Data are expressed as the mean ± SEM (n = 10) and were determined by two-way ANOVA with Bonferroni post hoc test. × $p < 0.05$ for dKO vs. WT mice fed a STD; # $p < 0.05$, and ## $p < 0.01$ for WT mice fed a STD vs. WT fed a HFD; + $p < 0.05$, ++ $p < 0.01$ and +++ $p < 0.001$ for dKO mice fed a HFD vs. dKO mice fed a STD; * $p < 0.05$, for dKO mice fed a HFD vs. WT mice fed a HFD. Area under the curve (AUC) from OGTT for (**C**) males and (**E**) females. Fasted glucose levels in (**D**) males and (**F**) females. Data are expressed as the mean ± SEM (n =). Insulin levels in (**G**) males and (**H**) females and data are expressed as the mean ± SEM (n = 6–10). Data were determined by one-way ANOVA with Bonferroni post hoc test. # $p < 0.05$, ## $p < 0.01$, and ### $p < 0.001$ for dKO vs. WT mice on the same diet; *$p < 0.05$, **$p < 0.01$, and ***$p < 0.001$ for STD vs. HFD mice of the same genotype.

4.4.4 HFD-Fed GPR10/NPFFR2-Deficient Female Mice Developed Fatty Liver

The liver weight was not different between dKO and WT mice fed STD (Fig. 25A, D). On the other hand, both female and male dKO mice fed HFD exhibited significantly increased liver weight compared to their WT controls. The quantitation of lipid content in the liver did not show differences between genotypes fed STD (Fig. 25B, C, E, F). Although the histological examination of liver tissue samples showed increased liver steatosis in male mice fed an HFD, no differences were observed between WT and dKO mice (Fig. 25B, C). On the other hand, female dKO mice that were fed HFD showed an increased accumulation of fat droplets in their livers compared to their WT controls (Fig. 25E, F).

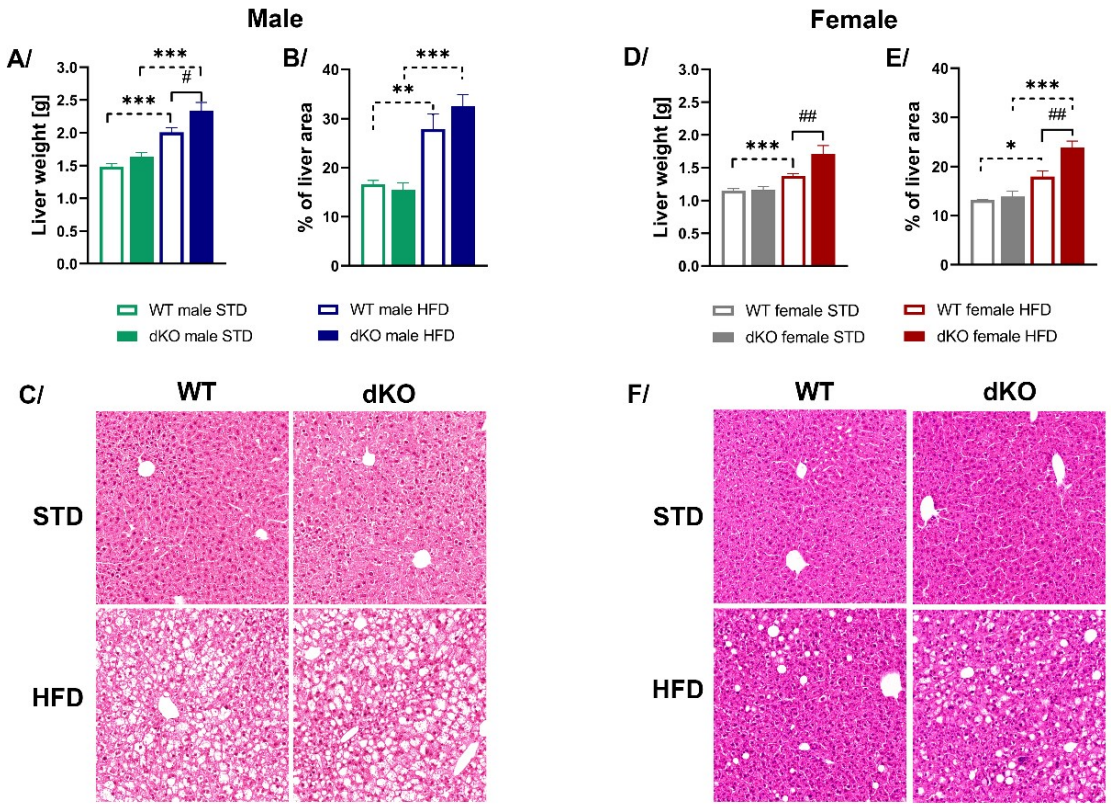

Figure 25: Female HFD-fed dKO mice showed increased accumulation of fat droplets. Liver weights in (**A**) males and (**D**) females. Data are expressed as the mean ± SEM (n = 10). Liver histology quantification in (**B**) males and (**E**) females as a percentage (%) of fat droplets in the liver area. Data are expressed as the mean ± SEM (n = 4–5). H&E staining of liver slices at a 200x magnification in representative photomicrographs of (**C**) men and (**F**) females. All data were analyzed by one-way ANOVA with Bonferroni post hoc test. # $p < 0.05$, ## $p < 0.01$, and ### $p < 0.001$ for dKO vs. WT mice on the same diet; *$p < 0.05$, **$p < 0.01$, and ***$p < 0.001$ for STD vs. HFD mice of the same genotype.

Even though no significant changes in hepatic PI3K/Akt/glycogen synthase kinase-3β (GSK-3β) pathway were observed in male mice of both genotypes fed STD and HFD (Fig. 26A), female mice on HFD displayed significantly decreased protein levels of PI3K p110α and Akt (Fig. 26B). Moreover, dKO female fed HFD mice showed significantly increased total protein levels of hepatic GSK-3β (Fig. 26B), which is involved in regulation of glycogen metabolism and insulin signaling.

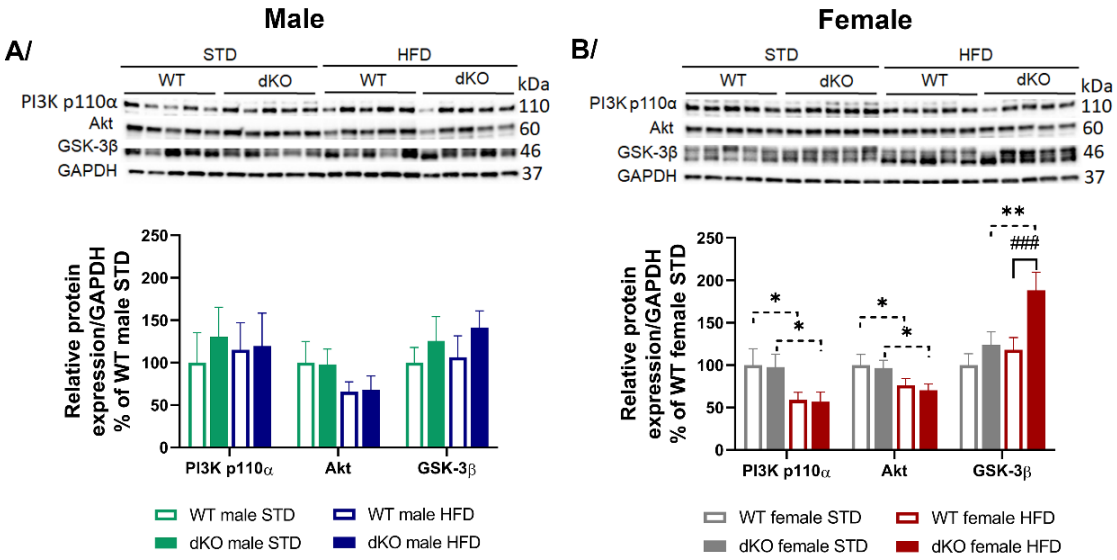

Figure 26: Female dKO mice fed HFD showed impaired hepatic PI3K/Akt/GSK-3β signaling.

Hepatic PI3K/Akt/GSK-3β signaling pathway in (**A**) males and (**B**) females. Immunoblots have been quantified densitometrically and normalized to GAPDH. Data are expressed as the mean ± SEM (n = 5). All data were analyzed by one-way ANOVA with Bonferroni post hoc test. # $p < 0.05$, ## $p < 0.01$, and ### $p < 0.001$ for NPFFR2 KO vs. WT mice on the same diet; *$p < 0.05$, **$p < 0.01$, and ***$p < 0.001$ for STD vs. HFD mice of the same genotype.

5. DISCUSSION

Obesity is a major health concern worldwide, and current treatments such as diet and exercise modifications and pharmacotherapy have limitations. The development of lipidized analogs of peptides has been a significant advancement in this field, as it has allowed for effective peripheral administration of these peptides.

Anorexigenic neuropeptides have a high potential to become a treatment option for obesity. The neuropeptide PrRP can reduce food intake after administration to the 3V (Lawrence et al., 2000; Lawrence et al., 2002), but when PrRP is administered peripherally, the ability to reduce food intake is lost. Lipidization of peptides helps enhance their stability in the bloodstream by binding to albumin and facilitates their central effect after peripheral administration. Lipidized analog of GLP-1 peptide is a prime example of this concept. It was initially used to treat type 2 diabetes mellitus and has recently been used to treat obesity as well (Gault et al., 2011; Larsen et al., 2001).

Our previous acute studies have demonstrated a substantial reduction in food intake in mice after peripheral administration of lipidized PrRP (Maletinska et al., 2015; Prazienkova et al., 2017). Moreover, DIO mice revealed reduction in cumulative food intake and body weight after chronic administration of lipidized PrRP (Pirnik et al., 2015; Pirnik et al., 2018; Prazienkova et al., 2017) and palm-PrRP31 and palm^{11}-PrRP31 emerged as key analogs in subsequent studies.

Recent studies have suggested that PrRP and its receptors may play a role in several physiological functions. However, the exact mechanisms underlying these effects are not well understood and require further investigation.

5.1 The Structure-Activity Relationship Study

In a previous study, we showed that lipidization of PrRP20 and PrRP31 with fatty acids of different lengths resulted in the preservation of the binding affinity towards GPR10 and an increase in their binding affinity towards NPFFR2. For the first time, we demonstrated that the s.c. administration of myristoylated-PrRP20, and palmitoylated- or stearoylated-PrRP31 analogs led to a significant reduction in food intake in overnight fasted mice (Maletinska et al., 2015). Even though PrRP, GPR10, and NPFFR2 are often linked with modulation of anxiety-like behavior (Lin and Chen, 2019; Maruyama et al., 2001; Matsumoto et al., 2000), no changes were observed after s.c. administration of palm-PrRP31 and myr-PrRP20 (Maletinska et al., 2015).

In vitro structure-activity study by Boyle *et al.* showed that last seven amino acids the C-terminal segment are essential for the biological activity of PrRP (Boyle et al., 2005). We previously designed several lipidized analogs with modifications at Phe^{31} using non-coded amino acids with an aromatic side chain. Analogs with 1Nal, $PheCl_2$, $PheF_5$, $PheNO_2$ or Tyr in position 31 displayed affinity towards the GPR10 receptor in nanomolar concentrations and $PheCl_2^{31}$PrRP31 palmitoylated at N-terminus also showed long lasting anorexigenic effect (Prazienkova et al., 2016). In this study, we designed a series of analogs with palmitoyl attached in positions 1 or 11 via various linkers and/or with $PheCl_2$ modification at the C-terminus.

Lipidization increased affinity towards GPR10 and NPFFR2. Moreover, new analogs 1-3 and analog 12 displayed really strong agonist activity at GPR10. In the off-target study, $palm^{11}$-PrRP31 and palm-PrRP31 revealed increased affinity towards NPFFR1 comparing to natural PrRP31 (more in following chapter 5.2; published in (Karnosova et al., 2021)). Therefore, we decided to study the affinity of these novel PrRP31 analogs towards NPFFR1 and our goal was to design analogs with similar or reduced affinity for NPFFR1 as natural PrRP31 in order to prevent any potential side effects. With the exception of $palm^{11}$-TTDS-PrRP31, and analogs 1-3, 6 and 7, the binding affinity of lipidized PrRP31 analogs towards NPFFR1 remained comparable to the natural PrRP31 or was decreased.

Analogs 1, 2, 8, 9, and 12 displayed the strongest anorexigenic effects in fasted lean mice. Analog 12, with a $PheCl_2$ modification at C-terminus and palmitoyl attached through the TTDS linker to Lys^{11}, displayed high affinity for receptors GPR10 and NPFFR2, strong agonist activity at GPR10, and had the most potent anorexigenic properties. Therefore, it was further tested in a chronic experiment in DIO mice, where $palm^{11}$-PrRP31 was used as a comparator. Analog 12 and $palm^{11}$-PrRP31 decreased body weight and adiposity after 3-week long treatment, but the effect of Analog 12 on body and adipose tissues weight showed to be more pronounced (results published in (Strnadova et al., 2023)).

Our results indicate that analog 12 could be a promising compound for treating obesity. However, stability testing in rat plasma showed that analogs with the TTDS linker had shorter stability compared to those without a linker or with a γE linker (Strnadova et al., 2023). There is the possibility that only small fragments of this analog after digestion in the plasma, are sufficient to mediate the anorexigenic effect, but this hypothesis must be further tested.

5.2 The Affinity for and Activity at Other Potential Off-Target Receptors of Lipidized PrRP31 Analogs

PrRP31 has a high affinity for its receptor GPR10, but it also binds to another receptor from the RF-amide peptide family receptor, NPFFR2 (Engstrom et al., 2003; Maletinska et al., 2015). PrRP and both its receptors, GPR10 and NPFFR2, are present in the brainstem and hypothalamus, regions that play a role in regulating appetite and energy expenditure (for summary of the distribution, see the Table 16). Furthermore, NPFFR1, another receptor for NPFF, is generally more abundant in the CNS than NPFF2 receptors. NPFFR1 and NPFFR2 share high amino acid sequence similarity (Bonini et al., 2000). Therefore, NPFFR1 was tested in this study as a potential target for the lipidized PrRP31 analogs using the two most potent previously published analogs palm-PrRP31 and palm^{11}-PrRP31 (Maletinska et al., 2015; Prazienkova et al., 2017).

Table 16. Summary of the distribution of PrRP, NPFF, and its receptors in the CNS of rodents.

		PrRP	GPR10	NPFF	NPFFR1	NPFFR2
Hypothalamus	ARC	+		+	+	+
	LHA			+		+
	VMN	+	+	+	+	
	DMN	+	+	+	+	+
	PVN	+	+	+	+	+
	PerVN	+	+		+	
	Anterior nucleus				+	
	Supraoptic nucleus			+	+	
	Preoptic nucleus	+			+	+
	Suprachiasmatic nucleus					+
Amygdala				+	+	+
Thalamus			+		+	+
Hippocampus				+	+	+
Brainstem	NTS	+	+	+	+	+
	Medulla oblongata	+	+	+	+	+
Spinal cord		+		+	+	+

(Vilim et al., 1999, Goncharuk et al., 2006, Nystedt et al., 2006, Zhang et al., 2018, Lin et al., 2016b, Fujii et al., 1999, Roland et al., 1999, Ibata et al., 2000, Iijima et al., 1999, Minami et al., 1999, Yano et al., 2001, Bonini et al., 2000, Hinuma et al., 2000, Liu et al., 2001, Higo et al., 2021, Waqas et al., 2017, Anko et al., 2006, Parker et al., 2000, Goncharuk and Jhamandas, 2008).

The palmitoylation enhanced the binding and agonist properties of both PrRP31 analogs to GPR10 and NPFFR2 receptors. The palm^{11}-PrRP31 analog had a stronger binding affinity for and agonist activity at the GPR10 receptor compared to the palm-PrRP31. They both revealed a stronger affinity towards NPFFR1 than natural PrRP31, hence NPFFR1 is now considered as a potential target of lipidized PrRP31 analogs. The potential for targeting NPFFR1 with lipidized PrRP31 analogs opens up new questions for the research of PrRP31 signaling and various physiological processes linked to NPFFR1.

The GPR10 receptor was discovered to have a high sequence identity with the NPY receptor family, with the highest homology to the Y1 receptor (Marchese et al., 1995). Moreover, also NPFFR2 has a high sequence similarity with NPY receptors and is located near the gene cluster for Y5, Y1, and Y2 receptors, suggesting NPFFR2 involvement in feeding regulation (Bonini et al., 2000). Neither PrRP31 nor its palmitoylated forms showed any binding to the Y2 receptor within the measured concentration range, but palm-PrRP31 showed low affinity towards the Y1 receptor. Palmitoylation increased affinity to and activity for the Y5 receptor, with palm-PrRP31 having much higher off-target activity at this receptor than palm^{11}-PrRP31. Additionally, we further tested palm^{11}-PrRP31 and the results showed the potential of palm^{11}-PrRP31 to be a positive allosteric modulator at the Y5 receptor, indicating that the palmitoylated PrRP31 analogs could partly regulate food intake also through the Y5 receptor.

the off-target properties of the palmitoylated PrRP31 analogs on the receptor of the orexigenic peptide ghrelin were studied. Palm-PrRP31 had a higher affinity for the GHSR receptor than palm11-PrRP31, but both analogs had negligible activity on GHSR.

NPFF and its receptors are connected with regulation of pain nociception (Gicquel et al., 1992; Gouarderes et al., 1993). Despite having a strong binding affinity for NPFF receptors, the ability of PrRP to influence pain perception through NPFFR1 and NPFFR2 has not been established yet. Previously, one study showed that PrRP reduced sensitivity to normally non-painful touch (tactile allodynia) in rats (Kalliomaki et al., 2004). In our study, no agonist or antagonist effects of PrRP31 palmitoylated analogs were seen at the MOR, DOR, and ORL-1 opioid receptors. Even though both analogs displayed very low affinity towards the KOR receptor, and they had only negligible ability to activate the KOR receptor, palm-PrRP31 showed stronger affinity and agonist activity towards KOR then palm^{11}-PrRP31. Overall, our results suggest that the potential pain-modulating effects of lipidized PrRP analogs would not be associated with opioid receptors.

Based on these result, palm^{11}-PrRP31 is a more suitable option than palm-PrRP31 for the potential treatment of obesity and neurodegenerative diseases due to its reduced potential for unwanted effects caused by increased off-target activity (results published in (Karnosova et al., 2021)).

5.3 Mechanism of Action of Palmitoylated PrRP31 Analogs *In Vitro*

Using CHO-K1 cells transfected with GPR10, NPFFR2 or NPFFR1 receptors the intracellular mechanism of action was studied. From previous studies, there was no clear answer whether GPR10 is coupled with Gq, Gi, or Gs proteins. After PrRP31 analogs stimulation of cells transfected with GPR10, we observed activation of intracellular Ca^{2+}, no activation of PKA, and partial inhibition of ERK and c-Fos activation after pretreatment with PTX. These results align with the findings of Hinuma *et al*., who demonstrated that GPR10 activation is mediated through both Gq and Gi/o, but not through Gs (Hinuma et al., 1998).

Hayakawa *et. al* previously suggested that activation of Akt by GPR10 is mediated through Gβγ subunits (Hayakawa et al., 2002). Because our results show that PTX completely inhibited phosphorylation of Akt in cells with GPR10 hence, the activation is mediated through the α subunit of Gi/o protein rather than Gβγ subunits. Moreover, we observed significantly increased phosphorylation of Akt at Thr308 and Ser473 in CHO-K1 cells that expressed GPR10, NPFFR2, and NPFFR1 after stimulation with palmitoylated PrR31 analogs.

Previously it was reported that PrRP activates members of the MAPK family, JNK and ERK, in GH3 cells (Kimura et al., 2000). Our findings demonstrate that palmitoylated analogs stimulated the activation of ERK, JNK, and p38, members of the MAPK family, in cells expressing GPR10, NPFFR2, and NPFFR1. MAPK are involved in a variety of cellular processes such as migration, cell growth, differentiation, and apoptosis (Sun et al., 2015). The phosphorylation of JNK and ERK can lead to the formation of the activator protein 1 (AP-1) complexes by activation of c-Fos and c-Jun transcription factors. The formation of AP-1 complexes is required to permit G1/S transition and cell cycle progression and hereby can promote the cellular processes mentioned above (Cargnello and Roux, 2011). Significant activation of c-Fos and c-Jun was observed after the cells with GPR10 and NPFFR2 were stimulated with PrRP31 and its palmitoylated analogs. In cells with NPFFR1, only palm-PrRP31 caused significant induction of c-Fos and c-Jun.

CREB can modulate gene expression in response to cellular signals which plays a role in the processes, such as memory formation, cell proliferation, differentiation, neuronal survival, or glucose metabolism (Wen et al., 2010). The phosphorylation of CREB was significantly increased in cells expressing GPR10 and NPFFR2 when stimulated with PrRP31 and its palmitoylated analogs and palm-PrRP31 also showed higher activity in cells transfected with NPFFR1.

The possible intracellular mechanism of action of lipidized PrRP31 analogs was suggested in the transduction pathway scheme (Fig. 27). Results in this chapter published in (Karnosova et al., 2021)).

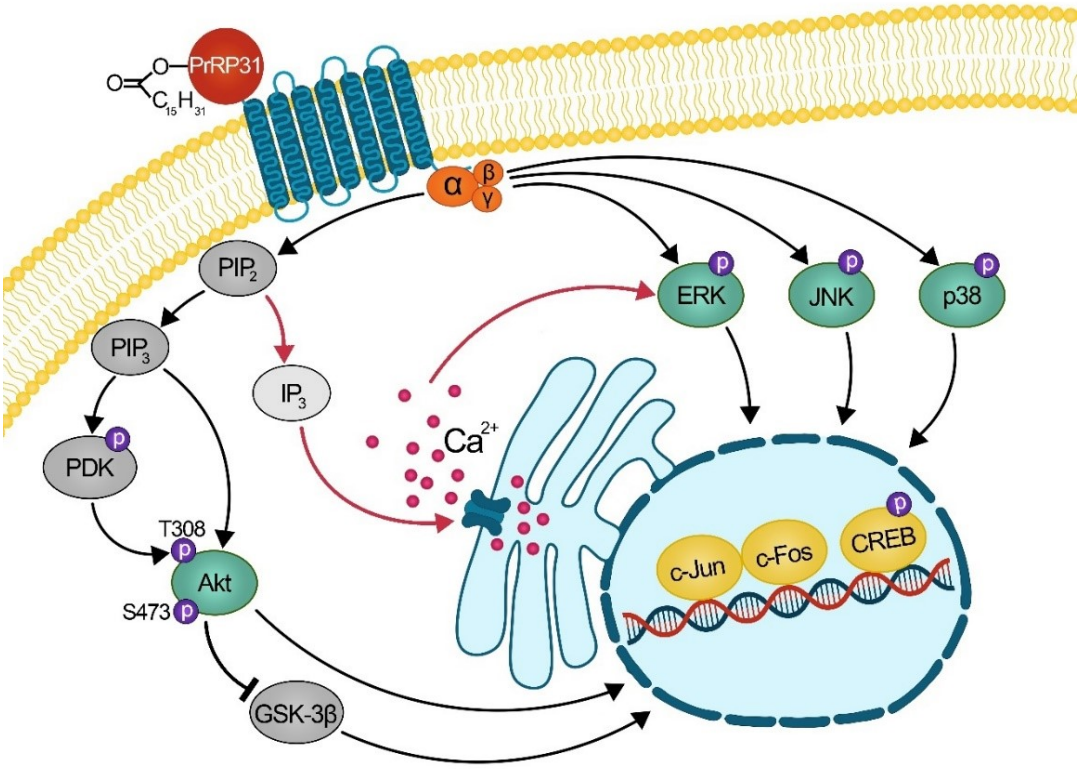

Figure 27: Scheme of mechanism of action of palmitoylated PrRP31 analogs (modified from (Karnosova et al., 2021)**.**
Black arrows symbolize mechanism of action through GPR10, NPFFR2 and NPFFR1 and red arrows only through GPR10. ERK, extracellular-signal-regulated kinase; JNK, c-Jun N-terminal kinase; CREB, cAMP-responsive element binding protein; PIP2, phosphatidylinositol 4,5-bisphosphate; IP3, inositol 1,4,5-triphosphate; PIP3, phosphatidylinositol (3,4,5)-trisphosphate; PDK, phosphoinositide-dependent kinase 1; Akt, protein kinase B.

5.4 Characterization Studies of Mice with Either NPFFR2 or GPR10/NPFFR2 Deletion

Because PrRP31 and its lipidized analogs exhibit strong dual agonist properties towards GPR10 and NPFFR2 receptors (Engstrom et al., 2003; Maletinska et al., 2015), we aimed

to characterize the impact of NPFFR2 deletion and GPR10/NPFFR2 (dKO) deletion in mice of both sexes fed either STD or HFD.

5.4.1 The Impact of NPFFR2 Deletion on Mice of Both Sexes Fed Either STD or HFD

As previously stated, the NPFFR2 KO showed a decrease in anxiety-like behavior in response to a single prolonged stress (Lin et al., 2020). Conversely, over-expression of NPFFR2 in mice led to increased depression- and anxiety-like behavior and a reduction in neurogenesis of neural stem cells caused by chronic stress (Lin et al., 2016b). In this study, WT and NPFFR2 KO mice fed HFD revealed reduced willingness to explore and a tendency to avoid open areas, but no difference was observed between the genotypes. Therefore, NPFFR2 deletion have no impact on behavior.

Both sexes of NPFFR2-deficient mice fed a STD revealed a lean phenotype. When given HFD, NPFFR2 KO male mice displayed reduced body weight, adipose tissue mass and liver weight, in addition to lower plasma leptin levels compared to WT controls. In contrary, study by Zhang *et al.* showed decreased body weight of male mice with NPFFR2 deletion fed STD, but when they fed HFD they revealed increased body weight, adipose tissue mass and leptin levels in serum (Zhang et al., 2018).

It has been found that NPFF directly regulates glucose balance. NPFF deletion led to improved glucose tolerance and lower blood glucose levels. Moreover, Zhang *et al.* suggested that signaling of NPFF mediated by NPFFR2 in the central nervous system modulate vagal output to peripheral tissues, including those crucial for controlling glucose metabolism (Zhang et al., 2022b). Our study revealed a significant impaired glucose tolerance in NPFFR2 KO male and female mice. Additionally, when given HFD, NPFFR2-deficient mice showed substantially greater glucose excursions compared to WT controls, without alterations in fasted glucose levels and plasma insulin levels between genotypes. The absence of NPFFR2 clearly resulted in a pronounced decrease in the ability to maintain glucose homeostasis, indicating the crucial role of this receptor in regulating blood glucose levels.

Earlier study had demonstrated that WT mice fed HFD exhibited a significant reduction in hypothalamic *Npffr2* expression. Additionally, HFD-fed mice also exhibit decreased *Npy* expression and increased *Pomc* expression in the ARC (Zhang et al., 2018). Given that the NPFFR2-deficient mice displayed pronounced glucose intolerance and that NPFFR2 is extensively found in the CNS (for summary of the distribution see the Table

16), we investigated insulin signaling in the hypothalamus and brainstem. NPFFR2 KO mice on HFD showed decrease in insulin signaling proteins levels leading to a disrupted central PI3K/Akt signaling pathway in the hypothalamus and brainstem. Moreover, female NPFFR2 KO mice fed HFD showed also impaired hepatic PI3K/Akt signaling. The results highlighted the importance of NPFFR2 in activation of kinases implicated in insulin signaling cascade. Collectively, these findings suggest that NPFFR2 plays a critical role in the regulation of energy balance and that dysregulation of this receptor together with increased caloric intake may contribute to metabolic disorders.

5.4.2 The Impact of GPR10/NPFFR2 Deletion on Mice of Both Sexes Fed Either STD or HFD

Previously, we characterized GPR10-deficient mice to understand the impact of the deletion on energy metabolism and to elucidate the mechanism of PrRP31 action through the GPR10 receptor (Prazienkova et al., 2021). Results from our GPR10 KO (Prazienkova et al., 2021) and NPFFR2 KO studies relevant for this study are summarized in the Fig. 28.

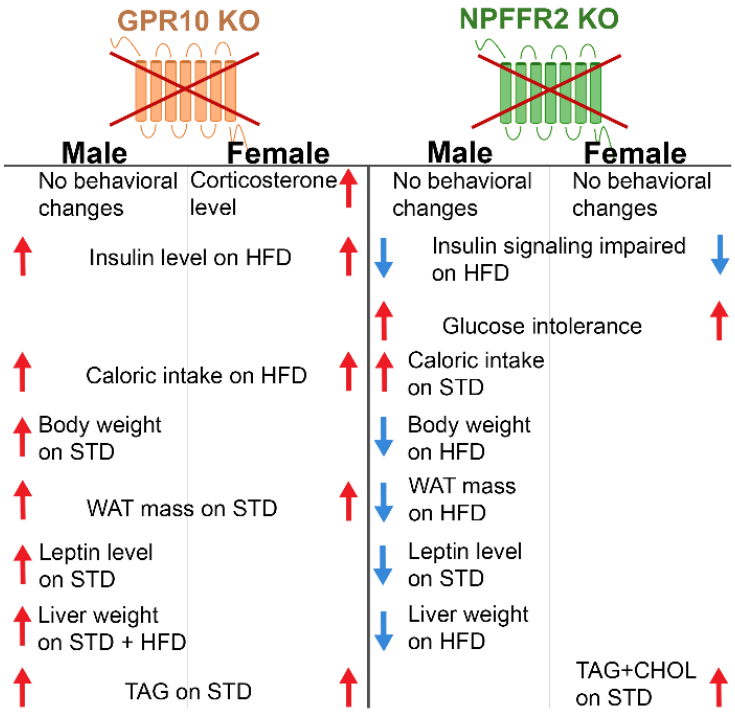

Figure 28: Overview of the results obtained from our GPR10 KO and NPFFR2 KO studies. The summary of the results from the GPR10 KO study is based on the research conducted by (Prazienkova et al. in 2021). WAT, white adipose tissue; TAG, triacylglycerol; STD, standard diet; HFD, high-fat diet; CHOL, cholesterol.

Male mice lacking GPR10 did not exhibit any signs of anxiety-like behavior. Although behavioral tests were only conducted on male mice, female mice lacking GPR10 showed elevated levels of corticosterone in their blood, indicating that deleting GPR10 may influence anxiety-like behavior in female mice (Prazienkova et al., 2021). Since NPFFR2 KO mice did not display any alterations in behavior, we speculated that male GPR10/NPFFR2-deficient mice would also not demonstrate any indications of anxiety-like behavior. As we expected no behavioral differences were observed between male WT controls and dKO mice. On the other hand, female dKO mice displayed increased anxiety-like behavior when fed STD and even more pronounced when fed HFD. Based on our previous results (Prazienkova et al., 2021) this behavior change could be caused by deletion of GPR10 rather than NPFFR2 receptor.

The outcomes of GPR10/NPFFR2-deficient mice correspond with the results obtained earlier from phenotyping studies with GPR10 KO (Prazienkova et al., 2021) and NPFFR2 KO (chapter 5.4.1) mice. In the study by Prazienkova *et al*. we showed that moderate obesity in GPR10 KO mice was more prominent in males than in females as a result of higher adiposity and increased plasma leptin level (Prazienkova et al., 2021). These results are in line with earlier studies (Bjursell et al., 2007; Gu et al., 2004). Moreover, in the study by Gu *et al.* GPR10-deficient male mice exhibited increased food consumption (Gu et al., 2004). Our study with NPFFR2 KO male (chapter 5.4.1) mice fed HFD showed decreased body weight compared to WT controls. Male dKO mice showed increased final body weight, energy intake, and ghrelin levels on STD, but when fed HFD the body and WAT weight were significantly decreased compared to their WT controls. Moreover, deletion of both receptors resulted in late-onset obesity in female mice fed HFD.

As previously mentioned (chapter 5.4.1) NPFFR2 KO mice had strong glucose intolerance when fed HFD. On the other hand, GPR10 KO mice on HFD exhibited significantly increased insulin plasma levels (Prazienkova et al., 2021). Hence, it is not unexpected that GPR10/NPFFR2-deficient mice showed impaired glucose tolerance on HFD along with elevated levels of insulin. Increased insulin levels indicate compensatory mechanisms to overcome the reduced insulin sensitivity, which led to hyperinsulinemia. An increased protein level of hepatic GSK-3β and insulin level suggest reduced insulin sensitivity in GPR10/NPFFR2-deficient female mice on HFD. This can subsequently lead to inhibition of the production of glycogen and glucose cannot be efficiently stored as

glycogen (Leavens and Birnbaum, 2011). This resulted in hyperglycemia in dKO female mice.

6. SUMMARY

A series of analogs with palmitoyl attached in positions 1 or 11 were designed and tested for affinity towards GPR10 and NPFFR2, as well as their anorexigenic effects. Analog 12, with a $PheCl_2$ modification at C-terminus and palmitoyl attached through the TTDS linker to Lys^{11}, displayed high affinity for receptors GPR10 and NPFFR2 and potent anorexigenic properties. Moreover, it showed only slightly increased affinity for NPFFR1 receptor compared to natural PrRP31. Analog 12 was further tested in a chronic experiment in DIO mice and was found to be a promising compound for obesity treatment.

The palmitoylation of PrRP31 analogs increased their binding and agonist properties for both GPR10 and NPFFR2 receptors. The palm^{11}-PrRP31 analog showed a stronger binding affinity towards GPR10 compared to palm-PrRP31. Both analogs exhibited a stronger affinity towards NPFFR1 than natural PrRP31, making NPFFR1 another potential target for lipidized analogs.

The GPR10 and NPFFR2 receptors are closely related to the NPY receptor family. Neither natural PrRP31 nor its palmitoylated analogs showed any binding to the Y2 receptor, while palm-PrRP31 displayed low affinity towards the Y1 receptor. Palmitoylation increased affinity and activity for the Y5 receptor, with palm-PrRP31 having higher off-target activity at this receptor than palm^{11}-PrRP31. Moreover, NPFF and its receptors are involved in regulation of pain nociception, but the ability of PrRP to influence pain perception through NPFFR1 and NPFFR2 was unclear. Both palmitoylated PrRP31 analogs did not exhibit agonist or antagonist properties to the opioid receptors MOR, DOR, and ORL-1. Although palmitoylated PrRP31 analogs showed negligible affinity and agonist activity towards KOR, palm-PrRP31 revealed stronger affinity and agonist activity than palm^{11}-PrRP31 for KOR. Therefore, it is evident that potential pain-modulating effects of PrRP31 analogs would not be mediated through opioid receptors. Clearly, palm^{11}-PrRP31 is more suitable candidate for obesity treatment due to its reduced off-target activity than palm-PrRP31.

In this study, we investigated the intracellular signaling of palmitoylated PrRP31 analogs, palm-PrRP31 and palm^{11}-PrRP31, in CHO-K1 cell lines expressing GPR10, NPFFR2, and NPFFR1 receptors. Stimulation with palmitoylated PrRP31 analogs resulted in significantly increased phosphorylation of Akt at Thr308 and Ser473 in CHO-

K1 cells expressing GPR10, NPFFR2, and NPFFR1. Palm-PrRP31 and palm^{11}-PrRP31 also stimulated the activation of MAPK family members, JNK, ERK, and p38. Moreover, stimulation with palm-PrRP31 and palm^{11}-PrRP31 resulted in significant activation of transcription factors c-Fos and c-Jun that form AP-1 complexes required for G1/S transition and cell cycle progression.

The second part of my study was focused on the metabolic phenotyping of NPFFR2-deficient and GPR10/NPFFR2-deficient mice fed either STD or HFD to determine the potential benefits of targeting these receptors with lipidized PrRP31. Both male and female NPFFR2 KO mice fed a STD revealed a lean phenotype. Interestingly we observed that HFD-fed NPFFR2 KO males had decreased body weight, white adipose tissue mass, leptin plasma levels, and liver weight compared to their WT controls fed HFD. Moreover, the absence of NPFFR2 resulted in glucose intolerance impaired on HFD and disrupted central PI3K/Akt signaling pathway in the hypothalamus and brainstem.

Deletion of both receptors GPR10 and NPFFR2 lead to increased anxiety-like behavior in female mice. Moreover, GPR10/NPFFR2-deficient mice resulted in late-onset obesity in male fed STD and female mice fed HFD and both sexes exhibited hyperinsulinemia when fed HFD. Female GPR10/NPFFR2-deficient mice fed HFD showed reduced impaired glucose tolerance and reduced insulin sensitivity due to increased hepatic GSK-3β and insulin levels. Sex-specific effects on metabolic parameters were observed in GPR10/NPFFR2-deficient mice, resulting in diet-dependent prediabetic symptoms.

These results show that both GPR10 and NPFFR2 receptors play an essential role in controlling energy balance and glucose metabolism. Targeting these receptors appears to be a promising approach for obesity treatment.

7. CONCLUSIONS

PrRP represents one of the most promising candidates of such anti-obesity neuropeptides. Our previous studies showed that peripheral administration of lipidized PrRP31 analogs led to a significant reduction in food intake and body weight in mice. Unfortunately, the mechanism of action of lipidized PrRP31 analogs remains unclear and here we aimed to further investigate it.

PrRP binds to its receptor GPR10 and with a high affinity also to the receptor NPFFR2. Palmitoylation increased the binding and agonist properties of two selected PrRP31 analogs, palm-PrRP31, and palm^{11}-PrRP, towards GPR10 and NPFFR2 receptors. Both analogs also revealed a stronger affinity towards NPFFR1 than natural PrRP31, suggesting NPFFR1 is a potential target of lipidized analogs and needs to be further investigated. Palm^{11}-PrRP31 exhibited reduced off-target activity, indicating that it is a more suitable candidate for obesity treatment than palm-PrRP31. Moreover, we demonstrated that stimulation with these analogs led to significant phosphorylation of Akt at Thr308 and Ser473, as well as activation of MAPK family members JNK, ERK, and p38 in cells expressing GPR10, NPFRR2 and NPFFR1. We also observed significant activation of transcription factors c-Fos and c-Jun that form AP-1 complexes necessary for G1/S transition and cell cycle progression. These results provide insights into the intracellular mechanisms of palmitoylated PrRP31 analogs at GPR10, NPFFR2, and NPFFR1 receptors.

To determine the effects of targeting GPR10 and NPFFR2 with lipidized PrRP31 analogs, we conducted the metabolic phenotyping experiments using NPFFR2-deficient and GPR10/NPFFR2-deficient mice fed either STD or HFD. The NPFFR2 deficiency resulted in glucose intolerance impaired on HFD and disrupted central PI3K/Akt signaling pathway in the hypothalamus and brainstem. The prediabetic syndrome and sex-dependent late-on set obesity was observed in GPR10/NPFFR2 KO. These *in vivo* experiments demonstrated the importance of GPR10 and NPFFR2 receptors in regulating energy homeostasis and glucose metabolism and their targeting with lipidized PrRP31 analogs is a promising strategy for obesity treatment.

8. REFERENCES

Alexopoulou, F., et al., 2022. Lipidated PrRP31 metabolites are long acting dual GPR10 and NPFF2 receptor agonists with potent body weight lowering effect. Sci Rep. 12**,** 1696.

Allard, M., et al., 1995. Mechanisms underlying the cardiovascular responses to peripheral administration of NPFF in the rat. J Pharmacol Exp Ther. 274**,** 577-83.

Anko, M.L., et al., 2006. Alternative splicing of human and mouse NPFF2 receptor genes: Implications to receptor expression. FEBS Lett. 580**,** 6955-60.

Arima, H., et al., 1996. Centrally administered neuropeptide FF inhibits arginine vasopressin release in conscious rats. Endocrinology. 137**,** 1523-9.

Bechtold, D.A., Luckman, S.M., 2006. Prolactin-releasing Peptide mediates cholecystokinin-induced satiety in mice. Endocrinology. 147**,** 4723-9.

Bi, S., et al., 2004. Differential roles for cholecystokinin a receptors in energy balance in rats and mice. Endocrinology. 145**,** 3873-80.

Bjursell, M., et al., 2007. GPR10 deficiency in mice results in altered energy expenditure and obesity. Biochem Biophys Res Commun. 363**,** 633-8.

Blouet, C., Schwartz, G.J., 2010. Hypothalamic nutrient sensing in the control of energy homeostasis. Behav Brain Res. 209**,** 1-12.

Boer, H.H., et al., 1980. Immunocytochemical identification of neural elements in the central nervous systems of a snail, some insects, a fish, and a mammal with an antiserum to the molluscan cardio-excitatory tetrapeptide FMRF-amide. Cell Tissue Res. 213**,** 21-7.

Bonini, J.A., et al., 2000. Identification and characterization of two G protein-coupled receptors for neuropeptide FF. J Biol Chem. 275**,** 39324-31.

Bonnard, E., et al., 2001. Identification of neuropeptide FF-related peptides in rodent spinal cord. Peptides. 22**,** 1085-92.

Boyle, R.G., et al., 2005. Structure-activity studies on prolactin-releasing peptide (PrRP). Analogues of PrRP-(19-31)-peptide. J Pept Sci. 11**,** 161-5.

Cargnello, M., Roux, P.P., 2011. Activation and function of the MAPKs and their substrates, the MAPK-activated protein kinases. Microbiol Mol Biol Rev. 75**,** 50-83.

Cline, M.A., Nandar, W., Rogers, J.O., 2007. Central neuropeptide FF reduces feed consumption and affects hypothalamic chemistry in chicks. Neuropeptides. 41**,** 433-9.

Cummings, D.E., Overduin, J., 2007. Gastrointestinal regulation of food intake. J Clin Invest. 117**,** 13-23.

Deluca, S.H., et al., 2013. The activity of prolactin releasing peptide correlates with its helicity. Biopolymers. 99**,** 314-25.

Desprat, C., Zajac, J.M., 1997. Differential modulation of mu- and delta-opioid antinociception by neuropeptide FF receptors in young mice. Neuropeptides. 31**,** 1-7.

Dockray, G.J., et al., 1983. A novel active pentapeptide from chicken brain identified by antibodies to FMRFamide. Nature. 305**,** 328-30.

Ellacott, K.L., et al., 2002. PRL-releasing peptide interacts with leptin to reduce food intake and body weight. Endocrinology. 143**,** 368-74.

Ellacott, K.L., et al., 2003. Repeated administration of the anorectic factor prolactin-releasing peptide leads to tolerance to its effects on energy homeostasis. Am J Physiol Regul Integr Comp Physiol. 285**,** R1005-10.

Elphick, M.R., Mirabeau, O., 2014. The Evolution and Variety of RFamide-Type Neuropeptides: Insights from Deuterostomian Invertebrates. Front Endocrinol (Lausanne). 5**,** 93.

Elshourbagy, N.A., et al., 2000. Receptor for the pain modulatory neuropeptides FF and AF is an orphan G protein-coupled receptor. J Biol Chem. 275**,** 25965-71.

Engstrom, M., et al., 2003. Prolactin releasing peptide has high affinity and efficacy at neuropeptide FF2 receptors. J Pharmacol Exp Ther. 305**,** 825-32.

Fan, W., et al., 1997. Role of melanocortinergic neurons in feeding and the agouti obesity syndrome. Nature. 385**,** 165-8.

Fehmann, H.C., et al., 1990. The effects of two FMRFamide related peptides (A-18-F-amide and F-8-F-amide; 'morphine modulating peptides') on the endocrine and exocrine rat pancreas. Neuropeptides. 17**,** 87-92.

Findeisen, M., Rathmann, D., Beck-Sickinger, A.G., 2011. Structure-activity studies of RFamide peptides reveal subtype-selective activation of neuropeptide FF1 and FF2 receptors. ChemMedChem. 6, 1081-93.
Fujii, R., et al., 1999. Tissue distribution of prolactin-releasing peptide (PrRP) and its receptor. Regul Pept. 83, 1-10.
Fukusumi, S., Fujii, R., Hinuma, S., 2006. Recent advances in mammalian RFamide peptides: the discovery and functional analyses of PrRP, RFRPs and QRFP. Peptides. 27, 1073-86.
Gault, V.A., et al., 2011. Administration of an acylated GLP-1 and GIP preparation provides added beneficial glucose-lowering and insulinotropic actions over single incretins in mice with Type 2 diabetes and obesity. Clin Sci (Lond). 121, 107-17.
Gicquel, S., et al., 1992. Analogues of F8Famide resistant to degradation, with high affinity and in vivo effects. Eur J Pharmacol. 222, 61-7.
Goncharuk, V., Jhamandas, J.H., 2008. Neuropeptide FF2 receptor distribution in the human brain. An immunohistochemical study. Peptides. 29, 1544-53.
Goncharuk, V.D., et al., 2006. Neuropeptide FF distribution in the human and rat forebrain: a comparative immunohistochemical study. J Comp Neurol. 496, 572-93.
Gouarderes, C., et al., 1993. Antinociceptive effects of intrathecally administered F8Famide and FMRFamide in the rat. Eur J Pharmacol. 237, 73-81.
Gouarderes, C., et al., 1996. Role of opioid receptors in the spinal antinociceptive effects of neuropeptide FF analogues. Br J Pharmacol. 117, 493-501.
Gouarderes, C., Kieffer, B.L., Zajac, J.M., 2004. Opposite alterations of NPFF1 and NPFF2 neuropeptide FF receptor density in the triple MOR/DOR/KOR-opioid receptor knockout mouse brains. J Chem Neuroanat. 27, 119-28.
Gu, W., et al., 2004. The prolactin-releasing peptide receptor (GPR10) regulates body weight homeostasis in mice. J Mol Neurosci. 22, 93-103.
Havelund, S., et al., 2004. The mechanism of protraction of insulin detemir, a long-acting, acylated analog of human insulin. Pharm Res. 21, 1498-504.
Hayakawa, J., et al., 2002. Regulation of the PRL promoter by Akt through cAMP response element binding protein. Endocrinology. 143, 13-22.
Higo, S., Kanaya, M., Ozawa, H., 2021. Expression analysis of neuropeptide FF receptors on neuroendocrine-related neurons in the rat brain using highly sensitive in situ hybridization. Histochem Cell Biol. 155, 465-475.
Hinuma, S., et al., 1998. A prolactin-releasing peptide in the brain. Nature. 393, 272-6.
Hinuma, S., et al., 2000. New neuropeptides containing carboxy-terminal RFamide and their receptor in mammals. Nat Cell Biol. 2, 703-8.
Holubova, M., et al., 2018. Prolactin-releasing peptide improved leptin hypothalamic signaling in obese mice. J Mol Endocrinol. 60, 85-94.
Cheng, Y., Prusoff, W.H., 1973. Relationship between the inhibition constant (K1) and the concentration of inhibitor which causes 50 per cent inhibition (I50) of an enzymatic reaction. Biochem Pharmacol. 22, 3099-108.
Ibata, Y., et al., 2000. Morphological survey of prolactin-releasing peptide and its receptor with special reference to their functional roles in the brain. Neurosci Res. 38, 223-30.
Iijima, N., et al., 1999. Cytochemical study of prolactin-releasing peptide (PrRP) in the rat brain. Neuroreport. 10, 1713-6.
Jenickova, I., et al., 2021. Efficient allele conversion in mouse zygotes and primary cells based on electroporation of Cre protein. Methods. 191, 87-94.
Jhamandas, J.H., Mactavish, D., 2002. Central administration of neuropeptide FF (NPFF) causes increased neuronal activation and up-regulation of NPFF gene expression in the rat brainstem. J Comp Neurol. 447, 300-7.
Jhamandas, J.H., MacTavish, D., 2003. Central administration of neuropeptide FF causes activation of oxytocin paraventricular hypothalamic neurones that project to the brainstem. J Neuroendocrinol. 15, 24-32.
Jhamandas, J.H., et al., 2007. Neuropeptide FF and neuropeptide VF inhibit GABAergic neurotransmission in parvocellular neurons of the rat hypothalamic paraventricular nucleus. Am J Physiol Regul Integr Comp Physiol. 292, R1872-80.

Kalliomaki, M.L., et al., 2004. Prolactin-releasing peptide affects pain, allodynia and autonomic reflexes through medullary mechanisms. Neuropharmacology. 46, 412-24.
Karnosova, A., et al., 2021. Palmitoylation of Prolactin-Releasing Peptide Increased Affinity for and Activation of the GPR10, NPFF-R2 and NPFF-R1 Receptors: In Vitro Study. Int J Mol Sci. 22.
Kavaliers, M., Yang, H.Y., 1989. IgG from antiserum against endogenous mammalian FMRF-NH2-related peptides augments morphine- and stress-induced analgesia in mice. Peptides. 10, 741-5.
Kimura, A., et al., 2000. Prolactin-releasing peptide activation of the prolactin promoter is differentially mediated by extracellular signal-regulated protein kinase and c-Jun N-terminal protein kinase. J Biol Chem. 275, 3667-74.
Korinkova, L., et al., 2020. Synergistic effect of leptin and lipidized PrRP on metabolic pathways in ob/ob mice. J Mol Endocrinol. 64, 77-90.
Kotani, M., et al., 2001. Functional characterization of a human receptor for neuropeptide FF and related peptides. Br J Pharmacol. 133, 138-44.
Laguzzi, R., et al., 1996. Cardiovascular effects induced by the stimulation of neuropeptide FF receptors in the dorsal vagal complex: an autoradiographic and pharmacological study in the rat. Brain Res. 711, 193-202.
Langmead, C.J., et al., 2000. Characterization of the binding of [(125)I]-human prolactin releasing peptide (PrRP) to GPR10, a novel G protein coupled receptor. Br J Pharmacol. 131, 683-8.
Larsen, P.J., et al., 2001. Systemic administration of the long-acting GLP-1 derivative NN2211 induces lasting and reversible weight loss in both normal and obese rats. Diabetes. 50, 2530-9.
Lawrence, C.B., et al., 2000. Alternative role for prolactin-releasing peptide in the regulation of food intake. Nat Neurosci. 3, 645-6.
Lawrence, C.B., Ellacott, K.L., Luckman, S.M., 2002. PRL-releasing peptide reduces food intake and may mediate satiety signaling. Endocrinology. 143, 360-7.
Leavens, K.F., Birnbaum, M.J., 2011. Insulin signaling to hepatic lipid metabolism in health and disease. Crit Rev Biochem Mol Biol. 46, 200-15.
Lin, S.H., 2008. Prolactin-releasing peptide. Results Probl Cell Differ. 46, 57-88.
Lin, Y.T., et al., 2016a. Altered nociception and morphine tolerance in neuropeptide FF receptor type 2 over-expressing mice. Eur J Pain. 20, 895-906.
Lin, Y.T., et al., 2016b. Chronic activation of NPFFR2 stimulates the stress-related depressive behaviors through HPA axis modulation. Psychoneuroendocrinology. 71, 73-85.
Lin, Y.T., et al., 2017a. Activation of NPFFR2 leads to hyperalgesia through the spinal inflammatory mediator CGRP in mice. Exp Neurol. 291, 62-73.
Lin, Y.T., et al., 2017b. NPFFR2 Activates the HPA Axis and Induces Anxiogenic Effects in Rodents. Int J Mol Sci. 18.
Lin, Y.T., Chen, J.C., 2019. Neuropeptide FF modulates neuroendocrine and energy homeostasis through hypothalamic signaling. Chin J Physiol. 62, 47-52.
Lin, Y.T., et al., 2020. Ablation of NPFFR2 in Mice Reduces Response to Single Prolonged Stress Model. Cells. 9.
Liu, Q., et al., 2001. Identification and characterization of novel mammalian neuropeptide FF-like peptides that attenuate morphine-induced antinociception. J Biol Chem. 276, 36961-9.
Ma, L., et al., 2009. Prolactin-releasing peptide effects in the rat brain are mediated through the Neuropeptide FF receptor. Eur J Neurosci. 30, 1585-93.
Maixnerova, J., et al., 2011. Characterization of prolactin-releasing peptide: binding, signaling and hormone secretion in rodent pituitary cell lines endogenously expressing its receptor. Peptides. 32, 811-7.
Maletinska, L., et al., 2011. Biological properties of prolactin-releasing peptide analogs with a modified aromatic ring of a C-terminal phenylalanine amide. Peptides. 32, 1887-92.
Maletinska, L., et al., 2012. Characterization of new stable ghrelin analogs with prolonged orexigenic potency. J Pharmacol Exp Ther. 340, 781-6.

Maletinska, L., et al., 2013. Neuropeptide FF analog RF9 is not an antagonist of NPFF receptor and decreases food intake in mice after its central and peripheral administration. Brain Res. 1498, 33-40.
Maletinska, L., et al., 2015. Novel lipidized analogs of prolactin-releasing peptide have prolonged half-lives and exert anti-obesity effects after peripheral administration. Int J Obes (Lond). 39, 986-93.
Marchese, A., et al., 1995. Cloning and chromosomal mapping of three novel genes, GPR9, GPR10, and GPR14, encoding receptors related to interleukin 8, neuropeptide Y, and somatostatin receptors. Genomics. 29, 335-44.
Maruyama, M., et al., 2001. Prolactin-releasing peptide as a novel stress mediator in the central nervous system. Endocrinology. 142, 2032-8.
Maselli, D.B., Camilleri, M., 2021. Effects of GLP-1 and Its Analogs on Gastric Physiology in Diabetes Mellitus and Obesity. Adv Exp Med Biol. 1307, 171-192.
Matsumoto, H., et al., 1999. Distribution and characterization of immunoreactive prolactin-releasing peptide (PrRP) in rat tissue and plasma. Biochem Biophys Res Commun. 257, 264-8.
Matsumoto, H., et al., 2000. Stimulation of corticotropin-releasing hormone-mediated adrenocorticotropin secretion by central administration of prolactin-releasing peptide in rats. Neurosci Lett. 285, 234-8.
Minami, S., et al., 1999. Cellular localization of prolactin-releasing peptide messenger RNA in the rat brain. Neurosci Lett. 266, 73-5.
Mochiduki, A., et al., 2010. Stress response of prolactin-releasing peptide knockout mice as to glucocorticoid secretion. J Neuroendocrinol. 22, 576-84.
Mollereau, C., et al., 2002. Pharmacological characterization of human NPFF(1) and NPFF(2) receptors expressed in CHO cells by using NPY Y(1) receptor antagonists. Eur J Pharmacol. 451, 245-56.
Morton, G.J., et al., 2006. Central nervous system control of food intake and body weight. Nature. 443, 289-95.
Morton, G.J., Meek, T.H., Schwartz, M.W., 2014. Neurobiology of food intake in health and disease. Nat Rev Neurosci. 15, 367-78.
Motulsky, H., Neubig, R., 2002. Analyzing radioligand binding data. Curr Protoc Neurosci. Chapter 7, Unit 7 5.
Mrazikova, L., et al., 2021. Lipidized Prolactin-Releasing Peptide as a New Potential Tool to Treat Obesity and Type 2 Diabetes Mellitus: Preclinical Studies in Rodent Models. Front Pharmacol. 12, 779962.
Mrazikova, L., et al., 2022. Palmitoylated prolactin-releasing peptide treatment had neuroprotective but not anti-obesity effect in fa/fa rats with leptin signaling disturbances. Nutr Diabetes. 12, 26.
Murase, T., et al., 1996. Neuropeptide FF reduces food intake in rats. Peptides. 17, 353-4.
Myers, M.G., Jr., Olson, D.P., 2012. Central nervous system control of metabolism. Nature. 491, 357-63.
Nanmoku, T., et al., 2003. Prolactin-releasing peptide stimulates catecholamine release but not proliferation in rat pheochromocytoma PC12 cells. Neurosci Lett. 350, 33-6.
Nicklous, D.M., Simansky, K.J., 2003. Neuropeptide FF exerts pro- and anti-opioid actions in the parabrachial nucleus to modulate food intake. Am J Physiol Regul Integr Comp Physiol. 285, R1046-54.
Nieminen, M.L., et al., 2000. Expression of mammalian RF-amide peptides neuropeptide FF (NPFF), prolactin-releasing peptide (PrRP) and the PrRP receptor in the peripheral tissues of the rat. Peptides. 21, 1695-701.
Nystedt, J.M., et al., 2006. Identification of transcriptional regulators of neuropeptide FF gene expression. Peptides. 27, 1020-35.
Parker, R.M., et al., 2000. Molecular cloning and characterisation of GPR74 a novel G-protein coupled receptor closest related to the Y-receptor family. Brain Res Mol Brain Res. 77, 199-208.

Payza, K., Akar, C.A., Yang, H.Y., 1993. Neuropeptide FF receptors: structure-activity relationship and effect of morphine. J Pharmacol Exp Ther. 267**,** 88-94.
Pineda, R., et al., 2010. Characterization of the potent gonadotropin-releasing activity of RF9, a selective antagonist of RF-amide-related peptides and neuropeptide FF receptors: physiological and pharmacological implications. Endocrinology. 151**,** 1902-13.
Pirnik, Z., et al., 2015. Peripheral administration of palmitoylated prolactin-releasing peptide induces Fos expression in hypothalamic neurons involved in energy homeostasis in NMRI male mice. Brain Res. 1625**,** 151-8.
Pirnik, Z., et al., 2018. Repeated peripheral administration of lipidized prolactin-releasing peptide analog induces c-fos and FosB expression in neurons of dorsomedial hypothalamic nucleus in male C57 mice. Neurochem Int. 116**,** 77-84.
Pirnik, Z., et al., 2021. Cholecystokinin system is involved in the anorexigenic effect of peripherally applied palmitoylated prolactin-releasing peptide in fasted mice. Physiol Res. 70**,** 579-590.
Prazienkova, V., et al., 2016. Pharmacological characterization of lipidized analogs of prolactin-releasing peptide with a modified C- terminal aromatic ring. J Physiol Pharmacol. 67**,** 121-8.
Prazienkova, V., et al., 2017. Impact of novel palmitoylated prolactin-releasing peptide analogs on metabolic changes in mice with diet-induced obesity. PLoS One. 12**,** e0183449.
Prazienkova, V., et al., 2019. Prolactin-Releasing Peptide: Physiological and Pharmacological Properties. Int J Mol Sci. 20.
Prazienkova, V., et al., 2021. GPR10 gene deletion in mice increases basal neuronal activity, disturbs insulin sensitivity and alters lipid homeostasis. Gene. 774**,** 145427.
Price, D.A., Greenberg, M.J., 1977. Structure of a molluscan cardioexcitatory neuropeptide. Science. 197**,** 670-1.
Prokai, L., et al., 2006. Cardiovascular effects of neuropeptide FF antagonists. Peptides. 27**,** 1015-9.
Ravussin, E., Bogardus, C., 1989. Relationship of genetics, age, and physical fitness to daily energy expenditure and fuel utilization. Am J Clin Nutr. 49**,** 968-75.
Roland, B.L., et al., 1999. Anatomical distribution of prolactin-releasing peptide and its receptor suggests additional functions in the central nervous system and periphery. Endocrinology. 140**,** 5736-45.
Roumy, M., et al., 2000. Are neuropeptides FF and SF neurotransmitters in the rat? Biochem Biophys Res Commun. 275**,** 821-4.
Samson, W.K., Resch, Z.T., Murphy, T.C., 2000. A novel action of the newly described prolactin-releasing peptides: cardiovascular regulation. Brain Res. 858**,** 19-25.
Samson, W.K., et al., 2003. Prolactin-releasing peptide and its homolog RFRP-1 act in hypothalamus but not in anterior pituitary gland to stimulate stress hormone secretion. Endocrine. 20**,** 59-66.
Samson, W.K., Taylor, M.M., 2006. Prolactin releasing peptide (PrRP): an endogenous regulator of cell growth. Peptides. 27**,** 1099-103.
Seal, L.J., et al., 2000. Prolactin releasing peptide (PrRP) stimulates luteinizing hormone (LH) and follicle stimulating hormone (FSH) via a hypothalamic mechanism in male rats. Endocrinology. 141**,** 1909-12.
Schafer, M.K., et al., 1993. Gene expression of prohormone and proprotein convertases in the rat CNS: a comparative in situ hybridization analysis. J Neurosci. 13**,** 1258-79.
Schwartz, M.W., Porte, D., Jr., 2005. Diabetes, obesity, and the brain. Science. 307**,** 375-9.
Simonin, F., et al., 2006. RF9, a potent and selective neuropeptide FF receptor antagonist, prevents opioid-induced tolerance associated with hyperalgesia. Proc Natl Acad Sci U S A. 103**,** 466-71.
Spolcova, A., et al., 2015. Anorexigenic lipopeptides ameliorate central insulin signaling and attenuate tau phosphorylation in hippocampi of mice with monosodium glutamate-induced obesity. J Alzheimers Dis. 45**,** 823-35.
Spuch, C., et al., 2007. Prolactin-releasing Peptide (PrRP) increases prolactin responses to TRH in vitro and in vivo. Endocrine. 31**,** 119-24.

Strnadova, V., et al., 2023. Search for lipidized PrRP analogs with strong anorexigenic effect: In vitro and in vivo studies. Neuropeptides. 98, 102319.
Sun, Y., et al., 2015. Signaling pathway of MAPK/ERK in cell proliferation, differentiation, migration, senescence and apoptosis. J Recept Signal Transduct Res. 35, 600-4.
Sundblom, D.M., Panula, P., Fyhrquist, F., 1995. Neuropeptide FF-like immunoreactivity in human plasma. Peptides. 16, 347-50.
Sundblom, D.M., et al., 1997. Neuropeptide FF-like immunoreactivity in human cerebrospinal fluid of chronic pain patients and healthy controls. Peptides. 18, 923-7.
Sunter, D., et al., 2001. Intracerebroventricular injection of neuropeptide FF, an opioid modulating neuropeptide, acutely reduces food intake and stimulates water intake in the rat. Neurosci Lett. 313, 145-8.
Takayanagi, Y., et al., 2008. Endogenous prolactin-releasing peptide regulates food intake in rodents. J Clin Invest. 118, 4014-24.
Talmont, F., et al., 2010. Pharmacological characterization of the mouse NPFF2 receptor. Peptides. 31, 215-20.
Timper, K., Bruning, J.C., 2017. Hypothalamic circuits regulating appetite and energy homeostasis: pathways to obesity. Dis Model Mech. 10, 679-689.
Torz, L., et al., 2022. NPFF Decreases Activity of Human Arcuate NPY Neurons: A Study in Embryonic-Stem-Cell-Derived Model. Int J Mol Sci. 23.
Uchida, K., et al., 2010. Participation of the prolactin-releasing peptide-containing neurones in caudal medulla in conveying haemorrhagic stress-induced signals to the paraventricular nucleus of the hypothalamus. J Neuroendocrinol. 22, 33-42.
Vilim, F.S., et al., 1999. Gene for pain modulatory neuropeptide NPFF: induction in spinal cord by noxious stimuli. Mol Pharmacol. 55, 804-11.
Waclawczyk, D., Silberring, J., Grasso, G., 2021. The insulin-degrading enzyme as a link between insulin and neuropeptides metabolism. J Enzyme Inhib Med Chem. 36, 183-187.
Waqas, S.F.H., et al., 2017. Neuropeptide FF increases M2 activation and self-renewal of adipose tissue macrophages. J Clin Invest. 127, 2842-2854.
Watanabe, T.K., et al., 2005. Mutated G-protein-coupled receptor GPR10 is responsible for the hyperphagia/dyslipidaemia/obesity locus of Dmo1 in the OLETF rat. Clin Exp Pharmacol Physiol. 32, 355-66.
Welch, S.K., et al., 1995. Sequence and tissue distribution of a candidate G-coupled receptor cloned from rat hypothalamus. Biochem Biophys Res Commun. 209, 606-13.
Wen, A.Y., Sakamoto, K.M., Miller, L.S., 2010. The role of the transcription factor CREB in immune function. J Immunol. 185, 6413-9.
Yamada, T., et al., 2009. Prolactin-releasing peptide regulates the cardiovascular system via corticotrophin-releasing hormone. J Neuroendocrinol. 21, 586-93.
Yang, H.Y., et al., 1985. Isolation, sequencing, synthesis, and pharmacological characterization of two brain neuropeptides that modulate the action of morphine. Proc Natl Acad Sci U S A. 82, 7757-61.
Yano, T., et al., 2001. Developmental expression of prolactin releasing peptide in the rat brain: localization of messenger ribonucleic acid and immunoreactive neurons. Brain Res Dev Brain Res. 128, 101-11.
Yu, J.H., Kim, M.S., 2012. Molecular mechanisms of appetite regulation. Diabetes Metab J. 36, 391-8.
Yun, S., et al., 2014. Does Kisspeptin Belong to the Proposed RF-Amide Peptide Family? Front Endocrinol (Lausanne). 5, 134.
Zhang, L., et al., 2018. Diet-induced adaptive thermogenesis requires neuropeptide FF receptor-2 signalling. Nat Commun. 9, 4722.
Zhang, L., et al., 2021. Lack of neuropeptide FF signalling in mice leads to reduced repetitive behavior, altered drinking behavior, and fuel type selection. FASEB J. 35, e21980.
Zhang, L., et al., 2022a. NPFF signalling is critical for thermosensory and dietary regulation of thermogenesis. Neuropeptides. 96, 102292.
Zhang, L., et al., 2022b. Central NPFF signalling is critical in the regulation of glucose homeostasis. Mol Metab. 62, 101525.

Other references

WHO European Regional Obesity Report 2022. Copenhagen: WHO Regional Office for Europe; 2022. Licence: CC BY-NC-SA 3.0 IGO

LIST OF MY PUBLICATIONS

Publications related to Ph.D. thesis:

1. Karnošová, A.; Strnadová, V.; Holá, L.; Železná, B.; Kuneš, J.; Maletínská, L. Palmitoylation of Prolactin-Releasing Peptide Increased Affinity for and Activation of the GPR10, NPFF-R2 and NPFF-R1 Receptors: In Vitro Study. *Int. J. Mol. Sci*. 2021, 22, 8904. https://doi.org/10.3390/ijms22168904. **IF_{2021} = 6.208**

2. Strnadová, V.; Karnošová, A.; Blechová, M.; Neprašová, B.; Holá, L.; Němcová, A.; Myšková, A.; Sýkora, D.; Železná, B.; Kuneš, J.; Maletínská, L. Search for lipidized PrRP analogs with strong anorexigenic effect: In vitro and in vivo studies. *Neuropeptides*. 2023, 98**,** 102319. https://doi.org/10.1016/j.npep.2022.102319. **IF_{2023} = 3.286**

Publications not related to Ph.D. thesis:

1. Holá, L.; Železná, B.; Karnošová, A.; Kuneš, J.; Fehrentz, JA.; Denoyelle, S.; Cantel, S.; Blechová, M.; Sýkora, D.; Myšková, A.; Maletínská, L. A Novel Truncated Liver Enriched Antimicrobial Peptide-2 Palmitoylated at its N-Terminal Antagonizes Effects of Ghrelin. *J Pharmacol Exp Ther.* 2022, 383(2), 129-136. https://doi.org/ 10.1124/jpet.122.001322. **IF_{2022} = 4.402**

2. Pražienková, V.; Funda, J.; Pirník, Z.; Karnošová, A.; Hrubá, L.; Kořínková, L.; Neprašová, B.; Janovská, P.; Benzce, M.; Kadlecová, M.; Blahoš, J.; Kopecký, J.; Železná, B.; Kuneš, J.; Bardová, K.; Maletínská, L. GPR10 gene deletion in mice increases basal neuronal activity, disturbs insulin sensitivity and alters lipid homeostasis. *Gene*. 2021, 774, 145427. https://doi.org/10.1016/j.gene.2021.145427. **IF_{2021} = 3.913**

3. Kořínková, L.; Pražienková, V.; Černá, L.; Karnošová, A.; Železná, B.; Kuneš, J.; Maletínská, L. Pathophysiology of NAFLD and NASH in Experimental Models: The Role of Food Intake Regulating Peptides. *Front Endocrinol.* 2020, 11, 597583. https://doi.org/10.3389/fendo.2020.597583. **IF_{2020} = 5.555**

SUPPLEMENT

Supplement 1:

Strnadová, V.; Karnošová, A.; Blechová, M.; Neprašová, B.; Holá, L.; Němcová, A.; Myšková, A.; Sýkora, D.; Železná, B.; Kuneš, J.; Maletínská, L. Search for lipidized PrRP analogs with strong anorexigenic effect: In vitro and in vivo studies. *Neuropeptides*. 2023, 98**,** 102319. https://doi.org/10.1016/j.npep.2022.102319.

Supplement 2:

Karnošová, A.; Strnadová, V.; Holá, L.; Železná, B.; Kuneš, J.; Maletínská, L. Palmitoylation of Prolactin-Releasing Peptide Increased Affinity for and Activation of the GPR10, NPFF-R2 and NPFF-R1 Receptors: In Vitro Study. *Int. J. Mol. Sci*. 2021, 22, 8904. https://doi.org/10.3390/ijms22168.